



Electrocatalytic seawater splitting: Nice designs, advanced strategies, challenges and perspectives

Jie Liang^a, Zixiao Li^a, Xun He^a, Yongsong Luo^a, Dongdong Zheng^a, Yan Wang^a, Tingshuai Li^a, Binwu Ying^a, Shengjun Sun^b, Zhengwei Cai^b, Qian Liu^c, Bo Tang^{b,d,*}, Xuping Sun^{a,b,*}

^a Institute of Fundamental and Frontier Sciences, University of Electronic Science and Technology of China, Chengdu 610054, Sichuan, China

^b College of Chemistry, Chemical Engineering and Materials Science, Shandong Normal University, Jinan 250014, Shandong, China

^c Institute for Advanced Study, Chengdu University, Chengdu 610106, Sichuan, China

^d Laoshan Laboratory, Qingdao 266237, Shandong, China

H_2 has a sufficiently high energy density and a combustion process that emits no carbon, therefore being an appealing storable alternative to fossil fuels. With evident advantages of seawater resources available worldwide, electrochemically making H_2 from seawater holds a great development prospect towards the global deployment of H_2 -based energy plants. However, with current water splitting technologies, this is not an easy task, and the primary obstacle is impurities in natural seawater including halide salts, magnesium salts, organic matter, etc., which readily cause the electrocatalysis systems to shut down. We herein present a timely review of seawater electrolysis systems at both lab-scale fundamental research and pilot-scale reactor level on the basis of most representative studies. We analyze some of the crucial experimental details that are frequently ignored, such as seawater treatments, product detection, electrode assembly, reactors, electrolyte feeding modes, etc. We then systematically emphasize the latest and representative strategies and catalytic materials designs as well as whether corresponding electrodes are genuinely stable as two key quests to find out truly reliable and exploitable electrode engineering. Gas release behaviors/kinetics at high reaction rates are highlighted as well. In addition, we introduce valuable contents like how to learn from ocean life for electrocatalytic system design. We conclude by taking a look at the future research directions and opportunities for encouraging more practical applications of seawater electrolysis systems/technologies.

Keywords: Green hydrogen economy; Seawater electrolysis; Electrocatalysts; Self-reconstruction; Membrane

Introduction

Limited fossil fuel (LFF) supplies and ecological damages that their exploitation causes are calling for gradual upgrades of our energy landscape, which is currently dominated by the LFF, to renewable energy source-based production of chemicals and

fuels (e.g., through Power-to-X) [1]. Hydrogen (H_2) is a key feedstock to various sectors including Haber-Bosch process, petroleum refining, steelmaking, etc., and is a widely accepted energy carrier with clean combustion [2–5]. While the H_2 demand has soared since 2000 and was approximately 90 million metric tons in 2020, over 90% of that H_2 has come from energy-intensive and carbon-emitting technologies like natural gas reforming [3]. The hard trade-off between the current unsustainable

* Corresponding authors.

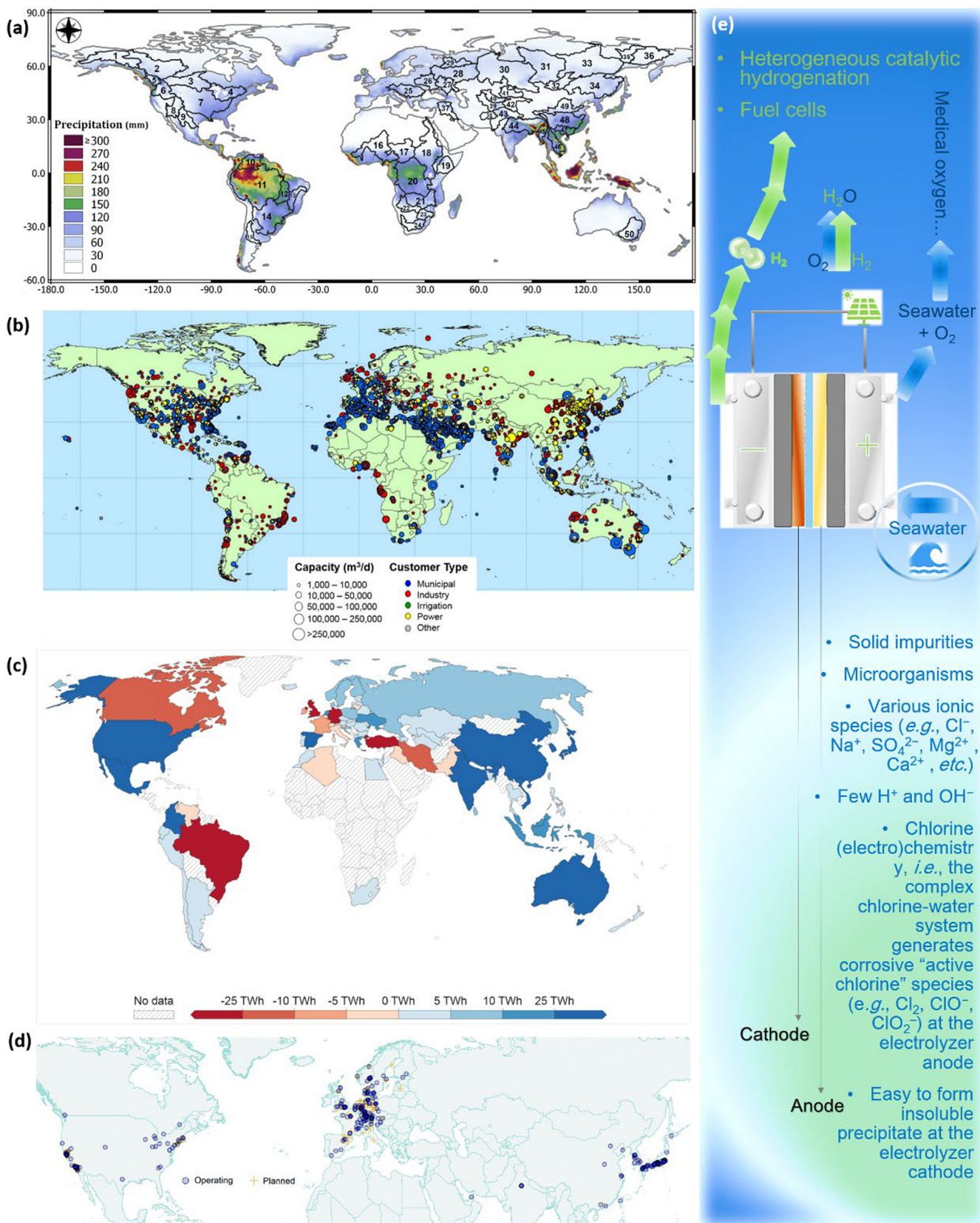
E-mail addresses: Tang, B. (tangb@sdnu.edu.cn), Sun, X. (xpsun@uestc.edu.cn), Sun, X. (xpsun@sdnu.edu.cn).

able H₂ production for the increasing H₂-related market and fast LFF depletion lead us to develop low-carbon H₂-based energy transition. Electrosynthesis of H₂ directly from ultra-high-purity water, powered by renewable energy, is green enough [6], but even if generating H₂ from water permits small water demand (~9 kg H₂O/kg H₂) [3], the Net zero Emissions Scenario in the future will result in an enormous rise in the volume of fresh water consumed for water splitting activities. It is known that although water covers about 70% of our planet, a tiny fraction of just ~ 2.5% is freshwater, and two thirds of that is either frozen in glaciers or inaccessible to humans in some other ways. Moreover importantly, fresh water resources are not evenly distributed around the world. The spatial distribution of rainfall (Fig. 1a) and the local climate type are the key determinants of the distribution of water resources [7]. One of the primary problems in numerous countries across the world, including Kuwait, Libya, Saudi Arabia, Jordan, the Republic of Yemen, Israel, Tunisia, Algeria, Burundi, etc., is a lack of water. Since lots of desalination plants have been built at great cost in the countries that lack freshwater resources (Fig. 1b) [8], it will be scarcely possible to electrolyze hard-won freshwater to make H₂ there.

Electrolysis of seawater to make H₂ (Fig. 1e) is a viable option in that vast seawater resources guarantee a solid foundation for such conversion. Moreover, many countries, including China, USA, India, Australia, and others, are developing renewable energy sources such as solar, wind, and geothermal energy (Fig. 1c) [9]. These countries have broad coastlines and lots of coastal cities, making large-scale seawater electrolysis powered by renewable energy highly attractive and easier to achieve. In fact, in addition to these countries, other countries with seawater resources can also rely on electrolysis to produce H₂, since deploying H₂ energy plants along the coast will significantly lower overall infrastructure and transportation costs. In addition, the locations and distribution of hydrogen filling stations around the world are not uniform, with the majority being centered in the United States and Japan (Fig. 1d) [10]. One the other hand, although water crisis is merely a vague idea to some people, the scarcity of life-sustaining water is putting people in water shortage regions at risk. In fact, seawater electrolysis, coupled with H₂-O₂ fuel cell technologies, are sustainable when used as an alternative possible solution for future on-site desalinizing saltwater into pure water. Accordingly, success in efficiently electrolyzing seawater would be a vital step in the worldwide deployment of clean energy technologies by exploiting ocean as the globe-spanning H₂ resources. Before starting this review, good review papers that are already available in this field are recommended for readers [11–21]. This article gives a summary of the most recent advances in the field as well as previously ignored findings.

Various impurities present in natural seawater, mostly inducing solid particles, microorganisms, organic matter, Ca²⁺, Mg²⁺, Sr²⁺, Cl⁻, Br⁻, and so forth, nonetheless, make the efficient and long-term generation of H₂ from seawater rather challenging. No matter how an electrolytic reactor is constructed, seawater electrolysis must occur there in order to obtain high-purity H₂. The anode, cathode and membrane are core parts of the reactor, but they are also the ones most vulnerable to pollution, corrosion, or poisoning from these impurities. Since natural saltwater

contains little H⁺/ OH⁻, the larger current densities (*J*), the more milky cathode precipitation (caused by pH drop) as well as the more severe anode corrosion (damaged by halide ions and more derived species). Direct oxidation of natural seawater would be ideal, yet since the pH is close to neutral and halide ions far outnumber OH⁻, the selectivity of O₂ would be limited. Some studies added used buffered seawater to attain relatively better performances, like seawater + 1 M KOH + 1 M phosphate (KPi) + 1 M borate (KBi) adopted by Nocera's group [22] as well as seawater + NaH₂PO₄ + Na₂HPO₄ (pH adjusted to 7) adopted by groups of Qiao and Liu [23]. Though such buffering seawater electrolytes may afford smaller pH gradients across the electrolytic cell and better catalyst performance, adding salts into seawater and then filtering actually has two little issues. (i) One-step seawater splitting becomes two-step pre-treated seawater (less Ca²⁺/Mg²⁺) splitting. (ii) Salts need to be added regularly to ensure stable reaction. Such issues are even more pronounced for alkalized seawater, because making seawater alkaline consumes KOH prior to the electrolysis. Even if some work removes Ca²⁺/Mg²⁺ using relatively cheaper salts (e.g., Na₂CO₃) and then adds NaOH/KOH to create alkalinity, direct electrolysis of natural seawater turns into indirect electrolysis of alkaline seawater. Materials that can afford high *J* at overpotentials < 480 mV ($\eta < \eta_{480}$) are being sought and designed for catalysis under alkaline seawater conditions (pH > 7.5 [11]) in that alkaline media can block chlorine electrochemistry at certain potentials. While it is possible to design such catalysts and some progress has been made (e.g., NF/NiMoN@Ni-FeN, 1 A cm⁻² at η_{398} , 1 M KOH + natural seawater [24]), artificially alkalizing seawater adds the complexity and energy penalty for industrial applications. Note that even though roughly 30% KOH solution is employed in industrial electrolysis of water, the catalysts in alkaline saltwater will degrade more quickly if it is overly alkaline (e.g., 6 M KOH + seawater [25]). Acidic seawater electrolysis is a different route with certain benefits like less precipitation and faster hydrogen evolution reaction (HER), yet it faces new issues (unsuppressed chloride oxidation and acid etching). At present, relevant studies based on acidic seawater are rare [26]. Though one-step direct electrolysis has much simpler equipment, it now has stricter requirements for both electrodes and membranes. Clearly, the cost-effectiveness of direct electrolysis can only be higher than indirect electrolysis if both the electrode and the membrane are durable enough. While OH⁻ concentrations in natural seawater are small, orders of magnitude lower than those in alkaline electrolytes, it is possible to directly electrolyze natural seawater at a good efficiency adopting appropriate catalyst designs (e.g., catalyst: Cr₂O₃-CoO_x, seawater: pH = 7.9, without solids/microorganisms, *J*: 0.4 A cm⁻² at 1.99 V with 75% *iR* compensation in a single-compartment cell, *J*: 1 A cm⁻² at 2.33 V in a proton exchange membrane (PEM)-based flow-type electrolyzer [27]). Alternatively, unconventional seawater electrolysis systems (SESSs) also exhibit great potential for cost-effective H₂ production. Overall, since residual cations and more unwanted anionic ions will still be present after chemical pre-precipitation treatment, H₂-evolving and O₂-evolving catalysts that show high selectivity and durability even in impure seawater electrolytes with impurity ions are highly desirable.

**FIG. 1**

(a) Annual mean precipitation over the period 1980–2018 from the Multi-Source Weighted-Ensemble Precipitation dataset. Reproduced with permission from Ref. [7] Copyright 2023, Elsevier. (b) Global distribution of operational desalination facilities and capacities (>1000 m³/day) by sector user of produced water. Reproduced with permission from Ref. [8] Copyright 2019, Elsevier. (c) Annual change in renewable energy generation, 2021 [9]. (d) Hydrogen refueling stations worldwide. Reproduced with permission from Ref. [10] Copyright 2019, Royal Society of Chemistry. (e) Schematic diagram of the SES.

People are curious in knowing distinctions between direct seawater splitting (DSS) and indirect seawater splitting (ISS, *e.g.*, reverse osmosis and subsequent conventional electrolysis) and whether the DSS is economically meaningful. Firstly, reverse osmosis (RO) plants are not deployed all over the world (Fig. 1b), and RO cannot manufacture any H₂. Large-scale seawater-to-H₂ electrolysis conversion, either directly or indirectly, will be a significant technical advance for our society as well as a nice opportunity for meeting H₂-based energy needs of coastal areas. Secondly, DSS will be more difficult if ISS shows low practicality/profitability. A fundamental issue is that water from RO treatments (OR technologies have been developed for many years and are quite mature) is still insufficiently filtered to support long-lasting functioning of current electrolyzers [19]. For industrial long-time electrolysis, concentrations of impurities in the seawater flowing through the electrolytic cell also gradually increases due to the consumption of H₂O, highlighting the value of developing electrodes/membranes tolerant to impurities in treated seawater that has not been thoroughly deionized/filtered and natural seawater. Our review tries to summarize such electrodes. In fact, the idea of ISS (purifying seawater prior to electrolysis) is never a bad one; rather, we need to leverage the best of both DSS and ISS. Take emerging electrolytic reactors as instances, a water vapor pressure difference-dependent natural SES developed by Xie et al. [28] (November 2022) and a multi-functional electrolyzer developed by Kim et al. [29] (February 2023), contain *in situ* seawater deionization/desalination compartment. Such devices also produce H₂ at good rates. Clearly, it is so vital to design genuine electrodes that are still active and stable in the presence of impurity ions (*e.g.*, Lewis acid-modified CoO_x [27]) and to explore unconventional SESs [28].

Despite the appearance of good catalysts, a few are electrolyzed in untreated natural seawater. Since 2021, nonetheless, the field has seen increasing inventive seawater-to-H₂ synthesis ideas via the adaptable use of membranes, ingeniously designed catalysts, electrolyte combos, and so forth. Effective strategies are becoming clearer, but there are still some trial-and-error catalyst designs. In this review (Fig. 2), we collect DSS/ISS system designs and innovative strategies, from both the lab-scale and pilot-scale work. A large number of representative work is taken from 2022 onwards to present the latest findings, new research trends and bottleneck issues (opportunities). Suggested research protocols regarding catalyst design are presented to encourage the sound development of the field, covering seawater treatments, product detection, electrolytic reactors and electrolyte feeding modes, and catalyst performance indicators. Moreover, the status of seawater reduction/oxidation (SR/SO) electrocatalysis is summarized in detail to reflect activity, selectivity, and stability of electrode (catalytic materials). We describe the seawater electrolytes used to evaluate the various catalysts in good detail to reflect their activity more fully. Strategies including local reaction micro-environment engineering, sandwich-like oxygen evolution reaction (OER) electrode construction, chloride-repelling layer/sites (*in situ* anion release), intrinsic (chlorine evolution reaction) CER-inhibition structure design, structural buffering and self-healing, *etc.*, can also be found in this review. We carefully selected SR (*i.e.*, HER) research work in recent years: almost all

of the chosen SR catalysts were tested in natural seawater, and sources of the seawater are given. In addition, some important but scattered directions are summarized, such as asymmetric seawater electrolysis, gas bubble detachment and release kinetics in water (including seawater), and possible bionic designs. In addition, the article summarizes some important but fragmented directions, such as asymmetric electrolysis, gas diffusion, and bionic design as an integrated picture of making H₂ from seawater. Finally, we offer exclusive perspectives that may guide future research in the field.

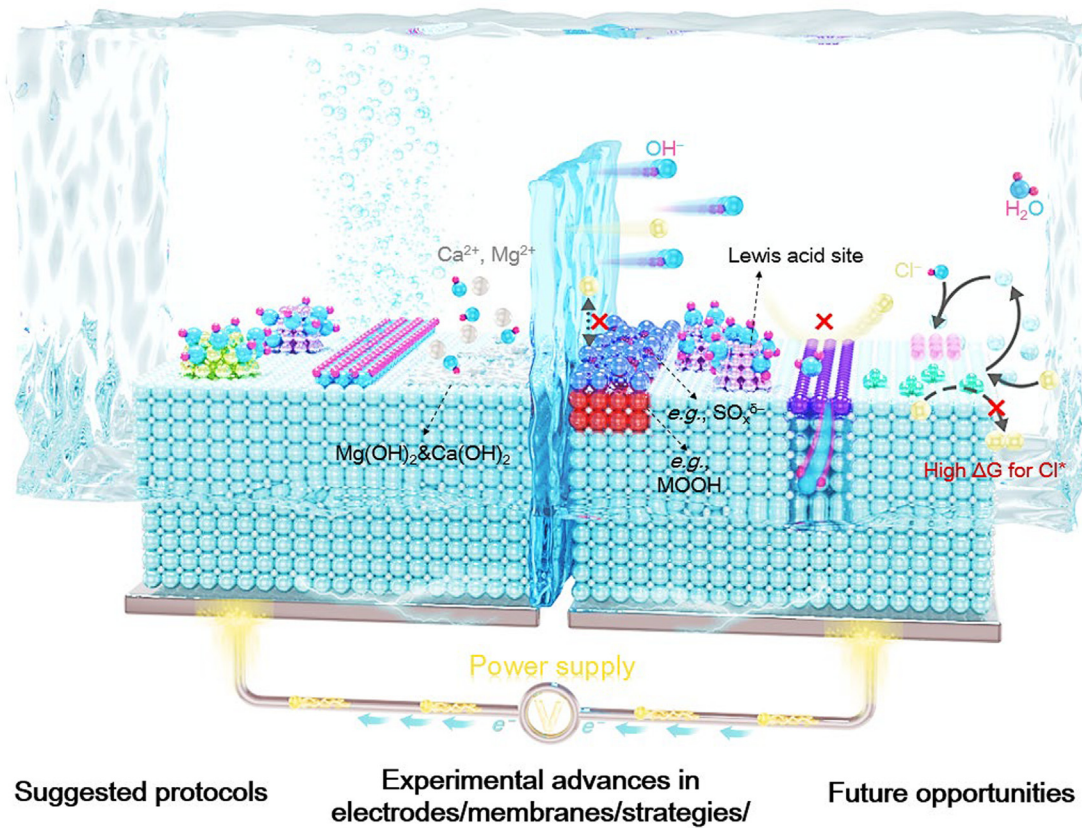
Present status and challenges in seawater splitting research

Latest experimental progress and best practices

To encourage and support a meaningful and practical breakthrough in this research field, we review and critically evaluate experimental details from representative recent studies, including (i) seawater treatment, (ii) product detection (especially for anodic products), (iii) electrolytic reactor and electrolyte feeding modes, and (vi) indicators that accurately reflect the catalyst performance and efficiency of electrolytic device. Relevant useful references are cited. Ultimately, we offer a flowchart of suggested procedures for conducting high-quality seawater splitting research.

Seawater treatment

Seawater is currently collected for research purposes in this field from a variety of sites, including Huanghai Sea in China (autumn) [27], Shenzhen Bay in China [28], San Francisco Bay in USA [30], Galveston Bay, Texas, USA (29.364 °N, 94.810 °W) [24], Barnet Marine Beach, Vancouver, Canada [31], *etc.*, and pre-treatment processes of the seawater varies. Guo et al. [27] filtered out solid impurities and removed microbes in natural seawater (pH = 7.9) prior to electrolysis. Wang et al. [31] performed OER in pH-neutral seawater: seawater + 1.0 M phosphate buffer solution. Alkalized seawater (*e.g.*, seawater + 1.0 M KOH) is one of the most common seawater electrolyte, and we must point out that evaluating OER catalysts in highly alkalized seawater is almost free of interference from *in situ* formation of precipitation of Ca²⁺/Mg²⁺. A pre-treatment may already remove most of Ca²⁺/Mg²⁺, and some researchers used less expensive Na₂CO₃ (compared to KOH) to save the cost of this pre-precipitation step (0.68 g Na₂CO₃ + 100 mL natural seawater [32]). The resulting supernatant is further used to make KOH-containing alkalized seawater. In fact, OER catalysts usually perform better in such alkalized seawater than in untreated seawater owing to (1) free of Ca²⁺/Mg²⁺ precipitation issues and (2) the presence of ample OH⁻. The catalyst performance for DSS, however, cannot be obtained in alkalized seawater. Catalysts with sufficiently high activities and durability for direct SO (or SR) are absolutely scarcer and apparently desirable. Acidified seawater is less used in current research for three reasons: (1) in acids, anodes favor the activation of adsorbed Cl⁻ rather than H₂O and thus more easily achieve high Cl₂ selectivity, but active chlorine must damage anodes; (2) acid leads to metal leaching; and (3) the demand for chlorine products like Cl₂ and NaClO may not be as high as the demand for H₂ in the future. Despite these, there are some

**FIG. 2**

Overview of recent seawater electrolysis findings discussed in this review. This figure shows some of the representative reported strategies.

possible benefits of acidic seawater, like faster HER kinetics and minimal precipitate production. It is arduous to find acidic seawater catalysts that can afford high activity while being resistant to oxidation, acid etching, and chlorine corrosion. However, we should note that there are already stable electrodes that can operate for eight to ten years [33]. We offer an open-ended cost comparison of various seawater treatment techniques (Table 1). To determine which pre-treatment method offers the best chance of achieving lower-cost H₂ generation from seawater, further pertinent studies are required.

Seawater electrolytes utilized have a significant impact on the activity, selectivity, and stability of the catalyst. Obviously, the seawater can be untreated natural seawater, natural seawater that filters out solids and microbes, natural seawater with salts/acid, or seawater with alkali (with pre-filtration process), simulated seawater, as well as other types. A lot of reported work did not provide the source of the seawater used, let alone the composition of seawater (concentrations of ions including Cl⁻, Br⁻, Na⁺, Mg²⁺, Ca²⁺, K⁺, Sr²⁺, SO₄²⁻, etc.) as well as the collection details, such as depth, season, longitude and latitude. In fact, electrode designs for DSS, which should receive great attention in future research, strongly relies on specifying the composition of the collected seawater and determining changes in the concentration of major ions in seawater electrolyte with electrolysis time. Solid impurities, organic matter, salt type, salinity, microorganisms, etc., of seawater in different regions vary greatly, which

would be reflected in catalyst performances. As seawater adopted in literature are not consistent, the performance can only be compared in similar electrolyte configurations. Performance measurements in simulated seawater with an identical standard would thus be a nice option, which would allow us to compare the performance of different catalysts more directly and effectively, but this simulated seawater cannot consist of chloride alone, or chloride plus alkali. We suggest to use simulated seawater with compositions similar to the compositions of real seawater reported in the recent literature [28], where certain amounts of Cl⁻, Na⁺, SO₄²⁻, Mg²⁺, Ca²⁺, K⁺, Br⁻, and HCO₃⁻ should be included. Some representative work adopted standardized artificial seawater electrolytes (e.g., Standard Practice for Preparation of Substitute Ocean Water [34] and Absolute Ocean standard [35]) with well-defined salinity and ion fractions. As for natural seawater, the compositions of seawater in Xie's work were Cl⁻ (9819 mg/L), Na⁺ (5745 mg/L), SO₄²⁻ (1566 mg/L), Mg²⁺ (699 mg/L), Ca²⁺ (223 mg/L), K⁺ (272 mg/L), Br⁻ (23 mg/L), Sr²⁺ (3.6 mg/L), F⁻ (1.7 mg/L), organic matter (12.3 mg/L), and microbe (6 CFU mL⁻¹), and the raw seawater was collected from Shenzhen Bay seawater, China [28]. The compositions of seawater in Zhang's work were Cl⁻ (14169.44 mg/L), Na⁺ (9733.84 mg/L), SO₄²⁻ (1927.52 mg/L), Mg²⁺ (1281.50 mg/L), K⁺ (432.52 mg/L), Ca²⁺ (393.46 mg/L), and HCO₃⁻ (54.71 mg/L), and Br⁻ (20.65 mg/L), and the raw seawater was collected from Marine Park Beach, Qingdao, China [36]. The compositions of seawater

TABLE 1

A simple comparison of the representative reported seawater pretreatment methods for electrolysis.

Treatments prior to electrolysis	Additional requirements	Seawater treatment cost	Ref.
Filtering out solid impurities & removing microbes in natural seawater	A catalyst capable of producing local OH ⁻ itself	Filtering costs	[27]
Without pre-treatment process	1. SDE solutions (<i>i.e.</i> 30 wt% KOH) 2 Porous polytetrafluoroethylene (PTFE) membrane	~0 (but with extra costs for PTFE membrane and 30 wt% KOH)	[28]
Adding phosphates, pH-neutral seawater	Adding extra 1.0 M phosphate buffer solution, filtering out some Mg/Ca precipitates	Phosphate costs, filtering costs	[31]
Adding Na ₂ CO ₃ and KOH (or just Na ₂ CO ₃), alkalinized seawater	Step 1: 0.68 g Na ₂ CO ₃ + 100 mL natural seawater, step 2: filtering out some Mg/Ca precipitates, step 3: adding 1.0 M KOH, step 4: filtering out some Mg/Ca precipitates	Na ₂ CO ₃ costs, KOH costs, filtering costs Notes: KOH costs more, but the alkaline condition it creates will achieve a lower overpotential, which will cut down electricity need.	[32]

in Liu's work were Cl⁻ (17683 ppm), SO₄²⁻ (2444 ppm), Na⁺ (9241 ppm), Mg²⁺ (1107 ppm), and Ca²⁺ (361 ppm), and the raw seawater was collected from Huizhou, Guangdong province, China [37]. A direct side-by-side comparison of catalysts developed by different research groups is made possible by using identical simulated seawater with the same composition. For one specific catalyst, performance differences found between simulated and local natural seawater reflect disparities between the simulated seawater and real seawater from a particular area. Such performance differences can be compared side-by-side again to illustrate effects of real seawater with different sources on catalyst performance. In short, electrodes that can be placed directly into untreated seawater for prolonged ampere-level *J* electrolysis are absolutely desirable. We point out that it is so important to quantitatively monitor the compositions (*e.g.*, Cl⁻, Mg²⁺, Ca²⁺, organic matter, and microbe) and pH values of seawater during electrolysis. The comparison of changes in the content of different substances in the seawater before and after seawater treatment and the comparison of seawater composition changes gives an indication of how electrolysis affects seawater. Whether used seawater can be discharged directly in the future will depend on this. Moreover, the comprehensive comparison also reflects which substances are consumed mostly and which substances may not be involved in the reaction.

Product detection

Measuring amounts of O₂ (*i.e.*, O₂ yield) over time and corresponding FEs is essential towards revealing whether side-reactions (*e.g.*, Cl⁻ oxidation) are suppressed as well as the SO catalyst is really efficient. O₂ yields at various electrolysis conditions (different *J*, applied voltage, electrolytes, *etc.*) can be measured by water drainage method or gas chromatography. The drainage collection can record the volume of produced O₂ (or H₂) over time, and the consumed electric energy to produce a certain amount of gas can be calculated based on electric power W (W = UI_t) over time. As for GC measurements, the generated gaseous products are blown from the anodic chamber to the GC with N₂ (or Ar) at a fixed flow rate. On the other hand, ample Cl⁻ in seawater makes the chlorine (electro)-chemistry almost unavoidable even if a significant amount of OH⁻ is added to the electrolyte. DSS with less OH⁻ is more conducive to Cl⁻ oxidation, which will lead to harsh electrolysis environments and consequent elec-

trode dissolution. Therefore, it is crucial to monitor the amount of active chlorine species. Direct use of active chlorine strips, commercial electronic/digital active chlorine sensor (or water quality analyzer), iodide titration [38–41], and colorimetric N, N-diethyl-p-phenylenediamine (DPD) assay [42] are common methods. Take the iodide titration as an example, active chlorine (hypochlorite + chlorine) can make the electrolyte turns yellow (even yellowish brown and dark red) after iodide titration, and possible key reactions includes: (1) NaOCl + 3KI + 2HCl → NaI₃ + H₂O + KCl, (2) OCl⁻ + 2I⁻ + 2H₂O → Cl⁻ + I₂ + 2OH⁻, (3) Cl₂ + 2NaI ↔ I₂ + 2NaCl. The solution is then reacted with Na₂S₂O₃ solution drops until it is faint yellow (I₂ + 2S₂O₃²⁻ → 2I⁻ + S₄O₆²⁻, NaI₃ + 2Na₂S₂O₃ → 3NaI + Na₂S₄O₆). Furthermore, adding a small amount of starch indicator to make the electrolyte becomes dark blue (*e.g.*, I₃⁻ + starch → [I₃][starch]), and finally adding Na₂S₂O₃ solution to complete the titration ([I₃][starch] + 2S₂O₃²⁻ + 3I⁻ + S₄O₆²⁻ + starch). Notably, since HClO is unstable and decomposes when exposed to light (2HClO + hν → Cl₂ + H₂O + O₂), strong light should be avoided during the electrocatalytic test to more accurately estimate the active chlorine yield. Additionally, the reaction selectivity towards OER and CER on catalyst surfaces, even in electrolytes with various pH values [43–45], can also be directly determined using a rotating ring disk electrode (RRDE) method, since the disk electrode and ring electrode can set two potentials separately at the same time (Fig. 3a) [43]. The principle of RRDE determines that it performs best in acidic system, and impurity ions will interfere with the accurate detection. Using strips is a cheap and straightforward measuring method, but the color change is subjective to our eyes. Also, using strips means discontinuous reading. Other methods offer more accurate data and of course is relatively expensive. DPD assay is susceptible to interfering substances and is not suitable for water samples with turbidity or high Chroma. According to the research work by Yokoyama et al. [46] and the research work by Guo et al. [27], RRDE can also detect changes in the local pH of catalyst surface during natural seawater electrolysis (Fig. 3b).

Electrolytic reactor and electrolyte feeding modes

Apart from establishing accurate product detection before, during and after electrolysis as well as seawater treatments, the electrolytic reactor is practically pivotal. A single-chamber

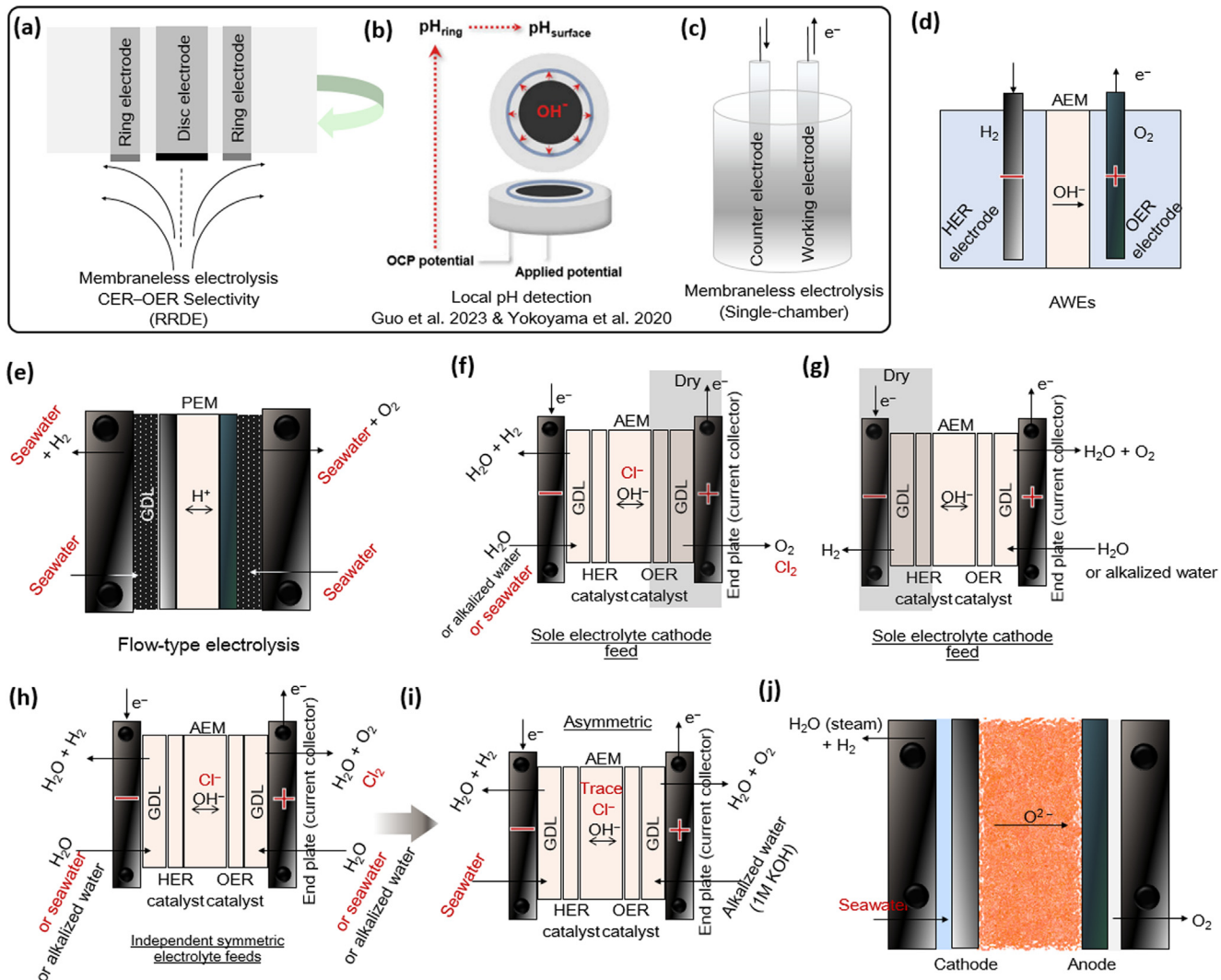


FIG. 3

Schematic drawing of water electrolysis devices and RRDE as a means of detection. Straightforward RRDE voltammetry towards facilely measuring (a) OER-CER competition, and (b) local pH change on catalyst in seawater. (c) Single-chamber electrolyzer. Brief illustrations of the basic working mechanisms of (d) AWEs and (e) PEM water electrolyzers. (f-i) A variety of AEM-based electrolytic cells in the case of different symmetric and asymmetric electrolytes feeding schemes. (j) High-temperature solid oxide electrolyzers.

electrolytic cell (Fig. 3c) (with a three-electrode system) was widely used in lab-scale experiments to screen catalysts, but there is a gap between such cell-based tests and practical production. Alkaline water electrolyzers (AWEs, Fig. 3d) and PEM water electrolyzers (Fig. 3e) are currently the most widely used electrolytic reactor technologies throughout the world. The AWE technology is well-developed and makes it simple to implement wide-scale applications, but there are still several issues with AWEs, including high energy consumption (*e.g.*, over 4 kWh/Nm³), relatively low J , sluggish startup times for temperature rise, enormous equipment sizes, *etc.* Alkaline electrolytes also react with CO₂ in the air to generate insoluble carbonates like K₂CO₃, which block/obstruct transfer of gases and reactants. Although PEM water electrolyzers can achieve smaller floor space and higher J , they also face a lot of pending issues including expensive equipment costs, high reliance on noble metals (anodes need to withstand acidic electrolytic environments), and complex preparation processes.

Additionally, there are a good deal of reactors that are still in the experimental/lab-scale stage but exhibit enormous potential, such as anion exchange membrane (AEM) and solid oxide electrolyzers, both of which utilize non-noble metal components. AEM electrolyzers have high J and long lifetimes, but they are still in the early stages of development and perform less effectively than PEM electrolyzers. Solid oxide electrolyzers (Fig. 3j) that convert water steam to H₂ demand additional heating and have issues with the unsatisfactory stability of the electrode material [47]. In fact, these existing devices are not designed for direct (even including indirect) seawater electrolysis. Unlike pure water, every impurity in seawater will constantly interfere with the proper functioning of the membrane and electrode materials, leading to membrane contamination/electrode decay and eventual electrolysis failure. Such incompatibility between natural seawater (and various seawater-based electrolytes) and pure water-based electrolytic reactors encourage researchers to redesign devices based on the characteristics of SR/SO. In a repre-

sentative study by Strasser's group (published on 20 May 2020) [48], asymmetric electrolyte feeds (*i.e.*, 0.5 M NaCl catholyte and 0.5 M KOH anolyte) achieved the best saltwater electrolysis activity, O₂ selectivity and stability among all different Cl⁻-containing electrolytes feed schemes. As shown in Fig. 3f-i, in the AEM-based electrolyzer with membrane electrode assemblies (MEAs), different electrolyte combos are used to attain maximized and stable *J* while improving the O₂ generation selectivity (*i.e.*, suppressing the unwanted Cl⁻ oxidation) and averting alkalization of saltwater. After this work, Chang et al. [49] (published in 2021) and Zhao et al. [50] (published in 2023) adopted similar asymmetric electrolysis strategies. By appropriately adjusting independent electrolyte feed configurations, it is possible to curb Cl⁻ oxidation while increasing electrolysis efficiency.

In a recent work by the groups of Han and Park, with the use of bipolar membranes (BPM) separating KOH solution at the anode chamber and H₂SO₄ solution at the cathode chamber, the electrolyte pH on both sides and cell voltage were maintained relatively stable over a 20-h operation, whereas the use of AEM, PEM, or cation exchange membrane (CEM) led to a decrease in anode electrolyte pH and consequent electrode damage and cell voltage increase [29]. Note that water can penetrate the BPM, and be further electro-dissociated into H⁺ and OH⁻ under at the bipolar junction of cation exchange layer-anion-exchange layer [51–53]. More operating features of BPM-based

electrolytic cells can be found in Table 2. Penetration of K⁺ and SO₄²⁻ through the membrane was suppressed when only BPM were used. Based on this feature, Kim et al. [29] realized *in situ* desalination of saltwater and co-production of HCl and NaOH using BPM, AEM and PEM simultaneously (Fig. 4a). During the electrolysis, the ionic conductivity of the salt solution decreased gradually and was accompanied by the rise in the Cl⁻ concentration of the acidic side and the rise in the Na⁺ concentration of the alkaline side. When this unitary device was developed into a stack device (Fig. 4a), the overall specific energy consumption (SEC) decreased further. In another work, depending on neutralization chemistry, a three-chamber electrolytic cell using CEM and AEM was assembled (Fig. 4b) to generate electricity and H₂ while desalting 4.0 M NaCl in the middle chamber [54]. The anode chamber contained alkaline solution with ample hydrazine and the cathode side contained pure acidic solution. Note that if the pH values are the same on both sides, just adding hydrazine to the anodic side will not generate electricity. A higher power density can be attained by concentrating more H⁺ at the cathode and OH⁻ at the anode, which supported successful conversion from low-grade heat (*i.e.*, waste heat sources [55]) in surroundings (*i.e.*, obtaining a positive entropic heat TΔS⁰) to electricity supply by this device. As shown in Fig. 4c, with this asymmetric neutralization cell design, H₂ production, desalination and power supply (*e.g.*, charging of a smartphone) are performed simultaneously. In addition, assuming hydrazine

TABLE 2

Reactor design comparison.

Reactor	Separator (ionic conduction)	Electrolyte	Main advantages	Main drawbacks
AWE (Commercialization stage)	A porous diaphragm (OH ⁻ migration)	Typically 20–30% KOH (or KOH + Seawater)	1. A mature technology 2 Low costs 3 Easy to achieve large-scale applications	1. High actual electricity consumption 2 Stable power supply needed (poor adaptability with renewable energy volatility) 3 Electrode-diaphragm gap causes an inherent high ohmic loss, limiting the current density
PEM-based electrolyzers (Commercialization stage)	A solid acid electrolyte polymer (Nafion)	Typically pure water	1. Small floor space 2. Strong adaptability to intermittent power supply 3. Easy integration with renewable energy 4. Production of compressed hydrogen	High equipment cost
AEM-based electrolyzers (Lab-stage)	A OH ⁻ transporting membrane	Typically 1 M KOH	1. High current density 2. Fast response, long life and low price 3. No need for precious catalysts 4. Production of compressed hydrogen	1. Still at the initial stage of development 2 Much lower performance than that of PEM-based electrolyzers
BPM-based electrolyzers (Lab-stage)	Water dissociation in a BPM drives H ⁺ and OH ⁻ toward the cathode and anode, respectively,	Typically an extreme pH gradient	1. Without restriction of operation to acidic (cation exchange membranes) or basic (AEM) conditions (<i>i.e.</i> flexibility in the choice of pH) 2 Less pH gradient, and thus better stability than mono-polar membranes	1. Under neutral pH or mild pH gradients co-ion leakage may become problematic, resulting in pH changes and thus energy loss in the device 2 High cost and short service life 3 High overpotentials driving water dissociation
High-temperature electrolyzers (Lab-stage)	A proton conducting ceramic membrane/A solid oxide membrane	Water	High-temperature electrolyzers have low energy consumption and use noble metal catalysts	1. Electrode stability is problematic 2 Requiring extra heating

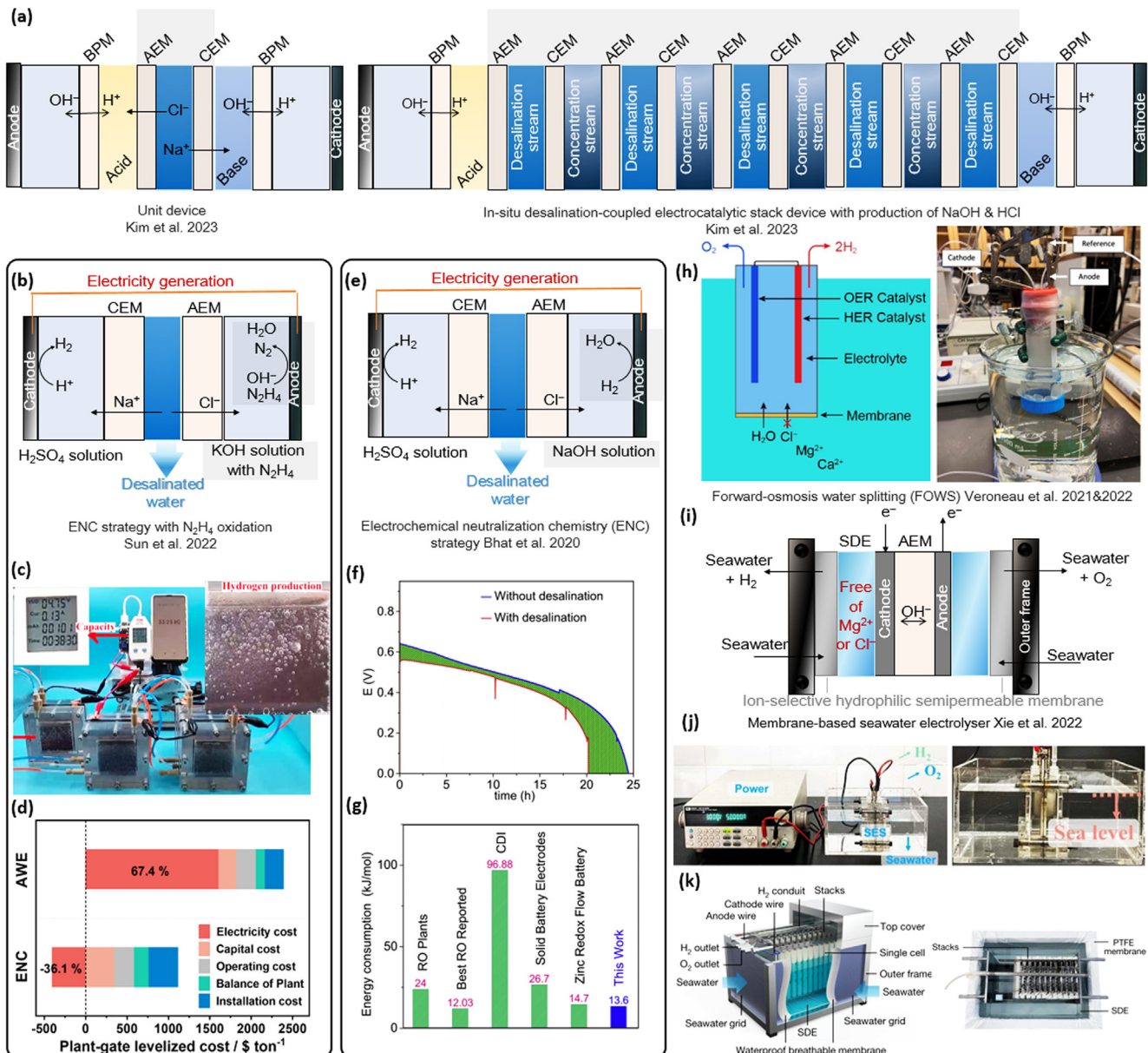


FIG. 4

Unconventional ways of generating H_2 from seawater. (a) Multifunctional seawater electrolysis unit device (left) based on BPM as the key component and corresponding stack device (right). (b) An electrochemical device that produces H_2 from saltwater and generates electricity. (c) Operation process: producing H_2 and charging mobile phone at the same time. (d) A rough cost comparison. Reproduced with permission from Ref. [54] Copyright 2022, John Wiley & Sons, Inc. (e) Schematic diagram of the electrochemical neutralization cell. (f) Discharge curves. (g) Comparison of energy consumption of different desalination technologies. Reproduced with permission from Ref. [56] Copyright 2020, Elsevier B.V. (h) In situ extraction of water for electrolysis from saltwater using concentration gradient. Reproduced with permission from Ref. [57] Copyright 2022, American Chemical Society. (i) H_2 production from natural seawater by combining physical phase equilibrium and electrocatalysis. (j) Lab-scale and (k) demo-type seawater electrolysis device. Reproduced with permission from Ref. [28] Copyright 2022, Springer Nature.

sewage, acidic and alkaline wastes can be used as feeding materials, and the cost demonstrated some competitive edge (Fig. 4d). Meanwhile, note that the power generation mechanism of this neutralization reactor is not quite the same as those of fuel cells consuming N_2H_4 and O_2 (or N_2H_4 and H_2O_2) through redox reactions. Moreover, Cl^- crossover into the anodic chamber, but no Cl^- oxidation products can be detected since the alkalinized electrolyte includes 1.0 M hydrazine. Just unplugging the external circuit can spontaneously produce only H_2 without discharging. In fact, back in 2020, Thotiyil's group [56] already demonstrated

the neutralization reactions-based on-site desalination process using acid and alkali as fuels, and the thermodynamic efficiency ($\Delta G^0/\Delta H^0$) of the former electrochemical neutralization cell (Fig. 4e) with a positive ΔS^0 was higher than that of the $\text{H}_2\text{-O}_2$ fuel cell with a negative ΔS^0 . Moreover, the device actually consumes less energy to desalinate saltwater than some commonly used desalination techniques (Fig. 4f and 4 g). Making H_2 from impure saltwater was made possible by Nocera's group when they incorporated an ion-selective membrane to a simple electrolytic reactor (Fig. 4h) [42,57]. The membrane selectively kept undesired

ions out of the electrolysis chamber that split water, and water molecules can move freely from outer saltwater into inner electrolyte due to ion concentration differences. Separate desalination and purifying procedures were thus avoided in Nocera's work. Xie et al. [28] developed membranes for *in situ* desalination and purification of natural seawater from Shenzhen Bay, and they achieved near-complete isolation of impure ions in seawater. As shown in Fig. 4i, a polytetrafluoroethylene (PTFE)-based waterproof membrane that only pass through water vapor are placed between natural seawater and KOH self-dampening electrolyte (SDE) solution. The pressure difference for the SDE-seawater combo makes gaseous H₂O to be continually extracted from seawater and to further migrate into the water-splitting compartment filled with SDE, thereby eliminating the need to design a catalyst that can repel unwanted ions like Cl⁻. Except for a lab-scale reactor (Fig. 4j), a scaled-up reactor (Fig. 4k), was developed to operate at the J of 250 mA cm⁻² for over 133 days without obvious membrane failure (*i.e.*, wetting and fouling), and impurities ions such as Mg²⁺, SO₄²⁻ and Cl⁻ were still excluded from the electrolysis compartment. In fact, membranes—in addition to the most important electrodes—are vital to split seawater stably and efficiently. Therefore, we focus here again on discussing and recommending two representative studies of seawater electrolysis with better membrane selections or improved membrane designs.

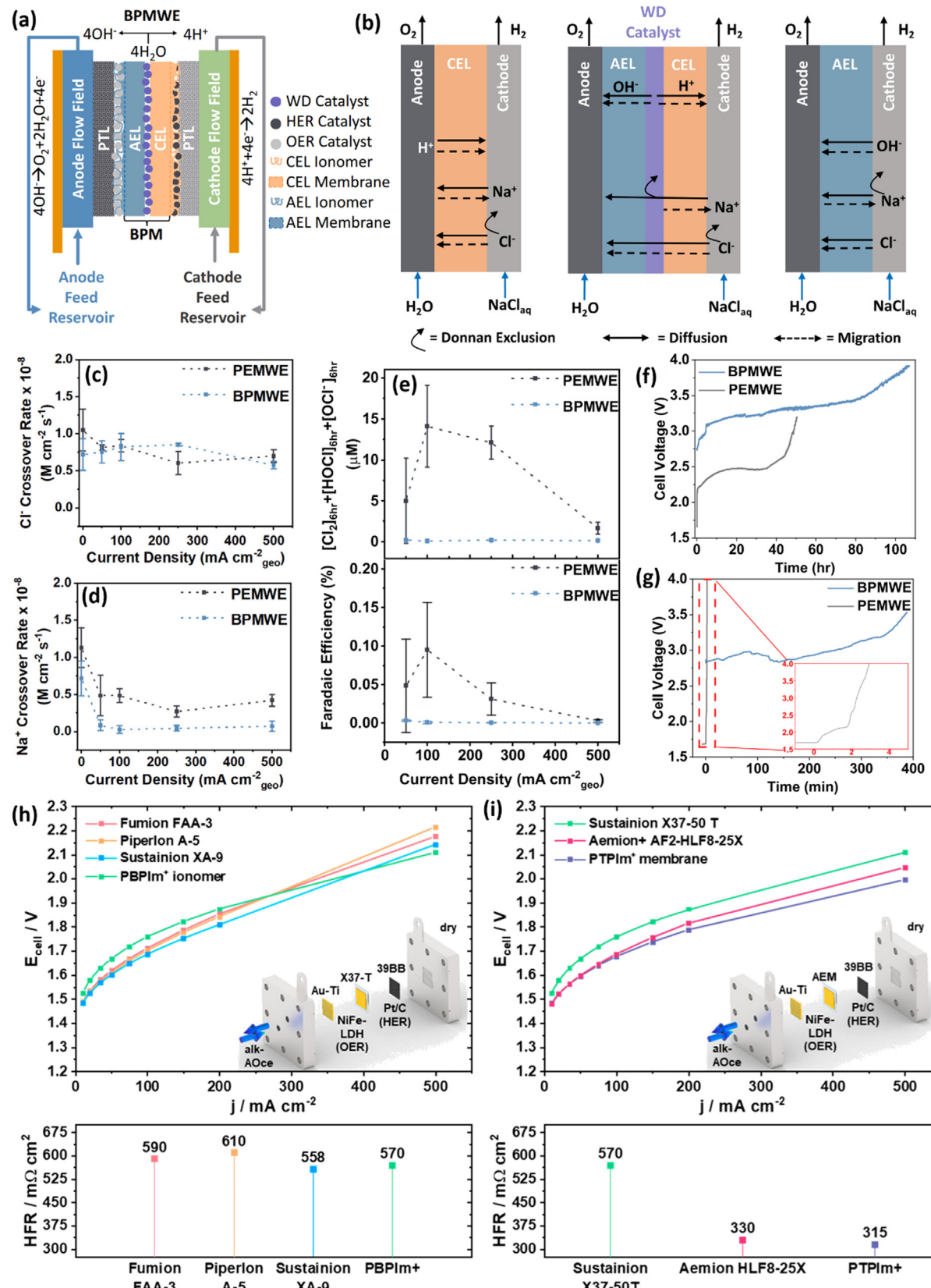
With almost identical configurations (*i.e.*, the same type of electrolyte feeds, circulation scheme, flow-fields, *etc.*), comparing the performance of electrolytic cells based on different ion-exchange membranes can find the most suitable membrane for seawater electrolysis. An electrolyzer based on BPM (Fig. 5a) was able to operate with natural seawater (Half Moon Bay, CA, USA) during sustained electrolysis to generate H₂ and O₂ at the J of 250 mA cm⁻², much better than that of the PEM cell [58]. Due to the extra energy needed for H₂O dissociation at cation exchange layer/anion exchange layer junction of BPM, the voltage demanded to attain a same J of 250 mA cm⁻² for the BPM-based electrolyzer (DI water as electrolytes) was 60 mV more than that for PEM-based cell (DI water as electrolytes). By comparing performances and ion transfers (Fig. 5c and 5d) of different electrolytic cells with NaCl catholyte and DI water anolyte, ion balance (Fig. 5b) can be speculated. Although the active chlorine FEs of the BPM-based and PEM-based electrolytic cells after electrolysis at different J were comparable (Fig. 5e), active chlorine in the anolyte (DI water) produced by the BPM-based electrolyzer were significantly less. This is in line with the lower Cl⁻ ion flux ($J_{avg}^{Cl^-}$) of the BPM-based electrolytic cell than that of the PEM-based one. Owing to the well-known Donnan exclusion effect at the cathode/cation exchange layer interface (Fig. 5b), both the BPM and PEM can inhibit Cl⁻ transport. Moreover, under galvanostatic 250 mA cm⁻² conditions with asymmetric unprocessed real seawater as the catholyte feed (Half Moon Bay, CA, USA), BPM-based and PEM-based cells showed voltage degradation over reaction time (Fig. 5f). Since the active chlorine FE after durability tests was lower than 0.01% for the BPM-based cell, instead of corrosive chorine spaces, growing pH gradients across the device may be the likely culprit for the voltage loss. Under galvanostatic 250 mA cm⁻² conditions with asymmetric real seawater as the catholyte feed (Half Moon Bay, CA, USA), both the

BPM-based and PEM-based cells showed voltage degradation over reaction time (Fig. 5f). As shown in Fig. 5g, under symmetric seawater feeds conditions, the voltage of the PEM-based electrolytic cell rapidly climbs until operation stops. This occurred primarily by substantial amounts of active chlorine produced in the acidic anode-cation exchange layer environment. In contrast, bipolar membranes are apparently able to provide the electrolyzer for longer periods of reaction time, possibly due to weaker Cl⁻ oxidation. In addition, Mg(OH)₂ can be found after electrolysis for both two electrolyzers. Strasser's group [35] proposed that the properties of OH⁻-conducting ionomer, such as ion exchange capacity (IEC), have a direct impact on mass transfer limitations and how well the saltwater-feeding electrolyzer operate electrochemically. A biphenyl-based ionomer (PBPIm⁺) with 2.17 ± 0.24 mmol g⁻¹ IEC value afforded lower E_{cell} at the same J when compared to other ionomer with lower IEC values (Fig. 5h), but similar high-frequency resistance (HFR) values were attained. In addition, a custom-made membrane (PTPIm⁺) with the lowest HFR (Fig. 5i) enabled smaller V_{cell} to achieve the same J for AEM-based saltwater electrolysis, outperforming commercial ones like X37-50 T. A PTPIm⁺-based MEA electrocatalytic device, using NiFe-LDH/Ni@Ni_xS_y for OER and CoP/C/Ni@Ni_xP_y for OER, respectively, achieved high O₂ FE during long-term and large- J electrolysis of 1.0 M KOH seawater with an average salinity of 3.5%.

From the latest advances in electrochemical reactor/system design and assembly, it is evident that unconventional ways of electrolyzing seawater as well as more efficient and robust systems designs deserve further development and optimization. In Table 2, we provided characteristics, benefits, and drawbacks of the various electrolytic reactors in order to compare the reactors more straightforwardly. In fact, to stimulate the sound development of the field of H₂ electrosynthesis from seawater, not only the simulated seawater with an identical standard is required (note that this does not mean that different seawater electrolytes cannot be used, and catalytic performances obtained in the same simulated seawater facilitates the direct comparison of different electrodes), but also a roughly uniform electrolysis measurement set-up. Even if two different groups have used PEM electrolytic cells for testing, the specific model of their PEM and the internal accessories are still different. And such differences can be even more evident in some of the work on innovations in seawater electrolysis reactor. Except for simple electrolytic cells like single-compartment (undivided) cell and H-cell for comparing the intrinsic activity of catalytic materials, all electrolytic devices should emphasize the electrode assembly and electrolyte supply modes and performance indicators including electrolyzer lifetime, electrolyzer cost, and electrolyzer efficiency, expected power consumption efficiency, *etc.* Therefore, testing in a conventional and common single-chamber electrolytic cell is still necessary towards scrutinizing catalyst performance, even though the microenvironment on the electrode surface varies greatly from one electrolytic reaction device to another.

Suggestions, initiative, and protocols

Based on the above discussion, we give an easily understandable flowchart of suggested procedures for the research of developing

**FIG. 5**

Latest and representative findings on membrane improvements towards more efficient and robust seawater electrolysis. (a) Cross-sectional BPMWE device. (b) Ion-transport dynamics in membrane electrolyzers. Crossover rates of (c) Cl⁻ and (d) Na⁺. (e) Product selectivity. (f) Device stability using seawater as the catholyte (anolyte: DI water). (g) Device stability using seawater as both catholyte and anolyte. Reproduced with permission from Ref. [58] Copyright 2023, Elsevier. (h) Effects of ionomer on electrolysis of seawater, with HFR values. (i) Effects of AEM on electrolysis of seawater, with HFR values. Reproduced with permission from Ref. [35] Copyright 2023, the authors of Ref. [35] Published by American Chemical Society.

catalysts for seawater electrolysis (Fig. 6). Seawater can be used as electrolyte after different pre-treatment steps (e.g., filtration) or directly as electrolyte. At this stage, the community still has not come to a consensus on the best pre-treatments of seawater. Whether or whether seawater should be alkalized is unknown based on the existing studies. Obviously, adding Na_2CO_3 and KOH/NaOH to seawater when alkalinizing natural seawater would increase the cost, but it also offers various benefits. Firstly, Cl^- oxidation can be inhibited and thus electrode lifetime is prolonged. Secondly, the power consumption is directly related to the electrolysis voltage, and the alkaline environment created by OH^- favored smaller potentials (for both H_2 and O_2 produc-

tion) than those of the direct natural seawater splitting. Thirdly, in comparison to commercial 30% KOH electrolytes for AWE, the majority of catalysts reported to accomplish long electrolysis periods (e.g., 500 h at 500 mA cm⁻², see Table 3) in alkaline seawater employ 1 M KOH + seawater, which uses substantially less KOH. Lastly, since OH⁻ continually forms at the cathode during electrolysis, it is not necessary to continuously add 1 M KOH + saltwater to the electrolysis system. Weakly alkaline seawater (e.g., 0.1 M KOH + seawater) or even seawater devoid of KOH can be fed into the electrolyzer for further seawater splitting when some water in the electrolysis system is consumed owing to gas generation. Thus, for the future seawater electrolysis sys-

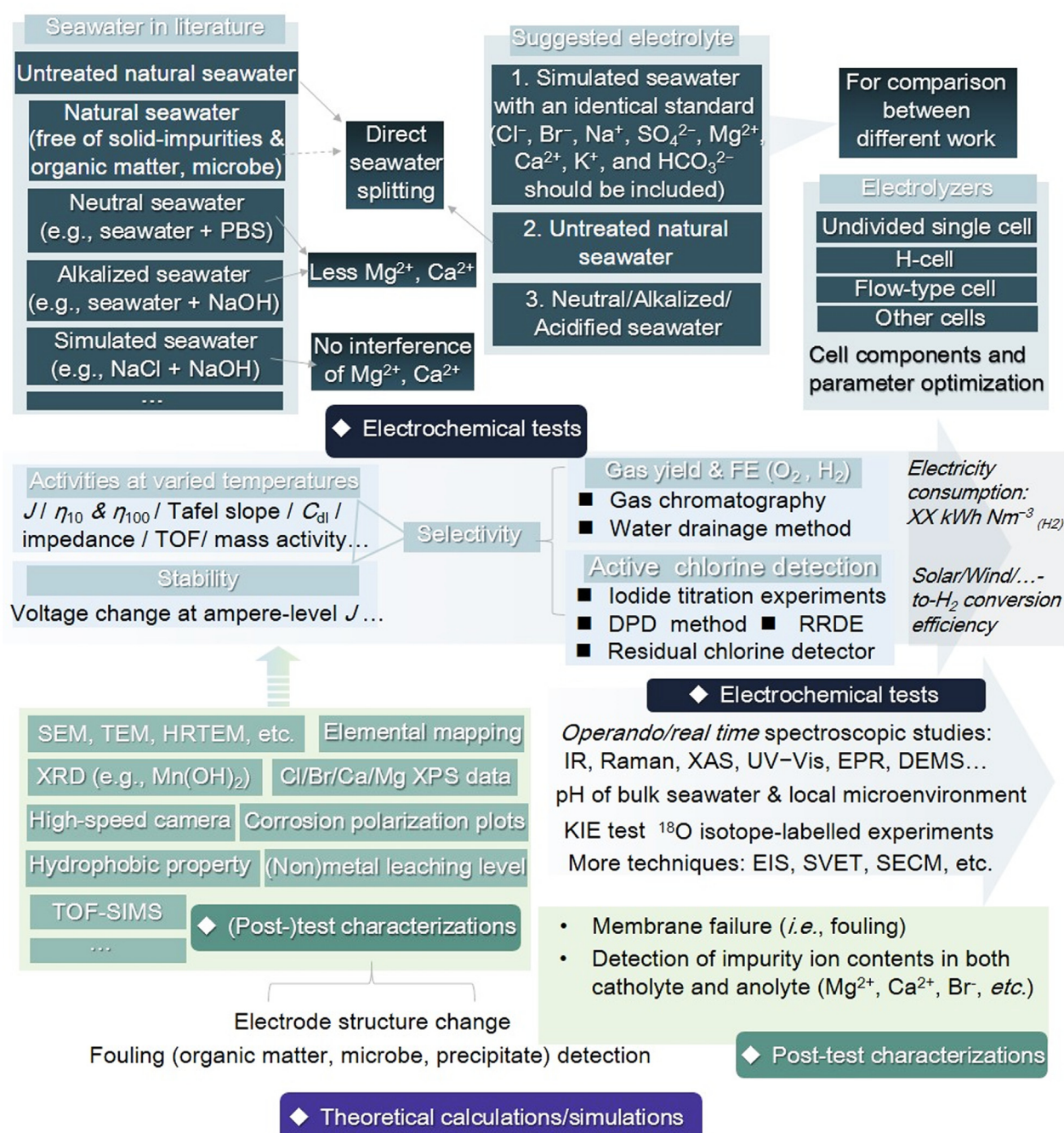


FIG. 6

A sketchy flowchart of suggested procedures including common experiments for conducting high-quality/reliable seawater splitting research.

TABLE 3

Representative seawater/brine water oxidation electrodes, electrolyzers, sources of seawater and seawater treatment before electrolysis, etc.

Catalytic materials	Substrate (Support)	Surface wettability	Electrolyzer (membrane)	Electrolyte	Seawater treatment	Stability	Ref.
NiMoN@NiFeN [24]	NF	N/A	N/A	1 M KOH + Seawater (Galveston Bay near Houston, Texas, U.S.A.)	ISS (alkaline seawater)	100 h@500 mA cm ⁻²	Nat. Commun. 10 (2019) 5106
Cr ₂ O ₃ -CoO _x nanorods [27]	CFP protected with Au (for batch-type electrolyser), or TFF (for flow-type electrolyser)	N/A	PEM-based flow type cell (Nafion 115)	Seawater (Huanghai Sea in China)	ISS (solids and microorganisms are filtered)	100 h@500 mA cm ⁻² (flow-type electrolyser)	Nat. energy 8 (2023) 264–272
Mo-Doped, Ni ₃ S ₂ [28]	NF	N/A	AEM-based homemade electrolyzer	Shenzhen Bay seawater	ISS (similar to <i>on-site</i> osmosis/filtration + conventional water electrolysis)	3200 h@250 mA cm ⁻² (in freshwater)	Nature 612 (2022) 673–678
NiFe/NiS _x [30]	NF (420 g cm ⁻²)	N/A	Single chamber cell (without membrane)	1 M KOH + Seawater (San Francisco Bay)	ISS (alkaline seawater)	1000 h@400 mA cm ⁻² (1 M KOH + Seawater) & 500 h@1000 mA cm ⁻² (1 M KOH + 0.5 M NaCl)	Proc. Natl. Acad. Sci. U. S. A. 116 (2019) 116624–6629
Fe ₃ P-NiSe ₂ [49]	Carbon paper	N/A	AEM-based electrolyzer (Fumasep FAB-PK-130)	Seawater (Florida local coast with a pH of ~ 8.7)	ISS (solids are filtered)	200 h@800 mA cm ⁻² (O ₂ FE: 92%)	Adv. Mater. 33, (2021) 2,101,425
Co _{3-x} Pd _x O ₄ [31]	NF/MnO ₂	N/A	AEM-based flow type cell	Natural seawater + 1 M phosphate buffered saline (PBS)	ISS	450 h@200 mA cm ⁻² & 20 h@1000 mA cm ⁻²	Adv. Mater. 35 (16) (2023) 2,210,057
Nilr-LDH [73]	Sulfuric NF	N/A	A three-compartment electrochemical glass cell	1 M KOH + seawater (Longfengtou Beach of Haitan Bay in Fujian Province of China, 119°48' E, 25°30' N)	ISS (alkaline seawater)	650 h@500 mA cm ⁻²	J. Am. Chem. Soc. 144 (2022) 9254–9263
MnO _x film-coated NiFe-LDH [95]	NF	N/A	A gas-tight H-cell	1 M KOH + Seawater (Shilaoren Beach in Qingdao, China, filtered with a membrane with a pore size of 0.2 μm)	ISS (alkaline seawater)	~40 h@50 mA cm ⁻² (Obvious attenuation)	Inorg. Chem. 61 (2022) 15256–15265
Ni-doped FeOOH [205]	NF	Superhydrophilic	AEM-based electrolyzer (X37-50 Grade T, Dioxide Materials)	1 M KOH + Seawater (Changwon, Republic of Korea)	ISS (alkaline seawater)	80 h@100 mA cm ⁻² (O ₂ FE: 92%)	J. Mater. Chem. A 9 (2021) 9586–9592
S-(Ni,Fe)OOH [179]	NF	Hydrophilic (~130° for hydrophobic NF)	N/A	1 M KOH + Seawater (Galveston Bay near Houston, Texas, USA)	ISS (alkaline seawater)	100 h@500 mA cm ⁻²	Energy Environ. Sci. 13 (2020) 3439–3446

(continued on next page)

TABLE 3 (CONTINUED)

Catalytic materials	Substrate (Support)	Surface wettability	Electrolyzer (membrane)	Electrolyte	Seawater treatment	Stability	Ref.
Fe _{0.01} &Mo-NiO [206]	NF, thickness: 1.6 mm, porosity: ~95%	N/A	N/A	6 M KOH + Seawater (Galveston Bay, Galveston, Texas, USA).	ISS (alkaline seawater)	80 h@~420 mA cm ⁻²	Energy Environ. Sci., 15, (2022) 3945–3957
NiFe-CuCo LDH [170]	NF	N/A	A gas-tight H-cell	6 M KOH + Seawater	ISS (alkaline seawater)	500 h@500 mA cm ⁻²	Proc. Natl. Acad. Sci. U. S. A. 119 (2022) e2202382119
CoFeS _x [198]	Single side catalyst coated membrane (for MEA), carbon paper	N/A	MEA-based flow-electrolyzer (Sustainion X37-50 Grade T), a three-electrode cell	Electrolyte 1: 0.1 M KOH + 0.6 M NaCl, electrolyte 2: 0.6 M NaCl + 0.03 M SO ₄ ²⁻ + 0.06 M Mg ²⁺ + 0.01 M Ca ²⁺	ISS (simulated seawater)	100 h@100 mA cm ⁻² in electrolyte 1 at 75 °C (for MEA), 700 h@100 mA cm ⁻² in electrolyte 1 (carbon paper) & 20 h@100 mA cm ⁻² in electrolyte 2 (carbon paper)	Adv. Sci. 9 (2022) 2,202,387
NiMoSx@NiFe-LDH [148]	NF	N/A	Single-chamber cell	1 M KOH + Seawater	ISS (alkaline seawater)	500 h@500 mA cm ⁻²	Inorg. Chem. Front. 10 (9) (2023) 2766–2775
BZ-NiFe-LDH [196]	Carbon cloth	N/A	Single-chamber cell	1 M KOH + Seawater	ISS (alkaline seawater)	500 h@100 mA cm ⁻²	Nano Res. Energy 1 (2022) e9120028.

Notes: CFP: carbon fibre paper. TFF: Ti fibre felts. ISS here: pre-filtration/chemical pre-precipitation/on-site seawater filtration + treated (sea)water electrolysis. Typical SO catalysts (can be seen in Table 3) invariably contain Fe-based elements, which on the one hand indicates the importance of these active elements, and on the other hand emphasizes the scarcity of exploring other metallic elements for SO. J of seawater electrolysis are generally large, and microenvironments of the electrode (including the formation/release of bubbles) is closely related to the electrolytic activity and lifetime. In future research, the hydrophobicity of the electrode should be provided as a basic information. Meanwhile, the majority of the substrates loaded with catalysts are NF, which is not strong enough mechanically to meet the demands of electrolysis in natural seawater, indicating the need for specially designed substrates with greater electrical conductivity, better loading capacity, stronger catalyst adhesion, etc.

tems, as long as the cell voltage is low enough (*e.g.*, 1.0 A cm^{-2} at 1.5 V) and/or the electrolysis time is long enough (*e.g.*, several years), no matter what seawater is used, such systems show the potential to be further developed. The economic viability of H_2 electrosynthesis from all kinds of seawater, based on carefully thought-out and precise calculations (*e.g.*, locations, wind or solar power or other energy, electrolyzer types and costs, costs associated with the pretreatment of seawater, input flow, cables and distribution infrastructure costs, *etc.*), is extremely desirable. In order to enable performance comparison between different research groups, it is required to examine catalyst performance in standardized simulated seawater with identical components in addition to the measurements in unprocessed/alkaline/neutral/acidic seawater. This is because catalysts achieve variable performance in different seawater. Another obstacle to performance comparison is the electrode assembly (*e.g.*, catalyst + substrate) and the difference in corresponding electrolyzers. Studies in this field used different electrolytic testing devices. For instance, the catalyst for zero-gap cell operation is usually sprayed onto the ion exchange membrane (see the sub-sections of *Lab-scale to pilot-scale*) and then hot-pressed. It costs smaller voltages to afford the same J with zero-gap cells than with H-cells or ordinary flow-type cells due to significantly lower ohmic resistance contribution from the electrolyte between the two electrodes, *i.e.*, zero-gap cells are easier to achieve less power consumptions. Since the seawater composition is changing during electrolysis, a slower voltage drop can also be expected for a flow-type cell compared to one with static electrolytes. Thus, zero-gap flow-type cells should be a nice choice for stably converting the seawater into H_2 with low power consumptions. Except for cutting down power consumption by lowering electrolyzer voltages, coupling other anode reactions with HER can also achieve less electricity consumption. Many chemicals, including the urea, hydrazine, sulfides, methanol/ethanol, benzyl alcohol, 5-hydroxymethylfurfural, chitin, glucose, amines, aldehyde, *etc.*, can act as the reactant to be oxidized at the anode. Alternative reactions should satisfy the following requirements: (1) thermodynamically more favorable than water oxidation (*i.e.*, having the potential smaller than 1.23 V); (2) low environmental pollution (*e.g.*, residual urea/hydrazine in electrolytes after reaction leads to secondary contamination of seawater); (3) low costs for anode reactants, for instance, urea itself is not cheap, so coupling the urea oxidation needs to achieve lower power consumption to offset reactant costs; (4) more valuable anodic products than reactants (*e.g.*, glucose to glucaric acid); (5) easy products separation (O_2 freely leaves the reactor without additional separation process). (6) Sufficiently high market demands for anode products. Though various conversion reactions may act as potential anodic reactions for enabling lowing power consumption targets, existing studies failed to clarify the possible impact on the environment and to provide sufficient evidences that certain reaction is the best candidate. Having sufficient data to confirm the best alternate anodic reaction is obviously essential. Future studies must pay attention to this. In terms of experimental measurements, we recommend enhanced detection of products as well as overall/in-depth examination of changes in electrodes and membranes. For electrode characterizations, the detection of metal/non-metal leaching level is important because corrosive

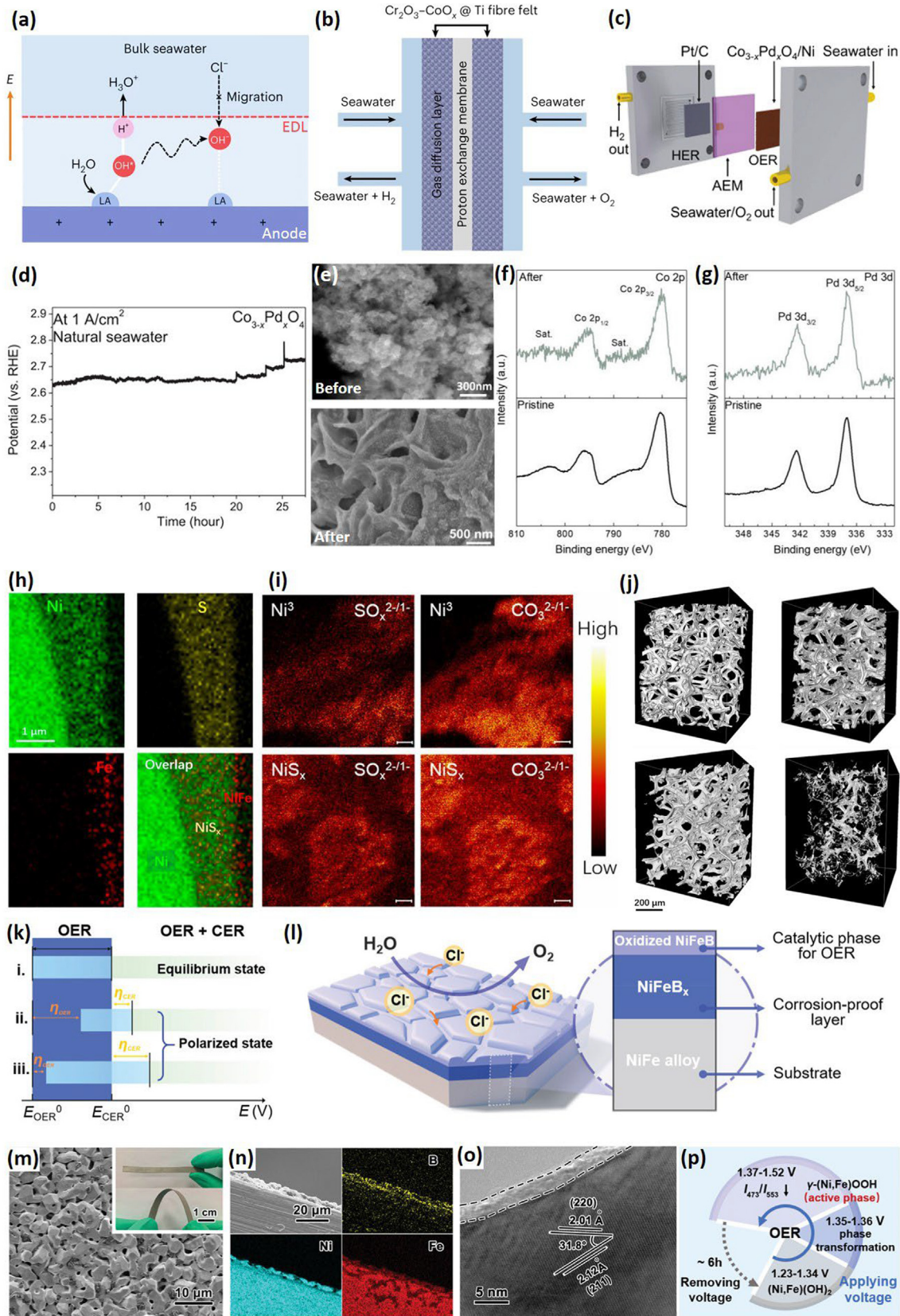
seawater environment usually leads to substantial chemical leaching and electrode fracture/crack. However, in some cases, leaching does not harm the electrode activity/stability. For instance, Mo leaching-derived MoO_4^{2-} can accumulate near the Mo-based electrode surface to minimize Cl^- attack [37], thereby enabling more stable SO. S leaching increases the stability of catalyst for a similar reason. Besides, in Yu's work, almost complete S leaching accelerated reconstruction of NiFe hydroxysulfide and Ni^{4+} species formation, thus improving the activity [59]. In future work, how the metal/non-metal leach out to the seawater and leaching-induced structural/performance changes are suggested to be identified. Moreover, the isotope-based tests, like kinetic isotope effect analysis and $^{18}\text{O}_2$ -labelled products detection, are rarely performed in previously reported seawater electrolysis research. By comparing NiOOH peaks and O_2 mass spectrometry (MS) signals of two different OER catalysts (NiFe hydroxysulfide and S-free Fe-Ni-OH), lattice oxygen mechanism (LOM), rather than adsorbate evolution mechanism (AEM) for S-free Fe-Ni-OH, was confirmed as the reaction mechanism for Fe-NiSOH [59].

Real stability of active anodes (catalytic materials)

Unlike many previous reviews that discussed designing catalysts for saltwater/seawater electrolysis [12,17,18,21,60–66], our review summarize electrode (catalytic materials) changes, in order to reflect their stability. Thus, research papers selected in this section covers relatively comprehensive electrode characterizations. Moreover, we discuss (1) representative electrode design strategies and (2) whether the corresponding catalysts is genuinely stable, which are two main quests to reveal truly stable/efficient catalysts, the most effective strategies, existing problems and potential opportunities.

Local reaction microenvironment engineering

For O_2 evolution anodes that survive and perform well in brine, ample OH^- should be a necessary premise. The "480 mV overpotential criterion" in alkaline media is not an idle one [38], and any strategy would be greatly compromised in the absence of OH^- . Adding or creating OH^- -rich reaction conditions is the most effective/practical strategy to restrain chlorine chemistry. The key role of catalytic surface microenvironment in practical SO is recently revealed by the groups of Qiao and Ling [27]. In their work, single-crystalline CoO_x nanorods, supported by Au modified carbon fibre paper, showed good overall seawater splitting activity in natural seawater with 1 M KOH (pH 14), but were much less active in natural seawater (pH 7.9). Cr^{3+} is a typical Lewis acid that preferentially combines to OH^- , and the anodic activity and stability of CoO_x in natural seawater can be profoundly improved by coating Cr_2O_3 particles as hard Lewis acid layer to the CoO_x . Under alkaline environments, the OER activity at the interface site was lower than that at the Co site, and the apparent activity decreased at higher Cr_2O_3 contents. Despite blocking some active Co sites, $\text{Cr}_2\text{O}_3\text{-CoO}_x$ exhibited performance in a neutral natural seawater comparable to that of CoO_x in an alkaline environment. This is achieved by the quick dissociation of adsorbed H_2O molecules on Cr_2O_3 to OH^* and H^* , whereas under an electric field, only H^+ diffuses quickly into bulk



seawater due to the presence of Lewis acid sites, thus elevating the local pH of the catalytic surface (Fig. 7a). Potential-dependent *in situ* IR data and DFT calculations together confirmed that Cr_2O_3 adsorb and split H_2O to produce excess OH^* and ample OH^- in the electrical double layer, thereby preventing unwanted Cl^- from entering. When the $\text{Cr}_2\text{O}_3\text{-CoO}_x$ was loaded on Ti fibre felt as both anodes and cathodes (Fig. 7b), the resulting two-electrode in a flow electrolyser configuration showed good and lasting activity, superior to $\text{Pt/C}||\text{RuO}_2$ pure water electrolyzer and many previous reports. However, the authors did not perform characterizations of the $\text{Cr}_2\text{O}_3\text{-CoO}_x@$ Ti fibre felt after the 100-h operation at high J (500 mA cm^{-2}).

Except for using a Lewis acid-modified anode electrode to intentionally build a local OH^- -rich micro-environment, according to strong-proton-adsorption strategy report by Wang et al. [31], the OER overpotential at 10 mA cm^{-2} followed the trend of $\text{Co}_{3-x}\text{Pd}_x\text{O}_4 < \text{Co}_{3-x}\text{Pt}_x\text{O}_4 < \text{Co}_{3-x}\text{Ir}_x\text{O}_4 < \text{Co}_{3-x}\text{Re}_x\text{O}_4 < \text{Co}_3\text{O}_4$ in simulated seawater (1 M phosphate buffer solution + 0.5 M NaCl). DFT results also confirmed that Pd₂₊ doping of CoOOH led to a decreased theoretical overpotential ((Pd,Co)OOH < CoO OH). Although increasing the Pd doping level provoked a gradual increase in the OER J of $\text{Co}_{3-x}\text{Pd}_x\text{O}_4$, potential-dependent Pd XAS data exhibited no apparent change in the electronic structure of Pd. Moreover, such J enhancements based on Pd doping cannot be observed in simulated alkaline saltwater (1 M KOH + 0.5 M NaCl). Like to the modification of CoO_x with Cr_2O_3 , the incorporation of Pd to Co_3O_4 brings the similar neutral OER activity improvement (no increase in alkaline media), thus illustrating the role of such additional metal sites in dissociating H_2O . And Pd adsorbs the H while splitting H_2O and did not act as an extra OER-active site. The design of this $\text{Co}_{3-x}\text{Pd}_x\text{O}_4$ catalyst is therefore similar to the Lewis acid-modified catalyst reported by groups of Qiao and Ling, because the $\text{Co}_{3-x}\text{Pd}_x\text{O}_4$ also has water-splitting/water-consuming sites. Note that the polarization curves of both Co_3O_4 and $\text{Co}_{3-x}\text{Pd}_x\text{O}_4$ in the protonic (H_2O) as well as deuterium (D_2O)-based electrolytes were collected/compared to investigate the kinetic isotope effects (KIE) of OER in neutral seawater. Substituting proton with deuterium led to more overpotential change for $\text{Co}_{3-x}\text{Pd}_x\text{O}_4$, thus confirming the critical role of Pd plays a role in water dissociation. Fig. 7c shows the AEM-based electrolytic cell with Pt/C/hydrophobic carbon paper for HER and $\text{Co}_{3-x}\text{Pd}_x\text{O}_4/\text{MnO}_2$ protected NF for OER, and humidified N_2 flows through the channels to bring H_2 out. According to V-t curves, the catalyst is stable at a J of 200 mA cm^{-2} , but decays in less than a day of electrolysis at a

J of 1 A cm^{-2} (Fig. 7d). Despite the relatively stable V-t curve, electrolysis at 200 mA cm^{-2} led to a significant change in the catalyst morphology (Fig. 7e). The crystal structure was still maintained. Chemical states of the surface, however, did not seem to change significantly (Fig. 7f and 7 g).

Multilayered (sandwich structured) anode design

Sandwich-like anodes integrate functions including fast water oxidation, Cl^- blocking, selective O_2 generation, etc., together [30,67–69]. A dual-layer NiFe hydroxide/ NiS_x -NF anode (Fig. 7h) was more stable than bare NF, NiS_x -NF, and NiFe hydroxide-NF at 400 mA cm^{-2} in Cl^- -rich alkaline electrolyte [30]. It self-activated during electrolysis: SO_4^{2-} derived from etching of NiS_x and other polyatomic anions like carbonate can be *in situ* embedded into NiFe structures (Fig. 7i). The top $\sim 200\text{-nm}$ -thick NiFe hydroxide layer split water actively, and the $\sim 1.5\text{-}\mu\text{m}$ -thick NiS_x sub-layer acted as a conductive interlayer and a sulfur source. Negatively charged polyanion-passivated NiFe/ NiS_x thus showed good capability against chloride corrosion (Fig. 7j). When paired with cathode Ni-NiO-Cr₂O₃, the anode showed unobvious activity loss for 1000 h in alkaline saltwater including 1 M KOH + seawater (23°C), 1 M KOH + 1.5 M NaCl (23°C), and 6 M KOH + 1.5 M NaCl (80°C). Ren et al. [67] reported a similar structure (NiFe hydroxide capped Ni_3S_2 nanopyramids on NF, NiS@LDH/NF) and revealed wettability transition from hydrophobic NF to superhydrophilic NiS@LDH/NF , yet whether Ni_3S_2 /NF is superaerophobic has not been studied. The corrosion resistance of SO electrodes must be improved due to a constrained O_2 evolution-only potential range (Fig. 7k) [69]. An oxidized NiFeB_x - NiFeB_x -NiFe alloy plate substrate sandwich (Fig. 7l-o) structure demonstrated nice synergistic action. According to *in situ* spectroscopic data, generation and stabilization of catalytic phases (*i.e.*, γ -(Ni,Fe)OOH) can be facilitated by the oxidized NiFeB_x (Fig. 7p), and surface B species were found as metaborate. No Fe-related Raman features can be found, suggesting the dopant role of majority of Fe in γ -NiOOH. In 1 M KOH + 0.5 M NaCl, the sandwich electrode with NiFeB_x interlayer and oxidized NiFeB_x top-layer did not corrode as quickly as the NiFe plate (electrode lifespan of $\sim 15 \text{ h}$) during electrolysis, but operated stably for 70 h , implying that metaborate-containing passivating layers may prevent excessive oxidative corrosion of the salty-water-splitting anode. Many other anodes can also be classified as multilayer electrodes, but the focus is placed on other aspects, such as *in situ* etching and redeposition, which are described in more detail later.

FIG. 7

Changing electrode local environments and typical sandwich structured (multi-layered) OER electrode design for the SO. (a) Local alkalinity on Lewis acid-modified CoO_x improves the OER activity and isolate harmful Cl^- species from the catalytic surface. (b) Brief schematic diagram of $\text{Cr}_2\text{O}_3\text{-CoO}_x@$ Ti|| $\text{Cr}_2\text{O}_3\text{-CoO}_x@$ Ti seawater electrolyzers. Reproduced with permission from Ref. [27] Copyright 2023, Springer Nature. (c) Brief schematic diagram of the MEA system, and the cathode is Pt-C catalyst on hydrophobic carbon paper. Humidified N_2 was flowed through the gas channels in the cathode, and seawater electrolyte was flowed through channels in the anode. (d) Stability tests of $\text{Co}_{3-x}\text{Pd}_x\text{O}_4$ catalysts on MnO_2 protected Ni foam (NF) at J of 1 A cm^{-2} . (e) Surface morphology changes. Surface XPS spectra in (f) Co 2p and (g) Pd 3d regions of $\text{Co}_{3-x}\text{Pd}_x\text{O}_4/\text{NF}$ before and after extended OER performed at 200 mA cm^{-2} . Reproduced with permission from Ref. [31] Copyright 2023, John Wiley & Sons, Inc. (h-j) NiFeS/NF after OER tests in 1 M KOH + seawater. (j) NiFeS after OER tests in 1 M KOH + seawater. Reproduced with permission from Ref. [30] Copyright 2019, PNAS. (k) Potential diagram in chloride-involved system. (l) Schematic diagram of the multilayer electrode. (m) SEM images and photos, (n) cross-sectional images, and (o) HRTEM image of the multilayered catalyst. (p) Surface structural transitions of the catalyst summarized from *in-situ* Raman data. Reproduced with permission from Ref. [69] Copyright 2021, John Wiley & Sons, Inc.

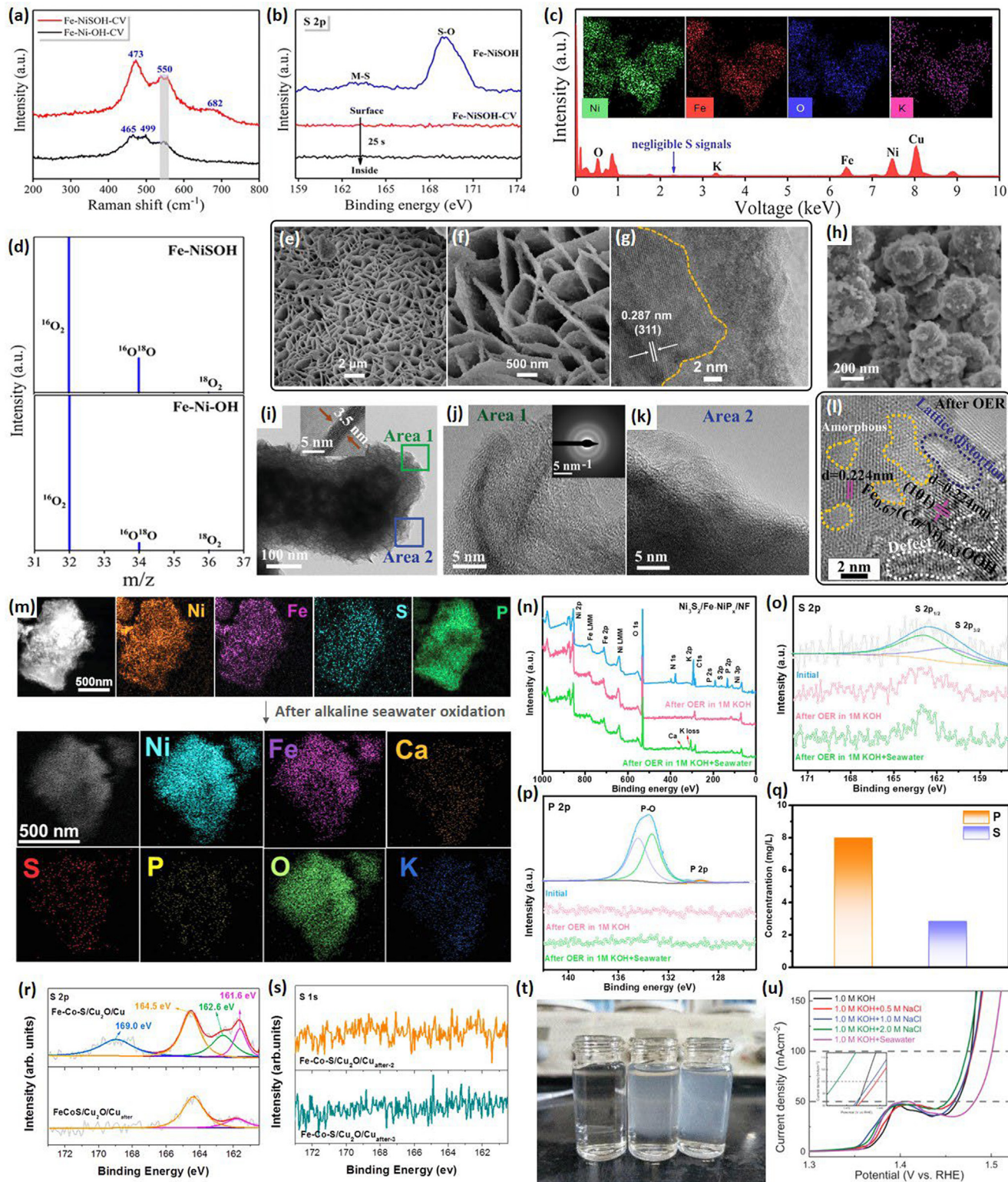
Sulfidation/selenization/more conversions

Many metal chalcogenides are known as good OER catalysts. As such, a great number of articles directly used these catalysts as SO catalysts. And with the gradual increase of corresponding research findings, like NiFeS/NF reported by Zhang et al. [30] in 2019, the synthesis of metal sulfides (other chalcogenides) itself seems to be a strategy. This review classifies developing metal sulfides for SO as a strategy because of the following three reasons. (1) Some works demonstrated that surface adsorbed SO_4^{2-} (leaching from the surface of sulfides) can prevent the Cl^- adsorption. (2) Even additive SO_4^{2-} (0.05 M) largely alleviate the chloride corrosion on NiFe-LDH/NF during alkaline SO (ASO) [70]. (3) Quite a few strong examples suggests the vital role of S in boosting SO performance, such as NiFe catalyst consisting of a mixture phase of sulfide, sulfate and hydroxide withstood 12 h of electrolysis in 1.0 M KOH + 0.5 M NaCl at 100 mA cm^{-2} [71], Fe-modified Ni hydroxysulfide (Fe-NiSOH) withstood 900 h of electrolysis in alkaline seawater at 500 mA cm^{-2} [59], S-doped $\text{Cu}_2\text{O}-\text{CuO}$ withstood 100 h of electrolysis in alkaline seawater at 500 mA cm^{-2} [72], etc. This sub-section will discuss the latest or reprehensive chalcogenides for SO, focusing on the changes that occur during the reaction. (4) Compared with the most widely used NF substrate, sulfuric NF can support the catalyst for a longer stability in alkaline seawater [73].

Huang et al. [59] synthesized Ni hydroxysulfide (NiSOH)/NF (wet chemical method, and NF was the Ni source) and Fe-NiSOH/NF (subsequent electro-oxidation in 0.01 M $(\text{NH}_4)_2\text{Fe}(\text{SO}_4)_2$ solution). Redox electrochemistry comparison of Fe-NiSOH/NF and its S-free counterpart, Fe-Ni-OH/NF, indicated more time-saving and energy-efficient growth of NiOOH and FeOOH on Fe-NiSOH/NF. Less NiOOH structures were formed with Fe-Ni-OH/NF (Fig. 8a). It is interesting that this process is accompanied by the complete loss of surface S (Fig. 8b and 8c). By the help of more *ex situ* and *in situ* characterizations and DFT calculations (such as ^{18}O isotope-labelled experiments results in Fig. 8d), Ni^{4+} species were identified as key catalytic sites for OER, and *in situ* S leaching facilitated the formation of such Ni^{4+} species. Moreover, the S-free Fe-Ni-OH/NF mainly followed AEM, whereas Fe-NiSOH/NF favored LOM. The Fe-NiSOH/NF showed good stability during ASO at J of 100 mA cm^{-2} for 100 h, but new elements (Mg, Ca, Na, Cl, etc.) can be found for the post-electrolysis electrode. This suggests that if the seawater-based alkaline electrolyte contains residual cations after the chemical precipitation treatment, then these cations will also attach to the anode. In addition, the Fe-NiSOH/NF afforded 900 h of water oxidation at the J of 500 mA cm^{-2} and 80 h of water oxidation at the J of 2 A cm^{-2} in alkaline seawater, respectively. Partially amorphous S-doped $\text{Cu}_2\text{O}-\text{CuO}/\text{Cu}$ foil afforded 100 mA cm^{-2} (stable) and 500 mA cm^{-2} (relatively obvious attenuation) for 100 h in 1 M KOH + seawater [72]. What is interesting is that signal of oxidized S enhanced in S 2p XPS region after the test. And S-Cu $^{+2/+3}$ redox couple were thus assumed as the catalytically active centers. Using Co_3O_4 core as the Co source, S- and S, B-codoped oxyhydroxides were fabricated as OER-active surface species [74]. Oxidized S species (or oxidized B species) may improve surface hydrophilicity, and S, B-codoped (CoFeCr)OOH showed higher affinity toward water

absorption than S-(CoFeCr)OOH (56.8° versus 121.9°). XPS data after OER tests in saline alkaline (1 M KOH + 0.6 M NaCl) environment show that peaks in the S 2p regain shifted toward higher binding energies, whereas the prominent peak in B 1 s regain was maintained. Cr dopants may maintain the oxidation state of electroactive Co sites through a so-called regulating effect. Moreover, the S,B-codoped (CoFeCr)OOH afforded 50 h of water oxidation at 50 mA cm^{-2} in 1 M phosphate-buffered saline + 0.6 M NaCl (pH = 7). In addition, the S, B-codoping strategy may lead to the LOM activation process [74,75]. Our group verified NiFeS/NF as a good bifunctional catalyst for ASO [76]. After preforming the OER in alkaline seawater for one day, the morphology of the catalyst (Fig. 8e and 8f) remained basically unchanged, and an amorphous NiOOH layer was derived (Fig. 8g). Typically, certain amorphous hydroxides can be produced from the surface of materials including metal sulfides, metal nitrites, metal phosphides, MOF, etc., during the anodic OER. These compounds serve as genuine reaction sites and may even shield the internal metal components. Such surface-derived catalysts (*i.e.*, precatalysts) are not unique in seawater electrolysis. In fact, how to precisely achieve the directional and qualitative growth of such *in situ* derived layer at the atomic level towards better protecting the inner material as well as exhibiting higher product selectivity would be considered necessary in this field. This is where the field really needs to break through to achieve direct SO. In another representative work, the authors prepared a series of metal sulfides on NF by electrodeposition and, with the exception of NiS_x (4.06 mg cm^{-2}) and NiCoS_x (3.97 mg cm^{-2}), the sulfides were loaded in amounts between 2 and 3 mg cm^{-2} [77]. The best-performing FeNiS_x are stacked nanospheres (Fig. 8h) that consists of amorphous sheet-like structures (Fig. 8i-k), with hydroxide derived from the surface (Fig. 8l) after prolonged testing at around 0.5 A cm^{-2} , leading to the crystalline/disordered materials. According to potential-dependent XAS data, Co was the first to experience oxidation when compared to Fe and Ni, and S leaching (from XPS analysis) may promote ternary metal (oxy) hydroxide formation. Reconstructed defective (oxy) hydroxide with parent multi-metallic amorphous nano-sulfides jointly showed relatively good activity and stability (97.6% J retention after 100 h in 1 M KOH, 92.2% J retention after 100 h in 1 M KOH + sweater). FeCoNi-LDH showed fast J decay (67.5% J retention) during 100 h in 1 M KOH, implying that electron coupling of metal sites may enhance the stability, and *in situ* reconstructed structure of sulfide has strong resistance to local pH drop and even the chloride (electro)-chemistry.

An Fe-doped $\text{Ni(OH)}_2/\text{Ni}_3\text{S}_2@\text{NF}$ electrode showed a relatively good OER stability (27 h@ 100 mA cm^{-2}) and high O_2 FE (95%) in 1 M KOH + 0.5 NaCl [78]. Note that XPS data of this electrode in S 2p region only showed one broad bump belonging to SO_4^{2-} . The control electrode, Fe-doped $\text{Ni(OH)}_2@\text{NF}$, showed a comparable activity to that of Fe-doped $\text{Ni(OH)}_2/\text{Ni}_3\text{S}_2@\text{NF}$ but inferior stability. This reflects the role of Ni_3S_2 in stabilizing the electrode, but hydrothermally prepared $\text{Ni}_3\text{S}_2@\text{NF}$ was not much more active than bare NF. Moreover, theoretical calculations revealed that Fe sites and Ni sites of (100) and (110) facets of Fe-doped Ni(OH)_2 were more suitable for OER and CER, respectively. Similar

**FIG. 8**

Vital role of S (oxidized S species) towards enhancing SO stability. (a) Raman spectra before and after CV activation. (b) XPS data before and after CV activation in the S 2p region, including the result after etching. (c) Element distribution of the Fe-NiSOH/NF after CV activation. (d) ¹⁸O-labelled mass spectrometry results. Reproduced with permission from Ref. [59]. Copyright 2022, Royal Society of Chemistry. (e) Low- and (f) high-magnification SEM images and (g) HRTEM image of post-OER NiFeS/NF tested in 1 M KOH + seawater. Reproduced with permission from Ref. [76]. Copyright 2021, Royal Society of Chemistry. (h) Surface morphology. (i-k) TEM images of the FeCoNiS_x. Inset in (j) shows the SAED pattern. (l) HRTEM image after OER tests. Reproduced with permission from Ref. [77]. Copyright 2022, John Wiley & Sons, Inc. (m) Changes of the distribution of elements. (n-p) XPS data. (q) Dissolved P and S species in solution. Reproduced with permission from Ref. [79]. Copyright 2022, John Wiley & Sons, Inc. (r,s) XPS data. Reproduced with permission from Ref. [80]. Copyright 2022, Elsevier. (t) Detection of sulfate ions in the electrolytes. (u) Effect of electrolyte salinity and impurity on electrode activity. Reproduced with permission from Ref. [81]. Copyright 2022, John Wiley & Sons, Inc.

to Fe-doped $\text{Ni}(\text{OH})_2/\text{Ni}_3\text{S}_2@\text{NF}$, *in situ* growth of NiFe-based Prussian blue analogs on a hydrothermally prepared $\text{Ni}_3\text{S}_2/\text{NF}$, followed by phosphidation led to $\text{Ni}_3\text{S}_2/\text{Fe-NiP}_x$ heterostructure/NF [79]. Grain boundaries and catalytically active $\text{Ni}(\text{OH})_2/\text{Ni}(\text{Fe})\text{OOH}$ were derived on the surface of $\text{Ni}_3\text{S}_2/\text{Fe-NiP}_x$ after OER tests in 1 M KOH + seawater. Interestingly, partial S and the majority of P were lost after ASO (Fig. 8m and 8o-8q), and K/Ca salts also appeared on the electrode surface (Fig. 8m and 8n). After electrolysis, not only valence states of surface Fe and Ni were greatly elevated, but also O vacancies were formed, while the XRD pattern did not change significantly, indicating surface oxidative reconstruction. In another work, Fe-Co sulfides were electrodeposited on $\text{Cu}_2\text{O}/\text{Cu}$ foam (CF), and the resulting Fe-Co-S/ $\text{Cu}_2\text{O}/\text{Cu}$ showed poor oxidation stability in 1 M KOH, 1 M KOH + 1 M NaCl, and 1 M KOH with real seawater [80]. XPS survey spectra of electrodes for electrooxidation in KOH + NaCl and KOH + seawater shows signal of Cl, and the electrode used in KOH + seawater adsorbed some Ca salts. The loss of sulfur species in KOH + NaCl and KOH + seawater (Fig. 8s) is more significant compared to that in KOH solution (Fig. 8r).

Partial sulfidation is proven as a good strategy by Zhang's group to prepare SO precatalyst [81]. $\text{Ni}_2\text{Fe-LDH}/\text{FeNi}_2\text{S}_4/\text{NF}$ with an η_{100} of 240 mV was a more active and robust electrode than $\text{FeNi}_2\text{S}_4/\text{NF}$ (271 mV) and $\text{Ni}_2\text{Fe-LDH}/\text{NF}$ (279 mV) in 1 M KOH solution. A small amount of $\text{Ba}(\text{NO}_3)_2$ solution was separately added to three different electrolytes (Fig. 8t, from left to right: unused 1.0 M KOH, 1.0 M KOH for $\text{Ni}_2\text{Fe-LDH}/\text{FeNi}_2\text{S}_4/\text{NF}$ after CV scans, 1.0 M KOH for $\text{FeNi}_2\text{S}_4/\text{NF}$ after CV scans) to visually demonstrate the S leaching. According to XPS and SEM results, there exists a stable Ni- and Fe-sulfate film over $\text{Ni}_2\text{Fe-LDH}/\text{FeNi}_2\text{S}_4/\text{NF}$ to hinder further oxidization after a continuous anodic scan. Without prior anodic CV scanning in 1 M KOH solution, the $\text{Ni}_2\text{Fe-LDH}/\text{FeNi}_2\text{S}_4/\text{NF}$ will deactivate rapidly in alkaline salty water and alkaline seawater. Moreover, the activity of the electrode after CV scan was not affected by the NaCl content in the alkaline salty water, and the activity was always weaker than that in alkaline seawater (Fig. 8u). Electroactivity of post-CV-scan $\text{Ni}_2\text{Fe-LDH}/\text{FeNi}_2\text{S}_4/\text{NF}$ was better than that of pristine $\text{Ni}_2\text{Fe-LDH}/\text{FeNi}_2\text{S}_4/\text{NF}$ in alkaline NaCl solution. In another study, similar surface S oxidation from incorporated S atoms to M–O–S species occurs on a partially sulfurized NiFe LDH catalyst after 12 h of anodic electrolysis at 100 mA cm^{-2} in 1 M KOH + 0.5 M NaCl [71]. Sulfuric NiFe LDH were much more stable than S-free NiFe LDH for alkaline salty water oxidation.

Metal selenides (M_xSe_y), with the more electronegative Se, appear to be a potential SO precatalyst. NiSe_2 doped with Fe/P was found to exhibit improved overall seawater splitting performance and high O_2 FE [49]. To prepare the Fe, P-NiSe₂, electrode-deposited NiFe alloy film was oxidized to nanoporous FeNiO_x for subsequent low-temperature phosphidation (using NaH_2PO_2) and selenization (using Se powder). This electrode operated stably for over 200 h in AEM electrolyzers with different electrolyte feeding modes and produced O_2 with high selectivity. The surface-derived passivation layer (P–O species) inhibited selenide dissolution, and Fe dopants enhanced the O_2 -evolving perfor-

mance, while the adjacent Ni sites acted as the HER active sites. Back in 2018, Qiao's group prepared a set of 3D Co selenide electrodes (from Co-Se1 to Co-Se5) via a straightforward selenizing method, using Co foil (thickness 0.1 mm) and Se powder with different Co-to-Se mass ratio [82]. Among these samples, Co-Se1 with the most negative charge transfer from Co to Se (*i.e.*, higher relative mole ratio of $\text{Co}^{3+}/\text{Co}^{2+}$ of 0.22:1, and higher coordination number of Co species) exhibited the best OER activity, whereas the Co-Se4 ($\text{Co}^{3+}/\text{Co}^{2+}$ ratio of 0.15:1) showed the best HER performance in 1 M KOH solution. The Co-Se1 experienced an activation process (main XRD peaks: from $\text{CoSe} + \text{Co}_9\text{Se}_8 + \text{Co}$ to $\text{CoSe} + \text{Co} + \text{Co}(\text{OH})_2$) after 1 h for stability electrolysis in 1 M KOH solution. The efficiency of the overall water splitting device consisting of Co-Se1 anode and Co-Se4 cathode exceeded that of the counterpart consisting of precious metals for in buffer solution (pH = 7.4) and seawater, showing the effectiveness of a simple charge state manipulation between negatively-charged Se active centers ($\text{Se}^{\delta-}$) with localized negative charges and positively-charged Co sites (*e.g.*, Co^{3+}) with positive charges.

In another representative work [83], a NiFe foam was soaked in NaHSe selenization solution for hydrothermal reaction to produce a selenized NiFe foam (Se/NiFe) with a selenide layer thickness of nearly 111 nm. Such Se/NiFe was further subjected to an electrodeposition process to prepare porous thickness 245 nm-thick NiFe LDH layer. According to cross-sectional TEM mapping of the resulting NiFe LDH/Se/NiFe, some Se diffused into the LDH layer during fabrication. When paired with Pt cathode for two-electrode electrolysis at the J of 100 mA cm^{-2} , the lifetime followed the trend of NiFe LDH/Se/NiFe (250 h) > Se/NiFe (180 h) > NiFe LDH/NiFe (150 h) > NiFe foam (85 h) in 1 M KOH + 1 M NaCl solution. Both TOF-SIMS mapping of SeO_3^- and depth-dependent XPS profile after 45 h of operation indicate that anionic Se species atop the NiFe foam, especially SeO_x^- intercalated in the LDH layer, can electrostatically shield a degree of corrosive Cl^- from approaching the electrode, thus protecting the electrode and guaranteeing the O_2 -evolution selectivity.

From the theoretical calculation results in the reported literature, it seems that usually S (or Se) is not considered as an active site, and the active site tend to remain the Fe-group elements. Among the Fe-based elements/sites, some elements tend to oxidize Cl^- and some elements tend to synthesize O_2 . The effect of S on the activity and selectivity still deserves further study. Besides, S will be oxidized and tends to leach from catalysts into electrolyte, and some $\text{SO}_x^{\delta-}$ may adsorb to the catalyst surface. Other non-metallic elements such as Se, P and B also follows such rules, the leaching degree of S species varies from work to work, and the corresponding impact on enhancing stability is also quite different. In addition, while sulfides-based electrodes showed exceptionally good stability in alkaline seawater [30], there are no conclusive results on the stability of such electrodes in untreated natural seawater. In the future design of sulfide-based/sulfur-containing SO electrodes, it is necessary to know, firstly, chemical states of sulfur prior to reaction, and secondly, whether sulfur species are catalytically stable and the amount of sulfur leaching/loss during electrolysis. Thirdly, the leaching rates of the sulfates for different S-containing electrodes should

be compared to guide the design of a custom S release SO electrode. Moreover, it would be helpful to at least qualitatively describe the relationship between sulfur loss and stability.

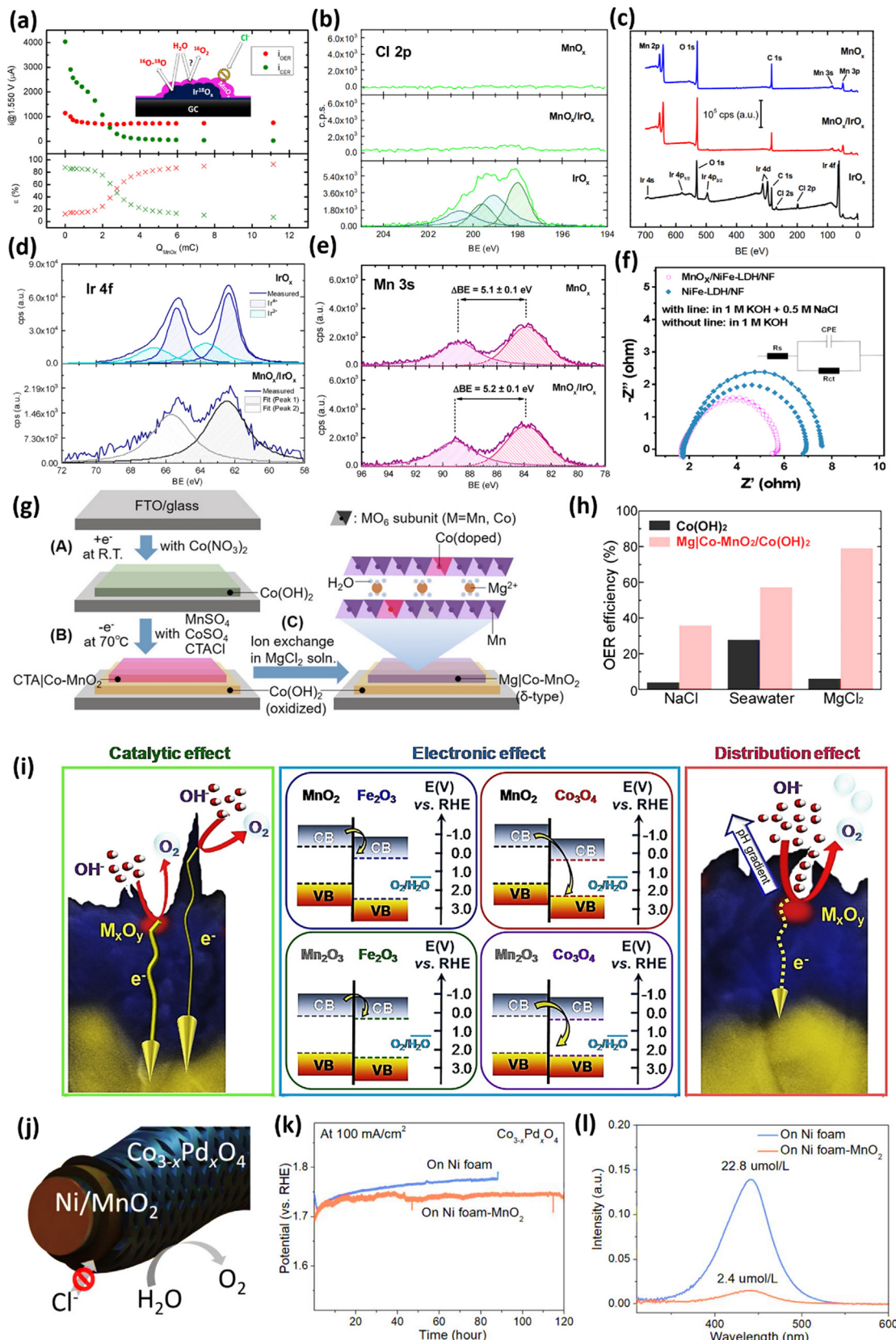
In the field of sulfides/selenides-based water electrolysis, Zhang's group investigated the evolution of Ni_3S_2 during OER in O_2 -saturated 0.1 M KOH solution and proposed hetero-anionic regulation mechanism [84]. Amorphous hetero-anionic-structured Ni hydroxides (*i.e.* Ni oxysulfides) were verified as the real active site of the sulfide pre-catalyst. Within such surface oxysulfides, S and O anions supplied an appropriate level of anionic polarization and optimized the cation electronic structure, which improved intrinsic water oxidation activity. As another example, even high-entropy sulfides like FeNiCoCrMnS_2 (acting as the pre-catalyst) transformed into sulfate-containing MOOH or MOOH-S (*i.e.* co-existence of M^{3+} and sulfate, the true OER-active center) during anodic water oxidation electrolysis [85]. Note that sulfate (SO_4^{2-}) further boosted the activity of FeNiCoCrMnOOH , such a conclusion is consistent with previously reported finding of boosted activity by the deliberate S incorporation [86]. Except for a 6-h leaching of S (S content in electrolyte: from ~ 37 ppm to ~ 110 ppm), Cr leaching lasted for at least 8 h (Cr content in electrolyte: from ~ 3 ppm to ~ 15 ppm), other metals including Co, Fe, Mn and Ni showed small leaching amounts (lower than ~ 2 ppm). S and Cr leaching had little to do with one another. OER performance was not affected by Cr leaching; rather, Cr acts as a pore-forming agent that increased the number of active sites that were exposed. According to these work [84–86], it appears that SO_4^{2-} -containing metal oxyhydroxides can be viewed as the active center for OER. However, Feng et al. [87] demonstrated that the active sites for OER were S-Fe and S-Ni sites buried in the sub-layer of S-FeNi catalyst rather than SO_4^{2-} -based sites. Thus, factors that may play a key role in improving the activity of sulfide pre-catalyst include (1) *in situ* creation of high-valence metal centers during the pre-activation process, (2) metal oxysulfides *in situ* formed on the surface of sulfide, (3) the surface SO_4^{2-} adsorption/incorporation (SO_4^{2-} can also repels Cl^- in seawater), (4) the sub-layer metal-S components, (5) enhanced specific surface area, *etc.* In fact, despite the above reported structure–performance relationships, the community has not yet come to a firm and compelling conclusion about the actual structure of the active sites of sulfide/selenide-based electrodes under working conditions. Thus, more studies, with systematic experimental research and comprehensive *operando* characterizations, are needed on this subject.

Of note here is that metal phosphides are more suitable for electrocatalytic SR [35,88], and little research has been done on whether $\text{PO}_x^{\delta-}$ can protect the surface of the electrode from being corroded by chloride during SO. We recommend the readers PO_4^{3-} -decorated $\text{Ni}_3\text{Fe-LDHs@CoP}_x$ for near-neutral seawater splitting, one of the latest and a representative work [89]. The authors discovered that the phosphate layer (1) mitigated a local pH drop due to its capacity to bind the H^+ , (2) aided in adsorption of OH^- , and (3) repelled Cl^- . As a result, PO_4^{3-} -decorated $\text{Ni}_3\text{Fe-LDHs@CoP}_x$ enabled more stable seawater splitting than $\text{Ni}_3\text{Fe-LDHs@CoP}_x$. Similar to $\text{SO}_x^{\delta-}$ and PO_4^{3-} , $\text{B}_y\text{O}_x^{\delta-}$ may also be able to adsorb and concentrate on the electrode to prevent Cl^- from reaching the active sites, but credible and in-depth

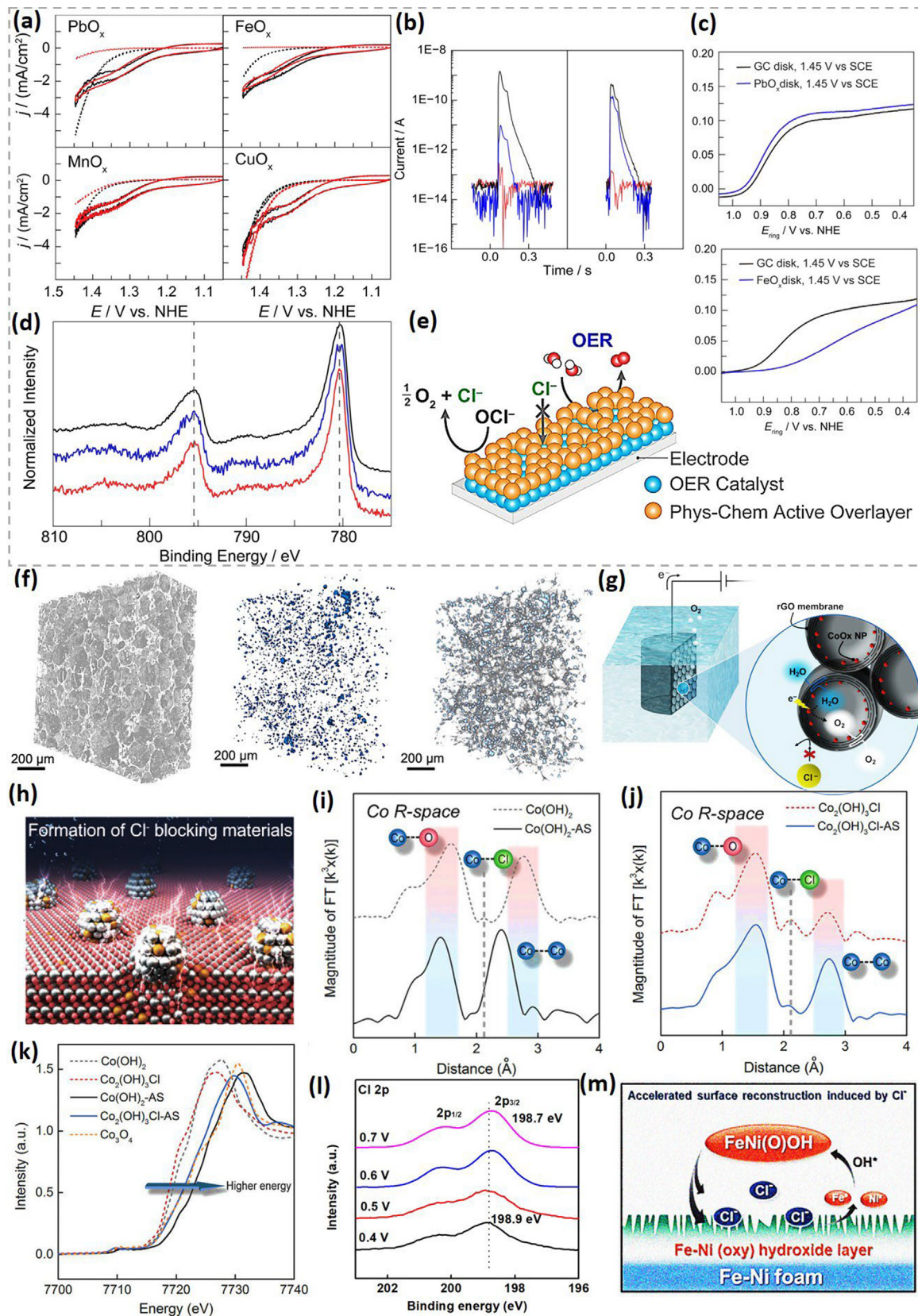
work is scarce. In any case, metal borides should be changed into boron oxide and a tiny quantity of soluble borates after OER electrolysis [90]. Fe-B-O@FeB_x showed good stability in alkaline simulated SO, and this catalyst converted to a layered structure of Fe (oxy)hydroxides/oxides/borides after anodic electrolysis [91]. Post-OER XPS results in the B 1 s region confirmed that surface B signals (contents) are weakened, where B–O signal was still present, but the Fe–B bond peak was absent. Another work that developed the anticorrosive oxidized $\text{NiFeB}_x\text{-NiFeB}_x\text{-NiFe}$ alloy for OER in saline water suggested that (1) NiFeB_x can act as a corrosion-proof layer and (2) metaborate was responsible for optimizing the electronic structure of Ni in outermost amorphous metaborate-modified $\gamma\text{-(Ni,Fe)}\text{OOH}$ [69]. Additionally, there are no works revealing the catalytic mechanisms of anionic S, Se, P, and B species (*e.g.*, $\text{SO}_x^{\delta-}$, $\text{SeO}_x^{\delta-}$, $\text{PO}_x^{\delta-}$ and $\text{B}_y\text{O}_x^{\delta-}$) atop the catalysts during natural SO for us to get more in depth understanding. Natural seawater can be even more corrosive than alkaline/neutral seawater to the electrodes, and it is worth studying how useful these anions can be in the presence of large amounts of interference impurities. The effect of these ions on the catalyst activity in natural SO is currently not known. Last but not least, where the dissolved S species go (*e.g.*, specific atomic-level distribution and truly stable existence state)?

Intrinsic inhibition of CER

Some materials do not rely on SO_4^{2-} adsorption (*i.e.*, S electro-oxidation, leaching, and adsorption) to repulse Cl^- , but rather have intrinsic Cl^- -repelling ability. According to early studies that developed O_2 -selective IrO_2 -coated Ti anodes for saltwater oxidation including $\text{Mn}_{0.87}\text{Mo}_{0.13}\text{O}_{2.13}/\text{IrO}_2$ -coated Ti (1999) [92], $(\text{Mn}_{0.89}\text{Mo}_{0.05}\text{W}_{0.06})\text{O}_{2.11}/\text{IrO}_2$ -coated Ti (2001) [93], $\text{Mn}_{1-x-y}\text{Mo}_x\text{Fe}_y\text{O}_{2+x-0.5y}$ IrO_2 -coated Ti (2002) [94], *etc.*, Mn is robust element that intrinsically hinders Cl^- oxidation. MnO_x can act as overlayer that disfavors the transport of Cl^- . In an acidic solution containing trace amount of Mn^{2+} and plenty of Cl^- , Koper's group used an IrO_x/GC rotating disk electrode (top) to show that the *in situ* formation of amorphous MnO_x on IrO_x can suppress CER while boosting OER (Fig. 9a) [45]. Mass spectrometry results corroborated improved O_2 selectivity resulted from MnO_x deposition. Chlorides were captured only on IrO_x (Fig. 9b) based on post-electrolysis XPS data. IrO_x appeared to be completely covered after the growth of MnO_x (Fig. 9c), as the remaining Ir signal was quite weak (Fig. 9d). XPS peaks in the Mn 3 s region hardly changed (Fig. 9e). Since the porous MnO_x network was found to possess low activity, subsurface IrO_x was the real O_2 -evolving activity source, which indirectly indicated that MnO_x reduced chloride diffusion coefficient and concentration gradient while transporting H_2O , H^+ and O_2 (inset in Fig. 9a). Similar to $\text{MnO}_x/\text{IrO}_x$ [45], Wang et al. [95] demonstrated better O_2 -generation stability of amorphous MnO_x layer/ NiFe LDH/NF compared to that of NiFe LDH/NF in 1 M KOH + 0.5 M NaCl solution as well as in 1 M KOH/seawater electrolytes. MnO_x facilitated charge transfer and reaction kinetics (Fig. 9f) and may act as a permeable metal oxide layer to restrain Cl^- transport. δ -type MnO_2 was simultaneously intercalated with Mg^{2+} and doped with Co ($\text{Mg}|\text{Co-MnO}_2$) by Masaharu's group to work as outer-layer of OER-active Co(OH)_2 (Fig. 9g) [96]. Although $\text{Mg}|\text{Co-MnO}_2/\text{Co(OH)}_2$ showed a greater overpotential

**FIG. 9**

Mn oxide-based structures that are inherently resistant to the CER. (a) Currents and selectivity. (b) XPS scans of the Cl 2p spectral peaks. (c) Survey spectra. XPS data in the (d) Ir 4f region and (e) Mn 3 s region. Reproduced with permission from Ref. [45] Copyright 2018, ACS publications. (f) Charge transfer resistance change. Reproduced with permission from Ref. [95] Copyright 2022, ACS publications. (g) Electrode fabrication. (h) OER efficiency. Reproduced with permission from Ref. [96] Copyright 2020, ACS publications. (i) Possible mechanisms. Reproduced with permission from Ref. [98] Copyright 2018, ACS publications. (j) MnO_2 as the protective shield. (k) Electrolysis difference before and after modification of protective layer. (l) UV-vis spectra. Reproduced with permission from Ref. [31] Copyright 2023, John Wiley & Sons, Inc.



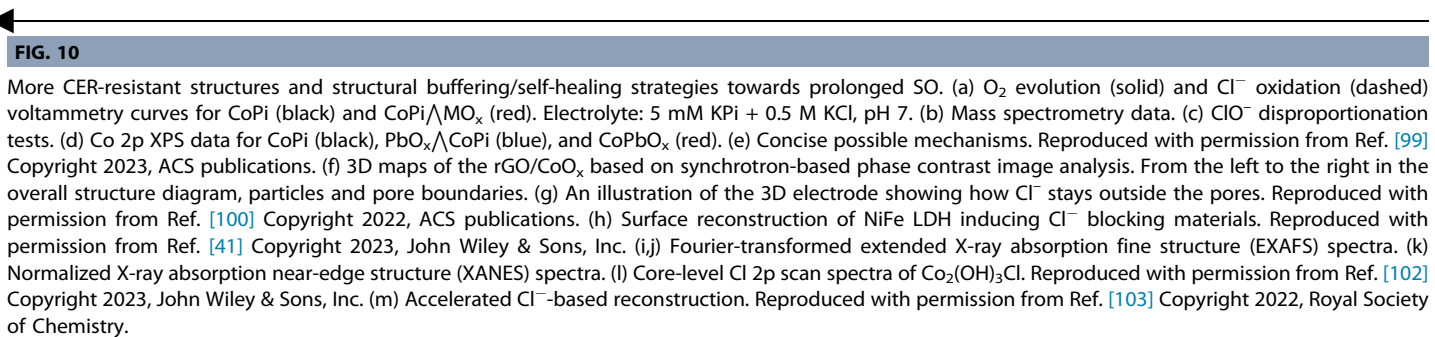
than Mg|MnO₂/Co(OH)₂ and Co(OH)₂ in 0.25 M MgCl₂, the O₂ production efficiency of the Mg|Co-MnO₂/Co(OH)₂ was far higher than that of Co(OH)₂ (Fig. 9h). Co dopants may make MnO₂ more negatively charge via electron transfer from intercalated OH⁻ to Co³⁺. Other work by Masaharu's group like Mg-intercalated layered MnO₂/IrO₂-coated Ti and Mn_{0.87}MnO_{0.13}O_{2.13}/IrO₂-coated Ti may provide us a more comprehensive understanding of the intercalation and doping strategies [92,97].

Unlike coating on catalysts, Mg oxides can be pre-coated on substrates like F-doped tin oxide (FTO) as a multifunctional layer. Bigiani et al. [98] successively deposited Mg precursors and Co oxides (or Fe oxides) onto FTO, followed by heating treatment under air (producing Co₃O₄-MnO₂/FTO or Fe₂O₃-MnO₂/FTO) or Ar (producing Co₃O₄-Mn₂O₃/FTO or Fe₂O₃-Mn₂O₃/FTO) to synthesis SO anodes. No Mn-Fe-O or Mn-Co-O phases were generated. For electro-production of O₂, Co₃O₄-MnO₂ was superior to Fe₂O₃-MnO₂, and Co₃O₄-Mn₂O₃ was superior to Fe₂O₃-Mn₂O₃ in simulated alkaline seawater. Fe₂O₃-based anodes were inferior to Co₃O₄ counterparts. All four anodes showed certain OER activities in alkaline Mediterranean seawater, and activities of the MnO₂-based anodes were better than those of the Mn₂O₃-based ones. According to *ex situ* studies, the following reasons can explain that why Mn oxide-based anodes was more active than Mn oxide-free anodes (*i.e.*, pure Co₃O₄ or Fe₂O₃) as well as why Co₃O₄-MnO₂/FTO performed the best (Fig. 9i). (i) Thin and thick arrows in the green box represent electrons transfer from Mn oxides and composites, respectively. Intrinsically, Co₃O₄ is more active than Fe₂O₃ for water oxidation. (ii) Electrons flow to Co oxides (*p*-type) via *p-n* heterojunctions, whereas they move from the higher energy conduction band of Mn oxides to the lower-energy one (*e.g.*, Fe₂O₃, *n*-type) via homologous path (see blue box in Fig. 9i). Additionally, MnO₂-based electrodes have greater energy difference than Mn₂O₃-based electrodes. (iii) Fe₂O₃ and Co₃O₄ differ in distribution, and more Co₃O₄ distributed at near-surface regions, possibly leading to its moderated pH gradient effects (see red box in Fig. 9i). Pre-coating a MnO₂ layer on NF that is not resistant to Cl⁻ etching inhibited CER (Fig. 9j and 9 l) [31]. Further synthesis of OER-active catalyst, Co_{3-x}Pd_xO₄, on such MnO₂-coated substrate achieved more durable electrolysis than MnO₂-free counterpart (Fig. 9k).

Various metal oxides were coated on a thin layer of CoPi as an overlayer (Fig. 10a) for O₂ electro-production in briny water [99]. Such deposition did not alter valence states of Co much (Fig. 10d), nor does it change valence states of Pb. If oxide layer

with a point of zero charge (pzc) value smaller than CoPi is deposited on the surface, the final OER selectivity will be improved (Fig. 10b, results for PbO_x-coated CoPi). Tests in 1 mM NaClO solution also showed that FeO_x enabled ClO⁻ disproportionation, thus achieving pure O₂ generation. Disproportionation on other catalytic surfaces, such as PbO_x, are not so obvious on the surface of FeO_x (Fig. 10c). Therefore, coating the catalytically active materials with a top-layer that can physically reject Cl⁻ and chemically drive ClO⁻ decomposition should achieve high O₂ selectivity from seawater electrolysis (Fig. 10e). Placing materials that repel Cl⁻ adjacent/close/near to OER active areas may stop Cl from adsorption. Surface reconstruction of Ni_{0.9}Fe_{0.1}-LDH transforming to a mixture of Ni-Fe oxyhydroxides and crystalline Ni-Fe alloy (Fig. 10h) was achieved by N₂-H₂ plasma treatment [41]. The *in situ* derived Ni₃Fe with high positive ΔG value for Cl^{-*} was believed to physically tune the surface potential to repel Cl⁻, thereby suppressing chloride corrosion at the surface of the Ni-Fe oxyhydroxides phase. Porous carbon-based electrodes can also be designed as a nice Cl⁻ impermeable architecture. Combination of CoO_x and rGO achieved O₂-selective SO as hydrated size of Cl⁻ is larger than the interlayer spacing between stacked rGO sheets [100]. Large aggregates of CoO_x (cubic Co₃O₄ + cubic CoO) internally decorated a porous carbon scaffold as the catalytic phase. Based on the different X-ray absorption of CoO_x and rGO, the phase contrast images visually and spatially present the rGO pore boundaries and enclosure of CoO_x particles inside such pores (Fig. 10f). The rGO/CoO_x was connected to a potentiostat using Ag paste layer or a cylindrical Ag mesh. In 1 M KOH + 0.5 M NaCl, bare Ag support was oxidized to Ag₂O as well as Ag₂O₃, affording little J due to low activities. The Co-free Ag/rGO exhibited only capacitive behavior. The two electrodes containing CoO_x showed a significant increase in J at + 0.75 V_{Ag/AgCl}, and the one using Ag mesh had better activity attributed to less ohmic voltage drop. The Ag mesh-based rGO/CoO_x showed an enhanced diffusive transport through the rGO structure. Due to the selective membrane-like pore walls composed of stacked rGO multilayer structures (Fig. 10g), the J values were stable for the Ag mesh-based rGO/CoO_x during the 3-h test, and the O₂ FE maintained at a high level. The closed macropores morphology and chemical composition did not change much after 25-h of testing.

To sum up briefly, manganese oxides (MOs), a material that tend to synthesize O₂ in acidic, neutral and alkaline saltwater environments, can be deposited directly on the catalyst to repel Cl⁻ [45] or on the substrate to protect it for more stable seawater



electrolysis [31]. Future research direction can focus on how to optimize the manganese oxide thin layer in terms of its thickness, chemical composition and conductivity, etc. The full comparison of MOs with more potential nice coatings such as lead oxides, chromium oxides, silicon oxide [101], aluminum oxides, etc. as the Cl^- -repelling protective layer also worth investigating. It is also crucial to reveal structural changes of this manganese oxide layer for real SO. Nocera's group reported that overlaying the catalyst (e.g., CoPi) with coating having a pzc (e.g., Fe_2O_3 , MnO_2 , and PbO_2) less than that of the CoPi would help to reject surface halide anions [99]. Recently discovered materials, like Ni_3Fe alloys [41], with a high adsorption energy for Cl^- are unfavorable to CER as well. Moreover, pore walls consisting of multi-layer rGO flakes behaved as selective Cl^- -filtering permeable membrane [100], due to large hydrated size of Cl^- compared to rGO interlayer distance. Developing such membrane-like layers/sites with intrinsic Cl^-/Br^- -filtering/repelling capabilities as catalytic sites, or the growth of such layers/sites in the vicinity of active sites deserves more research.

Structural buffer & self-healing strategies

A multifunctional layer (e.g., FeO_x [99]) with the intrinsic ability can inhibit CER, yet this layer may also block the active sites. There is a strategy that keeps the catalyst in regeneration. In Xu's work [102], the water oxidation performance of $\text{Co}_2(\text{OH})_3\text{Cl}$ far exceeded that of $\text{Co}(\text{OH})_2$ without lattice Cl^- species in 1.0 M KOH + 0.6 M NaCl electrolyte, including anodic J at fixed electrode potentials, Tafel slope (58.5 mV dec^{-1} vs. 83.2 mV dec^{-1}), charge transfer resistance (41.5Ω vs. 53.8Ω), electrochemical active surface areas-normalized mass activity ($46.88 \text{ A/g cm}_{\text{ECSA}}^{-2}$ vs. $1.21 \text{ A/g cm}_{\text{ECSA}}^{-2}$), turnover frequency (2.16 s^{-1} at 1.63 V vs. 0.04 s^{-1}), stability (99.9% J retention for 60000 s vs. fast J decay within 7000 s), OER FE ($99.6 \pm 0.2\%$ vs. $91.0 \pm 0.4\%$), etc. After the long-term test, XRD peaks of $\text{Co}(\text{OH})_2$ was weak and peaks of NaCl appears, and the corresponding lattice fringes were blurred. Peaks of NaCl also appeared for $\text{Co}_2(\text{OH})_3\text{Cl}$, but XRD peaks for $\text{Co}_2(\text{OH})_3\text{Cl}$ remained good and related lattice fringes remained clear. Moreover, *in situ* XAS (Fig. 10i-k) and *in situ* XPS (Fig. 10l) characterizations illustrate the Cl leaching and dynamic Cl replenishment/invasion on $\text{Co}_2(\text{OH})_3\text{Cl}$ surface. In Cl^- -containing electrolytes, etching of Fe-NF (Fe/Ni content ratio: 7/3) to Ni-rich surface was accelerated by Cl^- . Subsequent redeposition/assembly of OH^* and dissolved Fe^* and Ni^* can produce amorphous Fe-Ni (oxy)hydroxide layer (Fig. 10m) [103]. As a result of continuous etching/leaching, reconstruction and redeposition processes, the resulting catalyst can be electrolyzed for at least 100 h in 1 M KOH + seawater or in 1 M KOH + 1 M NaCl. After 100-h of electrolysis, the catalyst surface XPS signals did not appreciably alter, but morphologies did. By designing borate-intercalated Ni-Co-Fe oxyhydroxides (NiCoFe-Bi) properly as self-healing SO catalyst, the groups of Han and Li reported ultrastable electrolysis of artificial seawater ($\text{pH} = 14.95$, with 0.5 mM Fe(ii) ions) for 1000 h at the J of 500 mA cm^{-2} [34]. The reason why this catalyst can carry out 1000 h electrolysis is mainly dependent on Co-catalyzed Fe redeposition. Although both structural buffer (reported by Xu's group) and self-healing strategies utilized Cl^- , the corresponding etching-reconstruction process ceaselessly altered catalyst morphologies

and consumed electrodes, which can be reflected by decreasing electrode potentials for AC-FeNi(O)OH during 100-h operation in 1 M KOH + seawater [103]. Therefore, self-healing catalysts still face the problem of deactivation in practical long-term operation (e.g., at least several years). It can be anticipated that how to balance the rate of deposition and etching is the most important research.

Hybrid seawater electrolyzers (HSEs)

PEM-based electrolyzers and AWEs produce O_2 at half the volume of H_2 , but the anodic O_2 does not appear to be as valuable as H_2 . In fact, integrating electro-synthesized O_2 with traditional O_2 -consuming industries might actually end in lower costs. O_2 can also be inhaled as a medicine. O_2 use in sub-sea environments relies on pressurized storage tanks, so seawater electrolysis can act as an on-site O_2 generation technique. Moreover, H_2/O_2 generated by seawater splitting devices can be liquefied, stored, and used in H_2/O_2 fuel cells. Even so, the primary goal of seawater electrolysis remains the production of H_2 . Perhaps whether or not to synthesize O_2 can based on particular circumstances (local industries/markets). Chlorides also hinder anode from producing high-purity O_2 . Similar thermodynamic onset oxidation potentials of 4e^- OER ($1.229 \text{ V}_{\text{RHE}}$) and 2e^- CER ($1.358 + 0.059\text{pH} \text{ V}_{\text{RHE}}$) leads to OER-CER contest. Even in alkaline solutions, active chlorine species generate under high J (e.g., over 1 A cm^{-2}). Using other anolytes, even non-liquid electrolyte, can fundamentally prevent CER. To produce H_2 with less energy, create other useful anodic chemicals, and avoid CER, OER replacement is indeed an option. Affordable alternative to OER are key. Thus, we devote an entire section to reviewing HSEs, and focus on neglected contents in previous reviews.

Hydrazine oxidation is a known anodic reaction with a low thermodynamic potential of $-0.33 \text{ V}_{\text{RHE}}$ (Fig. 11a) [104]. Developing NiCo-MOF onto MXene-wrapped CF led to a 3D precursor, which was annealed under NH_3 to obtain a superaerophobic and porous NiCo-decorated carbon array/CF electrode (Fig. 11b-d, NiCo@C loading: 1.0 mg cm^{-2}). It acted as a bifunctional electrode in a HSE (separated by AEM) with neutral seawater ($\text{pH} = 8.3$, or alkaline seawater with pH of 13.8, Bohai Sea, Dalian, China) as the catholyte and 1.0 M KOH + 0.5 M N_2H_4 as the anolyte. The HSE achieved lower voltages than conventional alkaline seawater electrolytic devices, and it produced almost no ClO^- regardless of Cl^- crossover after a 60-h operation. NiCo@C/MXene/Cu quickly dissolved for ASO (Fig. 11e) due to severe active chlorine corrosion. Based on rough estimates (0.11 USD per kWh for electricity price), the energy equivalent input and CO_2 equivalent emission achieved by this HSE are lower than those achieved by current technologies (Fig. 11f). The HSE tops a lot of proficient seawater electrolyzers in terms of electricity costs (Fig. 11g). Self-powered systems were also demonstrated (Fig. 11h and 11i). There remain plenty of catalysts out there that are made to pair HER and N_2H_4 oxidation for HSE, like $\text{Ni}_2\text{P}/\text{Co}_2\text{P}/\text{NF}$ (June 2023 [105]) and Ru- $\text{Ni}(\text{OH})_2/\text{NF}$ (June 2023 [106]).

A NiFe foam (110 PPI, 1 mm thick) was converted to a 3D catalyst (Fig. 11j) consisting of bulk NiFe foam, $\text{Fe}_{0.25}\text{Ni}_{0.75}$ and hybrid of NiFeP and $(\text{Ni},\text{Fe})_3\text{S}_4$ as the outer array (Fig. 11k) for

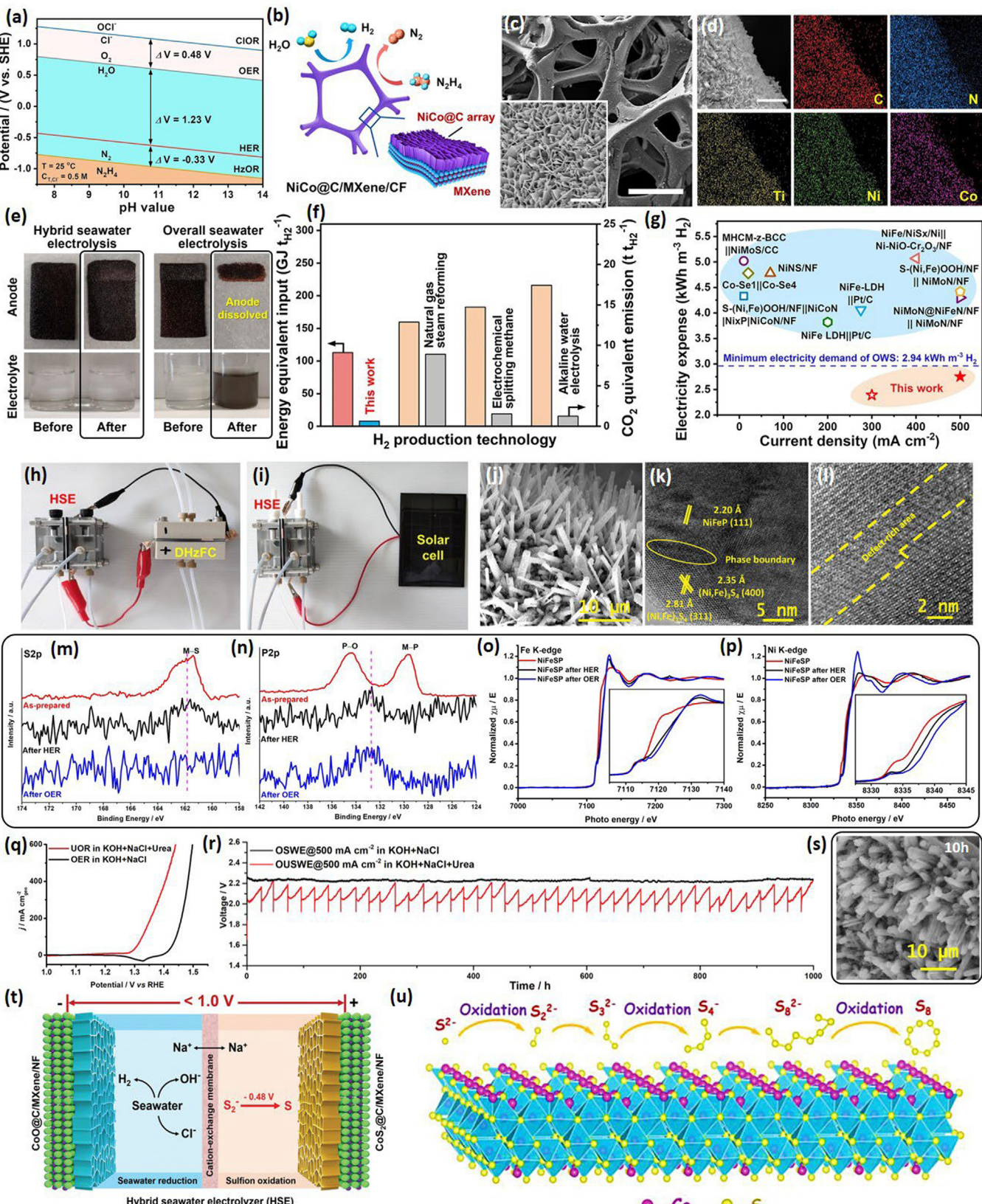


FIG. 11

Typical energy-saving SO (replace OER with HzOR, UOR, or SOR). (a) Pourbaix diagram. (b-d) NiCo@C/MXene/CF. (e) Prolonged anode life after replacing the OER. (f) Comparison of HSE with other H₂ generation techniques. (g) Comparison of HSE with other seawater electrolyzers. (h) DHZFC-powered HSE. (i) Solar-driven HSE. Reproduced with permission from Ref. [104] Copyright 2021, Springer Nature. (j-l) Catalyst characterization. (m and n) XPS data change after 10 h of electrolysis. (o and p) Fe and Ni K-edge XANES spectra. (q) UOR vs. OER. (r) V-t curves. (s) Catalyst morphology after 10-h electrolysis. Reproduced with permission from Ref. [107] Copyright 2022, John Wiley & Sons, Inc. (t) S²⁻ oxidation-based HSE. Reproduced with permission from Ref. [108] Copyright 2022, John Wiley & Sons, Inc. (u) S²⁻ oxidation pathways. Reproduced with permission from Ref. [109] Copyright 2022, John Wiley & Sons, Inc.

urea-mediated saline water electrolysis (*i.e.*, urea oxidation + HER) [107]. Such a NiFe phosphosulfide array showed phase boundaries and under-coordinated defects (Fig. 11*l*), which may enhance the activity. NiFeSP/NiFe foam was not much more active than NiFeP/NiFe foam and NiFeS/NiFe foam towards OER (or urea oxidation). *V-t* curves of NiFeSP/NiFe foam as OER and HER electrodes were recorded, for 1000 h of prolonged electrolysis, and the electrodes after 10 h of operation were characterized (see electrode change after 10 h OER or 10 h HER in Fig. 11m-p). Although the reaction was not carried out in real seawater but in 1.0 M KOH + 0.5 M NaCl, the intensity of XPS peaks were weaker in both S 2*p* and P 2*p* regions after only 10 h of operation, indicating that high *J* operation conditions easily results in S and P leaching. XPS data in Fe 2*p* and Ni 2*p* regions and X-ray absorption spectroscopy (XAS) characterizations (Fig. 11o and 11p) suggested that OER or HER catalysis led to oxidized Fe-/Ni-oxyhydroxide species. The catalyst surface experienced significant compositional reconstruction, while the array structure did not undergo notable changes (Fig. 11s). Moreover, the anodic onset potential of *J-V* curve decreased after the adding urea (Fig. 11q), whereas the cathode curve barely changed. Since NiFeSP/NiFe foam ran stably in saltwater for 1000 h, the OER was replaced with the more energy-efficient UOR. In the end, the catalyst also remained stable for 1000 h, with lower voltages (Fig. 11r).

The seawater-to-H₂ electrolysis energy efficiency can be improved by coupling HER with electro-oxidation of sulfion, which has a low potential barrier ($E_0 = -0.48$ V_{RHE}) and fast two-electron transfer: S²⁻ - 2e⁻ → S [108]. Similar to NiCo@C/MXene/CF reported by Sun et al. [104], CoS₂@C/MXene/NF was developed by Zhang et al. [108] for H₂ making from alkaline seawater at a low cell voltage (Fig. 10t). Unlike the rapidly changed NiFeSP under large OER *J* (or even HER *J*) [107], the CoS₂@C/MXene/NF showed no XPS peaks of oxyhydroxide or oxide species after 240 h at the *J* of 300 mA cm⁻². CoS₂@C nanosheets assembled on MXene/NF showed little damage. The anodic polarization curve achieves a smaller E_{onset} in the KOH solution with 1.0 M Na₂S, and much smaller voltages are required to achieve the same *J* in the two-electrode system using the seawater for the catholyte and Na₂S-containing KOH solution for the anolyte. The hybrid system can afford continuous electrolysis at 300 mA cm⁻² for 180 h, while its alkaline seawater counterpart quickly shuts down. During the reaction, the cathode keeps producing H₂, while the S²⁻ in the anode gradually become polysulfides (S_x²⁻, 2 ≤ x ≤ 4). H₂SO₄ can react with S_x²⁻ to produce solid sulfur. In addition, solar-driven HSE was assembled to stably operate at ~200 mA cm⁻² at ~0.9 V. In another work, Co₃S₄ nanowires/NF afforded same *J* in the presence of Na₂S at much smaller electrode potentials [109]. With the monolithic Co₃S₄/Ni catalyst as both anode and cathode, H₂ evolution catalysis coupling the electro-oxidation of S₂⁻ also achieved smaller overall saltwater splitting voltage. The HSE generated H₂ at 0.5 V for more than one day under the *J* of 100 mA cm⁻² and spent less energy than the alkaline saltwater splitting counterpart. Raman peaks of adsorbed sulfion gradually changed to that of S₈, S₈⁻, and S₄⁻ when the potential was measured from low (open-circuit potential) to high, thus disclosing a stepwise oxidation pathway on the Co₃S₄ (Fig. 11u). Except reactions like SOR, SR

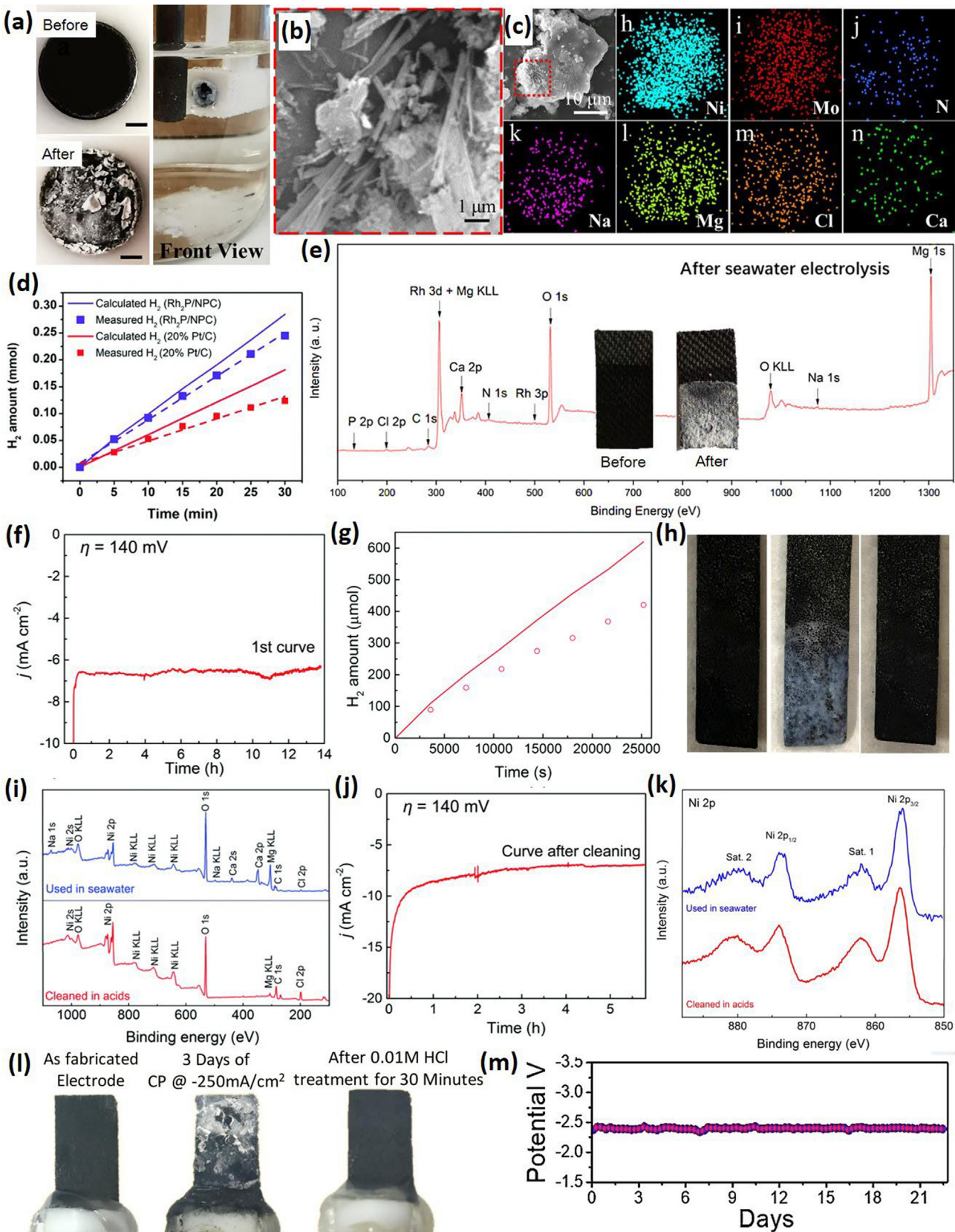
can be coupled to other anodic reactions that produce products with high added value (*e.g.*, xylose electrooxidation reaction [110], ethylene glycol oxidation reaction [111]), while ensuring the well-functioning and steadily cathodic synthesis of H₂. If the demand for the corresponding anode product (*e.g.*, formic acid [110]) is not as high as H₂, the anode reaction can be replaced periodically.

Recent HER electrodes in natural seawater

Without issues of chloride oxidation, local acidification at high *J*, catalyst self-oxidation (*e.g.*, carbon oxidation), etc., electrolysis environments of HER in seawater seem milder than those of SO. While most HER catalysts in fact cannot survive after relatively prolonged (*e.g.*, > 500 h) continuous SR electrolysis due to Mg²⁺/Ca²⁺ in natural seawater [112–119]. Many studies on developing HER catalysts in seawater used alkaline seawater, so Mg²⁺ and Ca²⁺ have actually been pre-precipitated (though some may still be left) [120]. We selectively review here catalysts electrolyzed in natural seawater to reflect the current status of direct SR research and to emphasize truly effective catalysts. All studies below nearly exclusively employed natural seawater, and seawater collection locations are also mentioned.

In 2019, Mn-doped NiS₂/NF showed comparable HER activity to that of Pt/C/NF in real seawater (Yellow Sea, China, pH = 7.9) and achieved better stability at η_{480} for 20 h [121]. This stability was attributed to the good adhesion of the Mn-doped NiS₂ to the Ni skeleton. In 2020, single-atom Pt anchored on CoP nanoarray on carbon fiber cloth was also reported to outperform the Pt/C counterpart for long-term SR (Shau Kei Wan, Hong Kong, China, pH ≈ 8.5) [122]. In 2020, core-shell NiMo@C₃N₅, supported by a glassy carbon electrode (GCE), showed better HER stability than the Pt/C counterpart in seawater (collected near Tsuen Wan, Hong Kong, pH = 7.4) [123]. Although the potential-time curve shows that NiMo@C₃N₅/GDE is relatively stable (a gradually rising potential), white impurity salts are kept depositing on the surface of the catalyst (Fig. 12a). The precipitation of Mg²⁺/Ca²⁺ and the physical adsorption Na⁺/Cl⁻ may lead to the gradual performance decay (Fig. 12b,c). NiMo wrapped by C₃N₅ shells can be protected from corrosion and poison of chemicals and biological impurities. The poor stability of Pt/C was attributed by the authors to its active sites, which would be quickly blocked by Pt-seawater ions interactions. Such inferior stability of Pt/C is consistent with earlier studies [117,124], showing the necessity of improving catalytic surface exposure and protecting active sites. In fact, stability experiments of HER catalysts in seawater were limited to relatively short periods of time (*e.g.*, < 500 h) or small *J* (*e.g.*, < 300 mA cm⁻²). See below for more examples.

In seawater (Bohai Sea, China), Co_{0.31}Mo_{1.69}C/MXene/N-doped carbon/GCE produced H₂ at η_{500} (around -43 mA cm⁻²) for 225 h [117]. At the *J* of lower than 10 mA cm⁻², Mo@(2H-1 T)-MoSe₂ performed a 12-h HER test in seawater (Bohai Sea, China) [125]. P-doped NiSe/NF afforded a *J* of -100 mA cm⁻² for 100-h SR (Persian Gulf, pH = 7.7), with significant electrode potential loss [126]. Both sub-2 nm Rh/N-doped hollow carbon spheres and its counterpart Ru/C afforded the fixed HER *J* of -10 mA cm⁻² for 12 h in seawater (Beidaihe, China, pH = 8.35), with obvious electrode potential loss [127].



Moreover, in seawater (Marine Park Beach, Qingdao, China), $\text{CeO}_2/\alpha\text{-MoC}/\beta\text{-Mo}_2\text{C}$ microrods on carbon cloth achieved a J retention of 87.5% after 100 h of HER electrolysis at an initial J of $\sim 1000 \text{ mA cm}^{-2}$ [36].

Mild acid treatment & low H_2 FE

Pan's group in 2020 demonstrated electrocatalytic reduction of seawater ($\text{pH} = 7.8$, Yellow Sea, China), using the GCE loaded Rh_2P NPs with catalytically active Rh-P centers/N, P co-doped porous carbon as the H_2 -producing electrode [128]. As shown in Fig. 12d, H_2 FE values of $\text{Rh}_2\text{P}/\text{N}$, P co-doped carbon and a Pt/C counterpart are below 100% (89.4% and 66.7%) throughout a 30-min test with a J of 10 mA cm^{-2} . Even so, J -t curves of the $\text{Rh}_2\text{P}/\text{N}$, P co-doped carbon including 24-h test at $\sim -0.25 \text{ V}_{\text{RHE}}$, 24-h test at $\sim -0.39 \text{ V}_{\text{RHE}}$ and 18-h test $\sim -0.42 \text{ V}_{\text{RHE}}$ were relatively stable. XPS data (Fig. 12e) confirmed the precipitates on the post-run catalysts mainly consists of Mg, Ca and Na salts. This work implies that even if the deposition of cations in seawater has occurred on the catalyst surface, the electrolysis V -t (or J -t) curve may not reflect the decline in H_2 FE in time. In 2018, Amal's group developed Mn-doped NiO/Ni array on NF for HER in seawater (Maroubra Beach, Sydney, Australia, $\text{pH} = \sim 8.2$) [129]. MnO_x and hetero-structured NiO-Ni existed in a composite on the NF. The electrode maintained a J of $\sim 6.5 \text{ mA cm}^{-2}$ for 14 h (Fig. 12f), but the H_2 FE got lower and lower after 1 h of electrolysis (Fig. 12g). White coating (Fig. 12h), i.e., Mg, Ca and Na salts (Fig. 12i), appeared on the Mn-doped $\text{NiO}/\text{Ni}/\text{NF}$, and these precipitates disappeared after a 20-min immersion in a dilute HCl solution (0.05 M). XPS data after a 14-h test and subsequent acid treatment (Fig. 12k) changed little. Residual Mg salts remained on the surface after acid pickling (Fig. 12i), but the activity and stability recovered to the initial/pristine state again (Fig. 12j). In another work, even at a small initial J , Co-Fe phosphate/(oxy)hydroxide/Fe foam (Co-FePO/OH/FF) showed fast performance decay during a 10-h electrolysis in seawater (Coogee beach, Sydney, Australia) due to *in situ* generation of white deposit layer, while such electrode was stable in 1 M PBS + 0.5 M NaCl [130]. Co-FePO/OH/FF recovered the HER activity after being treated in 0.5 M HCl solution, with good morphology integrity. A VS_2 /amorphous carbon (AC) catalyst showed relatively good stability without generating much active chlorine in seawater (the shores of the Bay of Bengal in Nagapattinam, Tamil Nadu, India, $\text{pH} = 8.25$, salinity = 3.38%) [131]. Although the monolithic VS_2/AC suffered from active sites blocking from the white salt coating (Fig. 12l), this electrode was cleaned in 0.01 M HCl solution every three days during the 21-day electrolysis test, and the J was fixed at 250 mA cm^{-2} (Fig. 12m). Regular electrode cleaning with diluted acid solution

extends cathode service life, yet doing so may raise the expense of real-world H_2 manufacture.

Though current cathodes can hardly sustain industrial-level J in seawater, electrodes that exceed the average performance level have emerged in some of existing studies. J of such electrodes during stability tests are obviously greater than $\sim 10 \text{ mA cm}^{-2}$ (e.g., Ref. [129] does not meet the standard, with a J during the long-term test of approximately $\sim 6.5 \text{ mA cm}^{-2}$), and the used seawater must be natural seawater (e.g., even Ref. [132] does not meet the standard due to the use of artificial seawater). For the catalysts mentioned below, while electrolytic curves are relatively stable, H_2 FE may not always be close to 100%. For instance, $\text{Rh}_2\text{P}/\text{N}$, P co-doped porous carbon achieved 24 h of HER electrolysis at the J of around $\sim 25 \text{ mA cm}^{-2}$ and at the J of around $\sim 140 \text{ mA cm}^{-2}$ (18 h of electrolysis at around $\sim 300 \text{ mA cm}^{-2}$), but the H_2 FE values within a 30-min operation were lower than 90% [128]. Despite dissatisfaction FEs, $\text{Rh}_2\text{P}/\text{N}$, P co-doped carbon afforded stable J -t curves. Carbon paper loaded Fe-doped Co_2P was stable for SR (Yellow Sea, $\text{pH} = 7.8$), which ran at $\sim 40 \text{ mA cm}^{-2}$ for least 100 h and at $\sim 200 \text{ mA cm}^{-2}$ for at least 48 h [133]. Carbon cloth supported 3D core-shell $\text{Ni}_5\text{P}_4@\text{amorphous Ni}^{2+\delta}\text{O}_{8(\text{OH})_{2-\delta}}$ was stable in catalyzing the reduction of real seawater ($\text{pH} = 7.8$) at different J ($\sim 10 \text{ mA cm}^{-2}$, $\sim 30 \text{ mA cm}^{-2}$, $\sim 50 \text{ mA cm}^{-2}$ and $\sim 100 \text{ mA cm}^{-2}$) for a total of 40 h [119]. In contrast, Ni_5P_4 -carbon cloth showed an obvious activity loss after electrolysis at an initial J of $\sim 10 \text{ mA cm}^{-2}$ for 20 h.

Many relatively stable cathodes contain erosion-resisting and conductive transition metal phosphides (TMPs), but a pure TMP catalyst is not enough. For instance, N, P co-doped porous carbon may act as the armor to prevent the etching, agglomeration and poisoning of Rh_2P [128]. Moreover, the protective layer can be a multifunctional layer. For instance, N-doped carbon shell of CoMoP@C improved SR performances by (1) making the etching rate slow down, (2) better dispersing the CoMoP , (3) acting as nice H^+ -enricher to raise H^+ concentrations around the CoMoP , and (4) providing porosity and conductivity [118]. Note that a thickness of 0.8–1.2 nm was proven as the best shell thickness than 1.6–2.0 nm (larger overpotential) and 2.6–3.8 nm (larger overpotential) due to optimal penetration of electrons. In another work, $\text{Ni}^{2+\delta}\text{O}_{8(\text{OH})_{2-\delta}}$ protective layer of a few nanometer-thick on the surface of Ni_5P_4 can effectively adsorb H_2O for further H-O cleavage as well [119]. And the interaction between the Ni-based protective layer and Ni_5P_4 also weakened the P-H_{ads} bond and facilitated the subsequent synthesis of H_2 . Despite the progress, electrocatalytic SR cathodes with sufficiently high durability and efficiency are rare. HER catalysis, especially in unprocessed natural seawater, is still facing several

FIG. 12

In situ formation of white Ca/Mg precipitates adhered to the electrodes during the SR electrolysis. (a) Photos of the catalyst before and after it was electrolyzed with seawater on a GCE. (b,c) SEM image and mapping images of the catalyst after the SR. Reproduced with permission from Ref. [123] Copyright 2022, Elsevier. (d) H_2 production efficiency. (e) XPS data. Inset shows the electrode before and after electrolysis. Reproduced with permission from Ref. [129] Copyright 2018, Royal Society of Chemistry. (f) J -t curve. (g) H_2 production efficiency. (h) The same electrode before electrolysis, after electrolysis and after acid treatment. (i) XPS data comparison. (j) J -t curve. (k) XPS data comparison. Reproduced with permission from Ref. [118] Copyright 2018, Royal Society of Chemistry. (l) The same electrode before electrolysis, after electrolysis and after acid treatment. (m) V-t stability test. Reproduced with permission from Ref. [131] Copyright 2021, ACS Publications.

significant obstacles. Firstly, even though some cathodes demonstrated good stability in alkaline seawater (see one of the most stable electrode, CF@Cu₂S@NiS@Ni/NiMo [134], for alkaline SR in Table 4), the H₂-producing capability of such cathodes has not been assessed in natural seawater, and such situations are not optimistic/encouraging. Cathodes that are stable in alkaline seawater are not necessarily stable in natural seawater because most of Ca²⁺/Mg²⁺ are removed in highly alkaline seawater. Moreover, if a two-electrode MEA electrolyzer is used, the precipitates formed inside will slowly poison the cathode and will quickly block the flow path of the electrolytic cell. Rapid gas release and corrosive conditions further trigger a catalytic site loss. Additionally, the geometric areas of most seawater splitting electrodes are merely 1 cm² or smaller, and reports on electrode scaling-up with good performance are thus needed.

Bubble traffic & gas release kinetics

Gas release becomes intense at industrial-level J . If such bubbles are able to escape the catalytic surface promptly, mass transfer will be much accelerated and there will always be sufficient active sites available for subsequent reactions. Bubble-based kinetics is of great significance for H₂ production from seawater for the following reasons. (1) Rapid bubble release ensures sufficient reaction sites. (2) Bubble release can even minimize damage to cathodes from Ca(OH)₂/Mg(OH)₂ because (i) huge amount of bubble release can flush out loosely connected deposits and (ii) even burst force derived from bubble splitting may push precipitates and some impurities away from active sites [135]. At present, most studies on bubble release are based on well-defined water environments (pH, composition) rather than impure seawater, and there are fewer in-depth studies on bubble release for changing the precipitation behavior and maintaining high catalyst activity in seawater. Yang et al. [136] synthesized 3D Pt/Ni-Mo with highly dispersed Pt NPs as a HER-active catalyst in saline water. When compared with carbon paper, NF, and Pt Foil, only the superhydrophilic Pt/Ni-Mo/NF (Fig. 13a) shows the great affinity to droplets. Moreover, a small dynamic contact hysteresis (θ_h) of Pt/Ni-Mo/NF further confirmed its low interfacial adhesion (Fig. 13b). In this way, the bubbles will easily escape the Pt/Ni-Mo and achieve efficient H₂ evolution. We will discuss more bubble release design examples in this section, which can serve as models for upcoming SO/SR electrodes designs.

Although less work has been done on bubble release studies in seawater, we can draw inspiration from recent advances in freshwater splitting. As a good example, to take away the gaseous H₂ generated on Pt strip catalysts quickly, Zhang et al. [137] introduced strips consisting of super-aerophilic (SAL) SiO₂ NPs adjacent to the Pt strip on both sides (Fig. 13e-g). The SAL stripes exhibited much higher H₂ bubble adhesive force than the Pt, and the bubbles produced on the Pt will eventually enter the SAL zone as they grow larger due to the asymmetric Laplace pressure between the bubble and the gas cushion. As shown in Fig. 13c and Fig. 13d, the finite element simulations demonstrate that the H₂ concentration at the interface of SAL/flat Pt is much lower than that of blank Pt electrode/bulk liquid, thus indicating that the diffusion of H₂ is greatly increased. The authors made

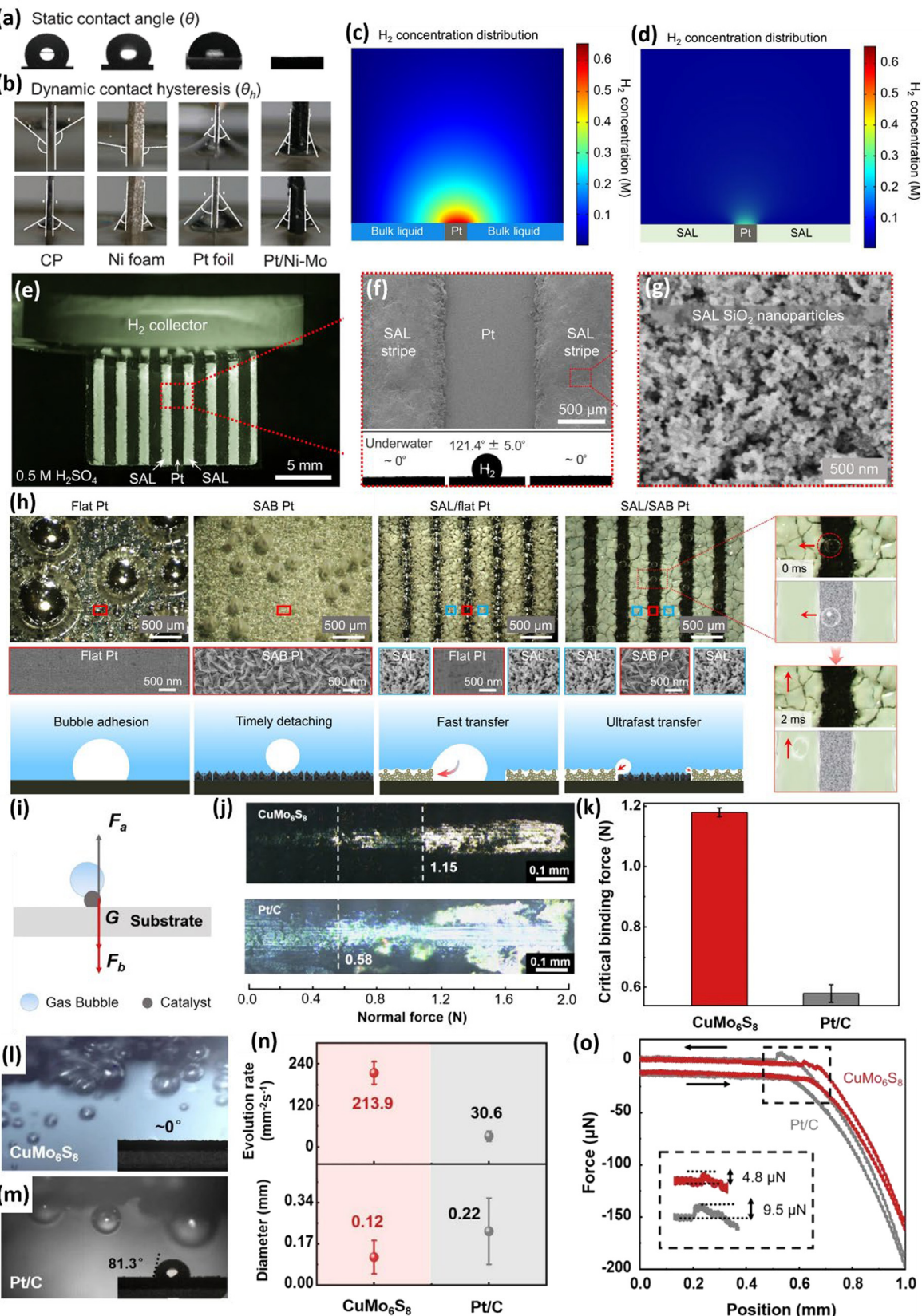
further observations of bubble evolution and migration at four different electrodes (Fig. 13h), the best combo: super-aerophilic (SAL) SiO₂ + super-aerophobic Pt) and again demonstrated their ultra-fast bubble transfer by exploiting the difference in bubble adhesion strength between different catalysts. Although this strategy performs a fair job of timely removing the H₂ off the surface of the HER-active material (e.g., Pt), it does so at an expense of about half of the area that could have been loaded with active Pt. In another work, annealing MoS₂/CF under Ar/H₂ resulted in a Chevrel phase CuMo₆S₈/Cu electrode that was highly stable for HER at large J including – 500, – 1000 and – 2500 mA cm⁻² [138]. As shown in Fig. 13i, in the simplified force analysis model, the interfacial bonding force between the catalyst and the support (F_b) will be balanced with the gravity of the catalyst itself (G) and the interaction between the catalyst and the bubble (F_a). The authors confirmed one of the reasons for the high electrolysis durability of CuMo₆S₈/Cu by using micro scratch tester and optical microscopy (Fig. 13j and 13 k), the high F_b . With *in situ* optical microscopy observations, CuMo₆S₈/Cu is more hydrophilic than Pt/C (Fig. 13l and 13 m), and small bubbles on the Pt/C surface typically aggregate into bigger bubbles while small bubbles on the CuMo₆S₈/Cu surface directly escape the catalyst surface. Smaller-diameter bubbles are produced more frequently on the surface of CuMo₆S₈ (Fig. 13n). According to the authors' derivations, the difference in interfacial energy pre- and post- the gas attachment determines whether the bubble can adhere to the catalyst, *i.e.*, the firmness of the gas adhesion. CuMo₆S₈/Cu has smaller transport overpotential (η_{trans}) as well as quicker bubble evolution kinetics than Pt/C. This is due to the smaller F_a of CuMo₆S₈/Cu (Fig. 13o). That is, the high stability of CuMo₆S₈/Cu is provided by a sufficiently high F_b and a low F_a . It is easy to predict that the same applies to seawater electrolysis. Active, selective and durable catalysts with near-zero adhesion to the bubbles and great adhesion to the substrate remain to be developed for both direct and indirect seawater electrolysis.

Shen et al. [139] compared the bubble traffic on three different OER catalysts including hierarchical Ni-Fe (oxy)hydroxides nanosheets on FF (FF-FN), RuO₂/FF and FF. The best-performance FF-FN electrode was far superior to the two other electrodes in terms of aerophobic nature (Fig. 14a, underwater gas bubble CA, CA_{bubble} of 150°) and hydrophilicity (Fig. 14b, CA_{H2O} of 0°). Moreover, the bubbles produced on FF-FN are also the smallest (Fig. 14c-e) and therefore the fastest to release from the catalyst surface. Similarly to FF-FN developed by Shen et al, compared to NiCo@C/CF with a larger CA_{H2O} of 102° and a smaller CA_{bubble} of 137°, NiCo@C/MXene/CF (CA_{H2O} of 57° and CA_{bubble} of 153°) featured a much better ability to release gas and displayed much more stable chronopotentiometric V-t curve (*i.e.*, less accumulation and timely detachment of bubbles,) as a result of more successfully mass diffusion and less bubble shielding effect (Fig. 14f and 14 g) [104]. As a result, the NiCo@C/MXene/CF acted as a more preferable HER electrode in alkaline seawater. The two work thus clearly show that for continuous seawater splitting at large J , gas-releasing ability (aerophobic properties) and availability of electrode surface/interface to H₂O (water adsorption capacity/rate) are necessary. The increase of the affinity of the electrode for H₂O (H-supplier) will boost

TABLE 4

Some representative SR electrodes, electrolyzers, sources of seawater and seawater treatment before electrolysis, etc.

Catalytic materials	Substrate (Support)	Surface wettability	Electrolyzer (membrane)	Seawater	Seawater treatment	Stability	Ref.
CeO ₂ /α-MoC/β-Mo ₂ C [36]	Carbon cloth	N/A	H-cell with Nafion membrane	Marine Park Beach, Qingdao, China, pH = 7.95	ISS (visible impurities and deposition are filtered)	100 h@ -1000 mA cm ⁻²	Appl. Catal. B Environ. 317 (2022) 121,774
NiCoN Ni _x P NiCoN [116]	NF	N/A	Single chamber cell (without membrane)	Galveston Bay near Houston, Texas, USA, pH ≈ 7.2	Direct electrolysis	24 h@ -10 mA cm ⁻²	ACS Energy Lett. 5 (8) (2020) 2681–2689
Co ₁₆ Mo ₁₆ P ₂₄ @C, Yellow Sea, China, pH = 8.35	ISS (visible impurities and deposition are filtered)			polyoxometalates (POMs) [118] 12 h@about - 20 mA cm ⁻²	Carbon paper Energy Environ. Sci. 10 (2017) 788–798	N/A	N/A
Mn-doped NiS ₂ [121]	NF	N/A	Single chamber cell (without membrane)	Yellow Sea, China, pH = 7.9	Direct electrolysis	20 h@about - 15 mA cm ⁻²	J. Mater. Chem. A 7 (44) (2019) 25628–25640
Single-atom Pt anchored on CoP [122]	Carbon fiber cloth	N/A	N/A	Shau Kei Wan, Hong Kong, China, pH ≈ 8.5	Direct electrolysis	24 h@about - 0.5 V _{RHE}	J. Mater. Chem. A 8 (2020) 11246–11254
Rh ₂ P/N, P co-doped porous carbon [128]	GCE or carbon paper	N/A	N/A	Yellow Sea, China, pH = 7.8	Direct electrolysis	18 h@about - 300 mA cm ⁻² 24 h@about - 200 mA cm ⁻²	J. Mater. Chem. A 8 (2020) 25768–25779
VS ₂ [131]	amorphous carbon (AC)	N/A	Single chamber cell (without membrane)	Shores of Bay of Bengal in Nagapattinam, Tamil Nadu, India, pH = 8.25, salinity = 3.38%	Direct electrolysis	504 h@about - 250 mA cm ⁻²	ACS Sustain. Chem. Eng. 9 (25) (2021) 8572–8580
Fe-doped Co ₂ P [133]	Carbon paper	N/A	N/A	Yellow Sea, China, pH = 7.8	Direct electrolysis	48 h@about - 200 mA cm ⁻²	J. Energy Chem. 55 (2021) 92–101
Cu ₂ S@NiS@Ni/NiMo [134]	CF	Superaerophobic surface	MEA-based electrolyzer	1 M NaOH + seawater	ISS (alkaline seawater)	2000 h@500 mA cm ⁻² (not the MEA device), for the MEA device, 675 h@500 mA cm ⁻² (60 °C)	Adv. Funct. Mater. (2023) https://doi.org/10.1002/adfm.202302263

**FIG. 13**

Studies on the bubble release during hydrogen evolution (a) Static θ and (b) θ_h . Reproduced with permission from Ref. [136] Copyright 2021, John Wiley & Sons, Inc. (c,d) Simulation of H₂ diffusion. (e) Optical image and (f) SEM image and wettability of the SAL/flat Pt. (g) SAL strip consists of SiO₂. (h) H₂ bubble behaviors on four electrodes. Reproduced with permission from Ref. [137] Copyright 2023, American Association for the Advancement of Science. (i) Force analysis. (j) Photos of micro-scratches. (k) Critical adhesive forces. (l,m) Bubbles and contact angles. (n) Bubble release data. (o) Catalyst-bubble interfacial adhesion force. Reproduced with permission from Ref. [138] Copyright 2023, Springer Nature Limited American Association for the Advancement of Science.

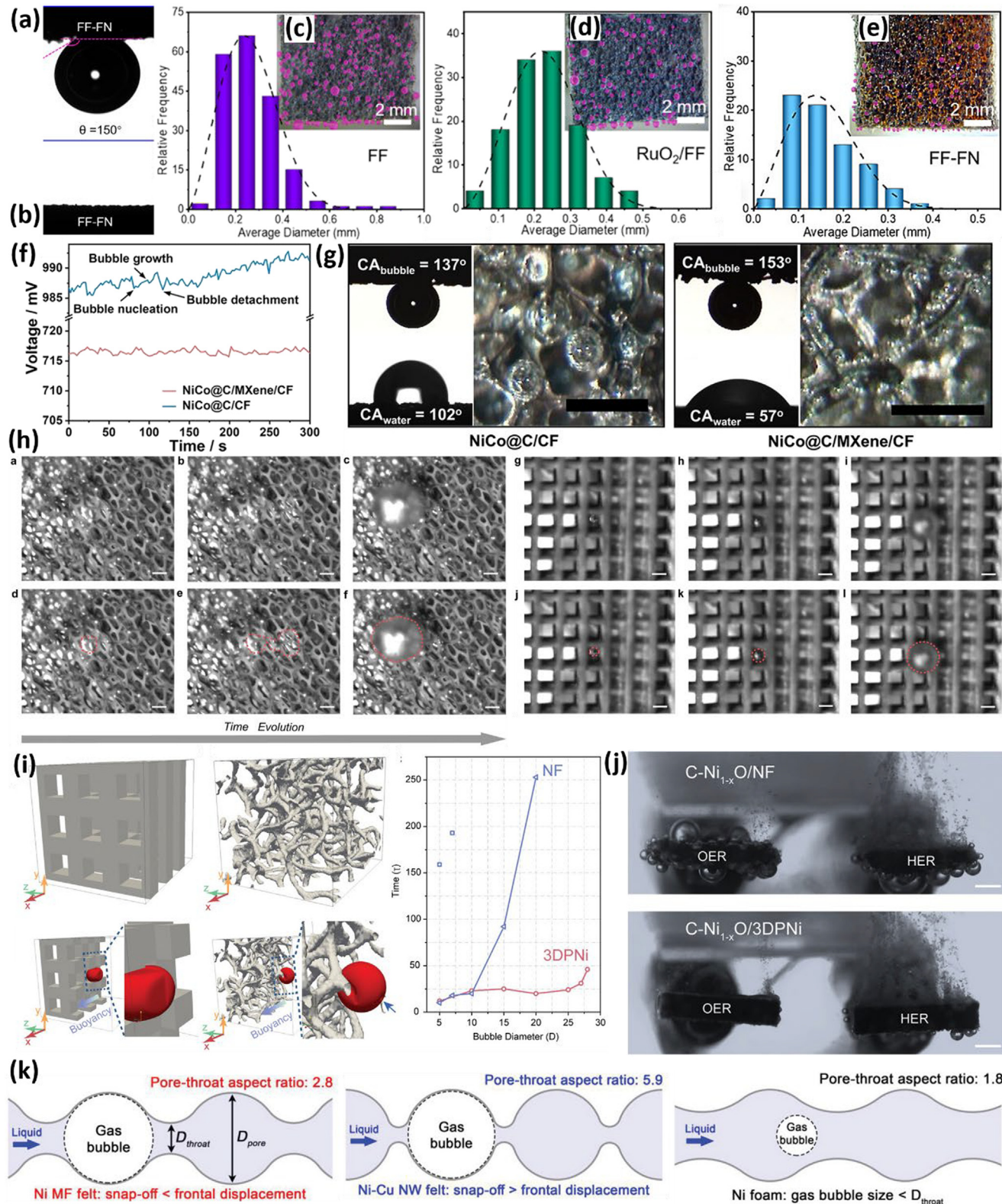


FIG. 14

Studies on the bubble release during H₂ evolution. (a) CA_{bubble} under water and (b) CA_{H2O} of FF-FN. Bubble diameter statistics of (c) FF (d) RuO₂/FN, and (e) FF-FN. Reproduced with permission from Ref. [139] Copyright 2022, John Wiley & Sons, Inc. (f) Stability comparison. (g) CA_{H2O} and CA_{bubble} on two different electrodes, with gas release images. Scale bars: 500 μm. Reproduced with permission from Ref. [104] Copyright 2021 Springer Nature Limited. (h) Bubbles pass through stochastic porous C-Ni_{1-x}O/NF electrode and C-Ni_{1-x}O/3DPNi with nicely controlled and periodic structures. Scale bars: 500 μm. (i) Structure model. The relative gas migration time through the two electrodes is correlated with the bubble diameter. (j) Gas coalescence and release. Scale bars: 2 mm. Reproduced with permission from Ref. [142] Copyright 2020, John Wiley & Sons, Inc. (k) How pore-throat aspect ratios influence bubble travel for different electrodes. Reproduced with permission from Ref. [143] Copyright 2023, John Wiley & Sons, Inc.

Volmer-Heyrovsky kinetics of the H₂ production in neutral/alkaline seawater electrolytes.

We then emphasize the great importance of understanding the porosity, tortuosity and spatial distribution of pores/channels of an electrode towards the authentically rational construction and design of porous electrodes that can withstand continuous seawater electrolysis at ampere-level J . The electrodes created by 3D printing techniques can have an organized electrode porous structure [140,141]. Additionally, since nucleation, growth, and detachment are all parts of the electrolysis-induced evolution of gas on the electrode, it is expected that the regular/periodic pore structure will help bubbles rise upward in the presence of buoyancy. That is, porous/channels of the electrode should be created in the same direction as the buoyancy to guide the bubble flow. Kou et al. [142] compared the bubble evolution behaviors and overall water splitting performances of two Ni substrates (NF and a 3D printed Ni lattice with periodic bubble flow channels) loaded with the same OER-active materials, *i.e.*, carbon-doped Ni oxide (C-Ni_{1-x}O) nanorods. Under high-speed camera observations (Fig. 14h), the C-Ni_{1-x}O/3D Ni is significantly effective at suppressing in-plane invasion and minimizing the pressure increase inside the 3D printed architecture. In contrast, for stochastic porous NF, certain pores in through-plane direction could be narrower than the ones in the in-plane direction. And bubbles would take a fancy to occupy a bigger pore due to the lower threshold entry pressure. This will inevitably result in bubbles staying in commercial NF with disordered pores for longer periods of time, and such bubbles will be subjected to a greater pressure increase before escaping the Ni electrode surface. Visualization tests with computational models (Fig. 14i) more intuitively reveal an increased bubble travel distance/time as well as the counteraction of the buoyancy effect in the NF at various gas bubble size. When the C-Ni_{1-x}O/3D Ni and C-Ni_{1-x}O/NF were used as bi-function electrodes (Fig. 14j), the 3D printed Ni was more effective in suppressing the bubble coalescence, mostly due to the higher probability of bubble collisions and merging in commercial NF. Accordingly, the C-Ni_{1-x}O/3D Ni not only attained a J of 1000 mA cm⁻² at the smaller η for both H₂ and O₂ production, but showed nice stability at a fixed J of 850 mA cm⁻² in 1.0 M KOH electrolyte at 80 °C. Similarly, Yang et al. [143] linked pore size and pore arrangement, bubble size, surface area, bubble traveling and bubble trapping, *etc.*, to water oxidation activities of three Ni electrodes (*i.e.*, NF, Ni microfibrous felt and Ni-Cu nanowire felt) and also proposed the general rule (Fig. 14k). The OER J followed the trend of NF < Ni-Cu nanowire felt < Ni microfibrous felt, but the ECSA-normalized OER J followed the trend of Ni-Cu nanowire felt < Ni microfibrous felt < NF. Though Ni-Cu NW felt had the highest ECSA, it exhibited 41 mV higher η than Ni microfibrous felt at the J of 100 mA cm⁻². Notably, the η of Ni-Cu nanowire felt ($\eta_{\text{Ni-Cu}}$) was initially smaller than that of Ni microfibrous felt ($\eta_{\text{Ni MFF}}$), but the $\eta_{\text{Ni-Cu}}$ quickly escalated to surpass $\eta_{\text{Ni MFF}}$ during pulse electrolysis measurements, indicating more serious bubble retention within Ni-Cu nanowire felt. The ratio of the pore diameter to pore-throat ($D_{\text{pore}}/D_{\text{throat}}$) can gauge how difficult it was to induce snap-off of bubbles to entrap bubbles in/on various electrodes. The higher $D_{\text{pore}}/D_{\text{throat}}$ (Fig. 14k) as well as a decrease in electrode permeability of the Ni-Cu nanowire felt indicates that

greater entrapment of bubbles limits its OER performance. Moreover, NF has the smallest ECSA despite having the smallest $D_{\text{pore}}/D_{\text{throat}}$. Only Ni microfibrous felt achieved the nice trade-off between the $D_{\text{pore}}/D_{\text{throat}}$ and surface area, thus showing the best activity and superb stability (25 A cm⁻² over 100 h). It is expected that the field of seawater electrolysis will require similar quantitative studies on the correlation between bubble entrapment/transport/removal phenomena and the efficiency of HER/OER catalysis. In addition, experimental results based solely on CA_{H2O} are insufficient since CA_{H2O} of certain electrodes that differ significantly in gas evolution behaviors are varied not much [143].

Summary and perspectives

Sufficiently efficient, long-term and scaled up electrolysis in impure natural seawater containing microbe, halides, various mono-, di-, and tri-valent ionic constituents (*e.g.*, Ca²⁺/Mg²⁺), suspended solids, micro-plastics, dissolved gases, *etc.* to make H₂ is a challenging yet rewarding task. Due to such complexity of seawater as well as extreme electrolysis conditions (*e.g.*, rich halide ions, a few OH⁻, industrial-level J and consequent local acidity/alkalinity), it is anticipated that seawater electrolysis will require catalytic systems that integrate the expertise of different disciplines/fields (*e.g.*, electrocatalysis, membrane science, corrosion science, bionics) and various effective engineering designs. Most of current H₂ production technologies from seawater remain in the lab-research stage, R&D for pilot-scale/large-scale level are not active worldwide, and we lack accurate/comprehensive techno-economic assessments of both DSS and ISS. Few SESs are powered by renewable energy sources (photovoltaic, wind, tidal, hydropower, *etc.*) in lab-scale studies, and on-site seawater-to-H₂ electrolysis is seldom coupled to downstream applications. Many catalyst design studies used processed seawater, and such seawater-based electrolytes are obtained by pre-filtration (solids and microbes) and further deep filtration (Mg²⁺, Ca²⁺, *etc.*) of seawater before entering the electrolyzer. Electrolytes used for scrutinizing catalyst performance in future work can be gradually switched from high-alkaline seawater to weakly alkaline seawater and to unprocessed natural seawater eventually.

For the anode side, voltage loss caused by local acidity or by Cl⁻ oxidation is different. In the worst case scenario, there will be a voltage loss spike results from simultaneous local pH drop and formation of corrosive chlorine species [58]. If only Cl⁻ oxidizes, the voltage will still rise. Note that acidic environments are conducive to Cl⁻ oxidation, so the electrode local alkalinity is necessary [27]. Fe-group elements are good HER-active and OER-active sites. For instance, Ni itself is capable of converting H₂O to O₂ (*e.g.*, NF) or H₂ (*e.g.*, Raney Ni). Various Ni-based oxides, nitrides, sulfides, *etc.*, and the composites are nice OER precatalysts. Ni is thus present in these catalysts in a variety of forms and naturally becomes the most common element for constructing seawater electrolysis electrodes. Lots of nicely built Ni-containing catalysts performed well in seawater media, including epitaxially *in situ* grown Ru cluster-Ni₃N heterostructure (30 November 2021) [144], NiIr LDH (10 May 2022) [73], amorphous FeCoNiS_x with reconstruction-derived crystalline/disordered

metal (oxy)hydroxide (30 September 2022) [77], etc. We point out that the combos of VIB (or VB) group elements and VIII group elements may achieve nice synergistic effects in seawater electrolysis. Take the combo of Cr and Co as an example, although CrO_x itself is not highly OER active, Cr seems to be a very good element to enhance performance of conventional OER catalysts. Cr exists in various states with different performance enhancement mechanisms. Taking Cr-doped CoP as a sub-example, in a work published in 2021, Cr doping endowed CoP more favorable H adsorption free energy and higher anti-oxidation ability, and such Cr-doped CoP was more active and stable than CoP for HER in H_2 -saturated 0.5 M H_2SO_4 solution [145]. In 2023, Song et al. [146] reported that Cr dopants ensured robust valence states of Co and alleviated the work function of Co_xP ($\text{CoP} + \text{Co}_2\text{P}$). Such Cr-doped Co_xP acted as both anode and cathode for 160-h alkaline seawater electrolysis. As another representative example, NiMoN nanorods is rather durable for alkaline water oxidation (e.g., NiMoN/NiFe LDH [147]) and even ASO (e.g., NiMoN@NiFeN [24]). Our group demonstrated that NiMoS_x microcolumn, hierarchically modified with NiFe LDH, also performed ASO at 500 mA cm⁻² for at least 500 h [148]. More future NiMo-based electrodes made from precursors like $\text{NiMoO}_4 \cdot x\text{H}_2\text{O}$ are likely to support longer ASO. There are many similar catalysts for seawater electrolysis as more instances, such as (1) $\text{Ni}_3\text{Se}_2@\text{MoO}_3/\text{CF}||\text{Ni}_3\text{Se}_2@\text{MoO}_3/\text{CF}$ (relatively obvious voltage loss at 100 mA cm⁻² in the 1.0 M KOH + seawater) [149], (2) Ni – Mo – Fe deposited on graphitic carbon felt (significant voltage loss at 50 mA cm⁻² within 20 h operation, electrolyte: filtered seawater, relatively obvious voltage loss at ~50 mA cm⁻² within 20 h operation, electrolyte: filtered seawater) [150], (3) MoN–Co₂N/NF||MoN–Co₂N/NF (significant voltage loss at 100 mA cm⁻² within 60 h operation, electrolyte: 1 M KOH + seawater) [151], (4) $\text{CoS}_2\text{-MoS}_2/\text{CC}$ (stable during stage stability test from 1 to 50 mA cm⁻² for a total of 50 min) [152]), (5) $\text{Ni}_3\text{N}/\text{W}_5\text{N}_4/\text{NF}$ (~9% anodic J loss for 45 h of electrolysis in alkaline seawater + plastics, initial J of ~200 mA cm⁻²) [153]. Therefore, although VIB (or VB) group elements can improve the stability and even activity of Fe group element-based catalysts in seawater according to many recent findings, the degree of improvement is unsatisfactory. How to make ultra-stable and efficient seawater electrolysis electrodes containing both Fe group elements and VIB group elements (even early transition metals including V, Nb, Mn, etc., and other elements such as Ag, Al, Pb, and Bi) will be one future direction in this field.

While reactions on both sides of seawater electrolysis have their own challenges, the anodic O_2 evolution can be replaced and the cathode cannot be replaced (unless AEM is employed with asymmetric electrolysis: H^+ production at anode) because producing H_2 is the most significant objective of seawater electrolysis. According to earlier studies, it is tricky to prevent forming precipitates. Even if the cathode consists of pure precious metals, as long as the electrolyte is unprocessed natural seawater, (e.g., Pt–IrO₂ for 10-h SR at a small J of about ~16 mA cm⁻², seawater source: Bohai Sea, pH 8.2 [154]), the electrode surface will definitely be masked by alkaline earth metal precipitation after a period of electrolysis. Most HER catalysts can only support natural SR with low J (e.g., $\text{Ag}_2\text{Se}-\text{Ag}_2\text{S}-\text{Co}$ carbonate hydroxide/NF for

a ~24-h test at about ~10 mA cm⁻², seawater source: Yellow Sea, China, pH = 7.2 [155]). For $\text{Cr}_2\text{O}_3\text{-CoO}_x$ reported by Guo et al. [27], when the pH was greater than ~9.3, precipitates can be produced near the CoO_x cathode, but the pH around the CoO_x was still lower than 9 even under a J of ~100 mA cm⁻², probably because the majority of OH^- produced by splitting H_2O is confined within the electrical double layer and only a small portion diffuses into the bulk seawater, which prevents the steep increase in pH. The presence of Lewis acid sites results in partial OH^- diffusion out of the EDL and neutralized by HCO_3^- into water molecules. A few cathodes were able to maintain natural SR relatively longer, but the J were too small (e.g., reconstructed $\text{CoC}_2\text{O}_4@\text{Mxene}/\text{NF}$ achieved 100-h test [156]) to determine the catalyst's resistance to the Ca/Mg precipitate formation and poisoning.

Thus, future study ought to focus on making catalysts to overcome this difficulty. Due to ample $\text{Ca}^{2+}/\text{Mg}^{2+}$, the solution pH on the cathode surface is expected to remain acidic/neutral/weakly alkaline. Note that the titration of Ca^{2+} in 1 M KOH can lead to fast increase in overpotential of Ni anode (~0.36 V at 0 μM Ca^{2+} , ~0.5 V at 500 μM Ca^{2+}) [22]. The research focus of developing future catalyst for natural SR is suggested to transition from simply designing catalysts with better conductivity and more active sites to build 3D structures with (1) enduring acidic/neutral surface microenvironment (prevent precipitates formation), (2) favorable water adsorption (achieve high access of H_2O to the inner Helmholtz plane above the catalytic surface/interface) [104], (3) great gas-releasing capability, and/or (4) positively charged electrode surfaces, etc.

Quite a few the latest and unconventional membrane-based electrocatalytic device designs, including the BPM-based natural seawater electrolyzer with Donnan exclusion for both Cl^- and Na^+ (asymmetrical electrolytes feeds) [58], the asymmetrical seawater electrolytic single-cell based on custom-made AEM (PTPIIm⁺) with a low HFR value [35], the Cl^- -selective membrane-based seawater electrolysis [42,57], the scalable, side-reaction-free and ultrastable seawater-to- H_2 conversion electrolyzer based on liquid–gas–liquid phase transition [28], the *in-situ* desalination-coupled device (feeding streams: 0.171 M NaCl or seawater, 1 M KOH, 1 M H_2SO_4) simultaneously equipped with BPMs, AEMs, and CEMs [29], the low-grade heat-based device (cathodic chamber: 0.5 M H_2SO_4 , anodic chamber: 1.0 M KOH + 1.0 M N_2H_4 , middle chamber: 4.0 M NaCl) equipped with AEM and CEM for H_2 production [54], etc., all yielded inspiring results. Research in this area looks forward to more unconventional, cutting-edge, practical seawater-based electrolysis devices, and it is fascinating to consider how such devices are going to evolve. For instance, since seawater impurities can pollute the membrane, and gases have the ability to cross the membrane (*i.e.*, gas crossover as potential explosive risks [157,158]), we may build the technology of uniquely designed membrane-less SES with lower cost, higher safety and efficiency [159]. Such SES can be developed on the basis of previous membrane-free fresh water electrolytic cell [160]). In following sub-sections, we divide more perspectives into 10 points to emphasize the easily overlooked research opportunities as well as to encourage more ground-breaking future work.

Lab-scale to pilot-scale

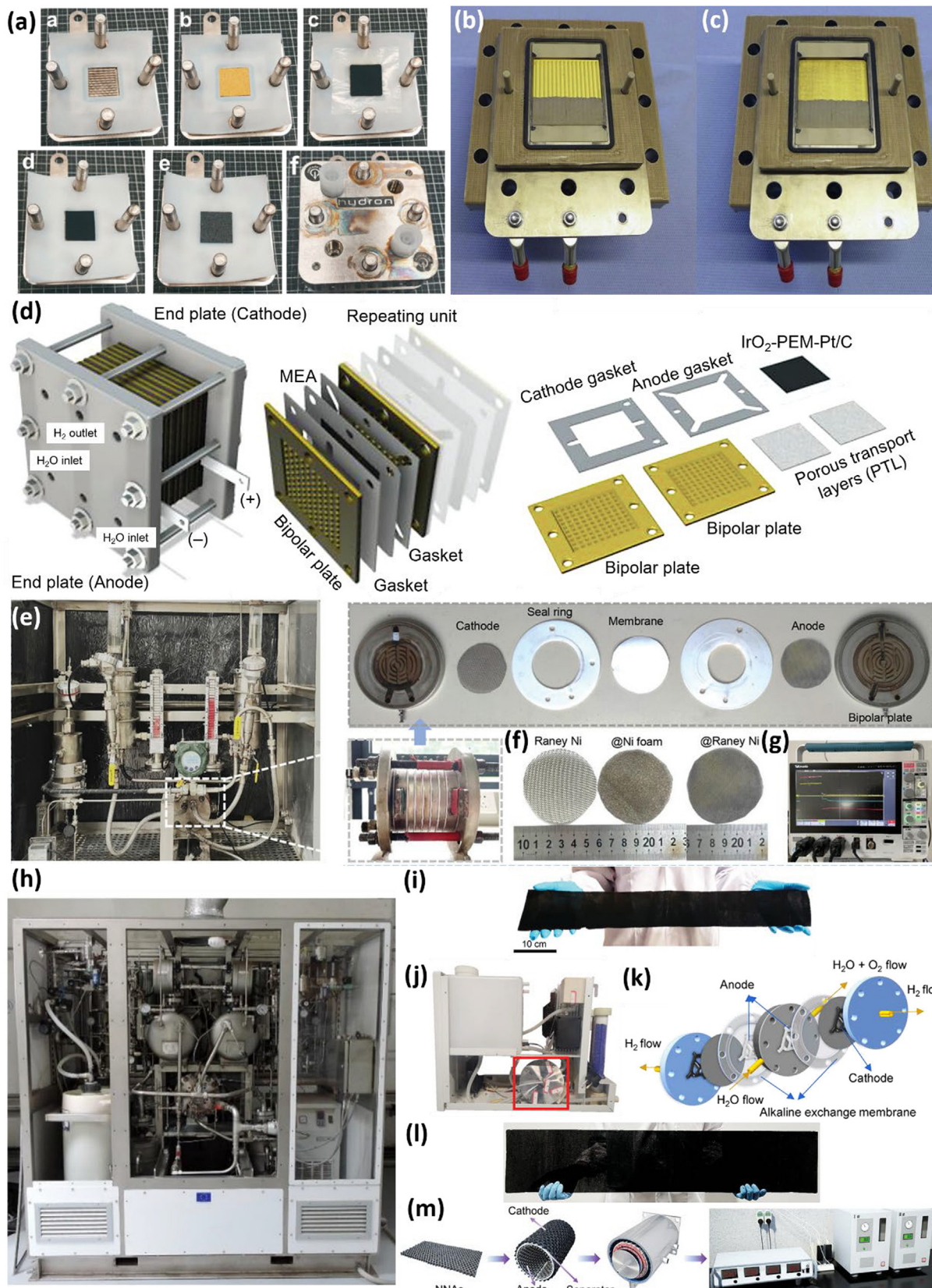
Various flow-type membrane-based electrolyzers were employed to probe the viability of electrodes for larger-scale seawater electrolysis. In order to clearly demonstrate this type of lab-scale flow electrolytic cell, actual photos and schematic drawings of such devices (Fig. 15a-d) from three published articles are chosen for demonstration. Peter Strasser and his team demonstrated detailed cell assembly processes (Fig. 15a) [48], including the arrangement and sequential assembly of gasket, porous transport layer (e.g., Au-coated Ti felt), MEA (e.g., AEM with catalysts spray-coated on both sides), another gasket, carbon-based gas diffusion layer, etc. These cell components can be clamped together with two endplates. For such membrane-based cells, factors including flow channels (with or without such channels, see Fig. 15b and 15c) [161], flow-rates, porous transport layer thickness, etc., may affect the performance, especially at ampere-level J . Fig. 15d also showed that porous transport layers, gaskets, and bipolar plates are assembled symmetrically on both sides with MEA as the center [162]. Repeating such units can attain larger H₂ production yield. A dual-cation-defects regulated NiFe catalysts, derived from Co, Mo co-doped NiFe LDH, operated in practical industrial electrolyzer system (Fig. 15e-g) with an energy consumption of $\approx 4.6 \text{ kWh m}^{-3} \text{ H}_2$ [163]. We point out that although work on empirical models, simulations and experimental analysis, etc., of pilot-scale PEM-based electrolyzers (Fig. 15h) [164,165] and alkaline water electrolyzers [166–168] were studied by different groups, semi-empirical models, data, and demonstrations of corresponding industrial-scale SESs have never been explored, which may determine the best operating conditions (e.g., temperature, J , seawater flow rate) and cell components. We selected two representative work in which the electrocatalyst capable of electrolyzing 1.0 M KOH [169] or alkaline saline water (1 M KOH and 0.5 M NaCl [136]) was prepared on a large scale (Fig. 15i and 15 l) and then assembled into different commercially available H₂ generators (Fig. 15j and 15 k and 15 m). Both two catalysts shared the same kind of substrate, NF, and were 3D array, i.e., NF supported Ni nano-pyramid array with low-coordinated atoms (22 April 2023 [169]) and Pt NPs anchored on dense Ni-Mo micro-column array/NF (12 March 2021 [136]). Notably, the Ni nano-pyramid array showed comparable HER performance to commercial Pt/Ti when used as cathode in asbestos diaphragm-based commercial H₂ generators (Fig. 15m) for 60-day test. Moreover, the Pt/Ni-Mo/NF cathode and a NF anode were assembled into an MEA electrolytic cell containing two HER cells and two OER cells that be separated by commercial AEM (Fig. 15j and 15 k). The Pt/Ni-Mo/NF far exceeded many Pt

group metal-based and non-precious metals-based catalysts for HER, and Pt/Ni-Mo/NF costs much less than them. Large-scale catalyst fabrication and the integration of catalysts into electrolysis stacks that are economically competitive should be an important direction in the seawater-to-H₂ conversion field.

There are actually some good seawater electrolysis catalysts that have emerged (e.g., NiFe hydroxide/NiS_x/NF [30], NiIr LDH-/sulfuric NF [73], NiMoS_x@NiFe-LDH/NF [148], and NiFe-CuCo LDH/NF [170] for ASO). Such anodes can be operated at the J of 0.5–1 A cm⁻² for >500 h in alkaline seawater. Moreover, as one of the most advanced SO catalysts, Cr₂O₃-CoO_x@Ti fibre felt showed relatively good stability at 500 mA cm⁻² for 100 h in a PEM-based electrolytic cell with filtered natural seawater as the feeding electrolytes [27]. However, that work did not provide characterizations of the Cr₂O₃-CoO_x@Ti electrodes after the 100-h electrolysis. Thus, structural changes and the upper limit of stable electrolysis time of Cr₂O₃-CoO_x@Ti cannot be known. Besides, for stable electrodes tested in alkaline seawater, we do not know how stable they will be in natural seawater. On the other hand, since many HER catalysts, such as interface-rich NiP₂-FeP₂ coupled with Cu nanowires on CF [171], were evaluated in alkaline seawater, which include less Ca²⁺/Mg²⁺, there are actually not many genuine SR catalysts. Even the state-of-the-art Cr₂O₃-CoO_x catalyst cannot run for too long or at too high a J (at least 2 h at the J of – 100 mA cm⁻²) in filtered natural seawater since notable precipitates may generate [27]. Developing DSS catalysts, especially for the HER side, seems to be stuck in a predicament where major breakthroughs are difficult to achieve. It is still vital to continue designing catalysts with specific surface micro-environments (e.g., (1) local acidity, (2) local alkalinity achieved by extra Lewis acid layer on OER-active catalysts [27], (3) *in situ* re-adsorption of SO₄²⁻ [30], (4) placing H₂O-dissociating sites near catalytic sites [31], (5) modification of CER-inert sites on the catalyst surface [41,45], (6) developing a phys-chem active overlayer with smaller pzc on catalytically active materials [99], (7) metaborate ions [69], (8) selenate/selenite ions [83], (9) molybdate ions [148], etc.). In fact, for some known good performance catalysts (e.g., NiFe-CuCo LDH [170]), they should be assembled into the membrane-based electrolyzers (PEM-based, AEM-based, BPM-based, etc.) for thorough performance testing, which would in turn reflect their practical application potentials. Currently, power consumptions of AWE are generally higher than those of PEM electrolytic cells, and the performance of AEM cells is not as good as that of PEM cells. The total energy consumption of solid oxide cells is quite high due to the additional heating required, although the power con-

FIG. 15

Water (including seawater) electrolysis at various scales. (a) A single cell stack assembly. The MEA is sandwiched between a carbon-based GDL on the cathode and a gold-coated Ti felt. Reproduced with permission from Ref. [48] Copyright 2020, Royal Society of Chemistry. Lab-scale cells that have an active area of 25 cm², (b) with and (c) without flow channels. Note that for (b) the channel-less cell, flow-field plate is replaced by a set of sheets of Ti spacers. Reproduced with permission from Ref. [161] Copyright 2017, Elsevier. (d) Detailed and intuitive drawings of commercial PEM electrolysis stack. Reproduced with permission from Ref. [162] Copyright 2023, John Wiley & Sons, Inc. (e) Industrial AWE systems with enlarged view and AEM cell stack structure (bipolar plate, electrode, membrane, seal ring, etc.). (f) Photos of the OER electrodes (g) Oscilloscopes for cell voltage recording. Reproduced with permission from Ref. [163] Copyright 2023, John Wiley & Sons, Inc. (h) A 46 kW PEM electrolyzer. Reproduced with permission from Ref. [165] Copyright 2018, Elsevier. (i) 700 cm² Pt/Ni-Mo/NF. (j) H₂ generator with the (k) cell stack structure. Reproduced with permission from Ref. [136] Copyright 2023, John Wiley & Sons, Inc. (l) 2000 cm² Ni nanoarray electrode. (m) A step-by-step assembly procedure of the Ni cathode in a commercial electrolyser. Reproduced with permission from Ref. [169] Copyright 2023, John Wiley & Sons, Inc.



sumption is not high. Their longer electrolysis at ampere-level J in membrane-based electrolytic cells and the corresponding post-electrolysis electrode/membrane characterizations are highly useful for further development and scale-up effort in the area of practical natural seawater electrolysis. Moreover, there are still many engineering details to be investigated in those studies. A comprehensive semi-empirical model is now needed for the field of seawater electrolysis (natural seawater, or acidic seawater, or KOH + seawater). In addition, the pilot-scale alkaline seawater electrolysis based on these high-performance O_2 -evolving (H_2 -evolving) electrocatalysts and the corresponding techno-economic analysis are worth studying.

Long-term stability tests

Considering that most of the work only offers electrolysis curves (V - t or J - t) for a fixed duration (e.g., 100 h, 200 h, 500 h) as well as the morphology and crystal structure of the electrode after prolonged seawater electrolysis, the assessment of electrode stability should be improved. To improve the quality of stability tests, the following perspectives can be taken into consideration by future researchers. (1) Rather than a fixed-time stable V - t (or J - t) curve, the long-term electrolysis curve that clearly shows when and how the electrode is broken should be provided. In short, no matter how high the voltage (or J) and how long the electrolysis time is adopted by the researcher, the electrode should be deactivated in the stability test to know the true upper limit of the electrolysis lifetime of the designed electrode. (2) V - t curve and J - t curve are not the same (i.e., the decay of the J and the decay of the voltage are not of the same magnitude) because the J mostly climbs quicker with the voltage. The two curves should be contrasted with each other. (3) A lot of studies failed to real-time measure/monitor O_2 FE, H_2 FE and active chlorine species during the stability process, and such long-term stability tests without selectivity data cannot reflect whether the electrode has a potential value of large-scale application, because even if the voltage (or J) is relatively stable, the product selectivity may decrease. Therefore, it is not clear whether the corresponding electrode can be used for practical seawater splitting. A good example of simultaneous product monitoring during a long-term stability test is stable Cl_2 synthesis by single-site Ru in NaCl solution in a recent work: the product selectivity and the Ru leaching amount during a 1000-h of testing were recorded [172]. (4) Apart from the characterizations of the catalytically active phase change, the impurity composition of the tested electrodes should be fully examined.

Alkaline seawater electrolytes

The majority of SO catalysts were found efficient only in alkaline seawater, as making seawater alkaline truly hinders Cl^- electrooxidation. However, the cost of chemical calcareous deposition should be taken into account when calculating total costs of H_2 generation. Importantly, identifying anodes that are genuinely high-selective for OER in seawater is hard because of high OH^- concentrations in the alkaline seawater, which may outnumber the concentration of Cl^- in solution. Therefore, there should be a top-priority demand for genuine catalysts that can electrolyze natural seawater to produce H_2 .

The conventional idea is to (1) start with previously reported OER/HER electrodes with high gas-evolving performance in pH-near-neutral electrolytes and (2) re-design (upgrade) them for seawater electrolysis. This idea may not be bad, so we recommend some past reviews here, such as the progress of 3d transition-metal-based catalysts for neutral/near-neutral water electrolysis written by Anantharaj and Aravindan (2019) [173], the development of water oxidation electrocatalysts at mild pH written by our group (2019) [174], and advances in HER catalysis under neutral pH conditions written by Chen's group (2020) [175]. It is necessary to be aware that PBS solution generally beats Na_2SO_4 solution for better electrocatalytic activity. Many catalysts for neutral OER/HER reported in previous studies were electrolyzed in PBS, whereas seawater has few buffer ions. Moreover, salts in seawater has lots of chlorides, and Cl^- oxidation is easy to occur. How to obtain O_2 efficiently while repelling Cl^- (or to produce H_2 while inhibiting calcareous precipitation on the cathode) became a nearly unavoidable task for DSS.

Theoretically, anions are heavily adsorbed on anodes to lose electrons for conversion, yet anodes can be negatively charged to repel Cl^- . High concentrations of OH_{ads}/OH^- can be obtained by efficiently splitting the H_2O at local catalytic sites, thus avoiding the need to obtain OH^- from the bulk electrolyte. Correspondingly, if acidic seawater is not used, the cathode generates H_2 by direct cleavage of H_2O . To prevent the formation of Ca/Mg salts on the surface, cathodes should be built in a design that unfailingly prevents a local pH boost that would result from producing H_2 at high J . This is required since natural SR to H_2 at industrial-level J results in residual OH^- . It would be beneficial to inquire into (1) local and bulk pH changes [27], (2) atomic H consumption-generation balance, (3) the state of H^+ on the surface of the electrocatalyst [176], etc.

Electrode assembly

Catalytically active materials (CAMs) are typically deposited, coated or synthesized on various supports (substrates or membranes) for electrolysis. The sub-section begins by discussing such a unit mainly consisting of CAMs (e.g., NiFe LDH) and supports (e.g., NF) in the seawater electrolysis field, as the support is fundamentally critical to overall performances. Currently, heterogeneous CAMs based on supports including 2D (carbon paper, thin Ti plate, FTO, etc.) and 3D (e.g., various thick metal foams) types are being intensively explored. Owing to its macroporous feature, continuous 3D framework and intrinsically good OER activity, metallic NF has been frequently used in hosting CAMs [177]. Many papers calculate the J of NF-type seawater electrolysis catalysts based on geometric area, while the great specific surface area, internal capillary action and self-oxidation of NF may lead to an overestimation of the performance. For the assembly of MEA for SO/SR, we recommend a recent review paper by Wu and his co-workers [178].

NF and more sweater oxidation substrates in the future

In fact, the majority of recent good saltwater (seawater) oxidation electrodes including NiFe/ NiS_x -NF (2019) [30], S-(Ni,Fe)OOH/NF (2020) [179], CoVFeN@NF (2020) [180], NiFe-LDH@FeNi₂S₄/NF (2022) [81], Ni_3S_2 @Fe-NiP_x/NF (2022) [79], Fe-NiSOH/NF (2022) [59], NiOOH@FeOOH@NiFeP/NF (2022)

[181], Cr-doping Co_xP/NF (2023) [146], etc., employed NF as the substrate due to the 3D metallic structure of the NF and the good intrinsic OER activity of Ni itself. However, the lifetime of metallic NF is rather limited in untreated natural seawater due to severe seawater corrosion (NF dissolves in seawater under oxidation potentials and is thus easily broken). Recent work used more robust NF substrates without compromising the performance of NF, *i.e.*, sulfuric NF [73] and MnO₂ protected NF [31], to reinforce corrosion resistance of the Ni supported electrodes. Moreover, in alkaline environments, the mechanical strength of NF might not even be sufficient to afford practical seawater electrolysis. This all speaks to the need for more robust/durable substrates under SO conditions. At present, it is quite necessary to build physico-chemically enhanced NF by techniques like structure engineering, in accordance with actual electrolysis conditions in untreated natural seawater. Further, catalysts supported by NF are rarely evaluated in flow-type electrolyzers (PEM-based or AEM-based).

Designs of new-generations of metal foams (except for widely used NF, FF and NiFe foam), Ti-based substrates (except for widely used Ti foil, Ti plate, Ti mesh, Ti fibre felts), tin doped indium oxide (ITO), FTO, stainless steel mesh/plate, boron-doped diamond (BDD), and home-made substrates are imperative and desirable. For instance, while the Ti plate is stable during SO electrolysis, its own passivation is not conducive to long-term electrolysis (the *J* attained by the catalyst at the initial SO state may drop rapidly/gradually). The substrate itself can be regarded as a catalyst with low activity. If the substrate is not durable enough, the overall ultra-long electrolysis lifetime cannot be achieved. Developing next-generation substrates that are better than conventional substrates such as NF (a 3D OER-active network that is not resistant to acid, chlorides and other impurities), Ti fibre felts (stable but easily form passivation insulating layer), carbon fiber cloth (carbon oxidizes under electrode potential ranges of OER) and FTO (limited catalyst loading area). Future scientific research work is expected to aim at achieving industrial-level *J* seawater electrolysis by developing truly innova-

tive next-generation substrates (low-cost, high electrical conductivity, strong corrosion resistance, high mechanical strength, structures facilitating mass transport and ion diffusion, OER-active nature, *etc.*).

Ti substrates for seawater oxidation electrolysis

Though NF is a widely used catalyst substrate for ASO, and we encourage designing more robust upgraded NF, Ti ought to be the reasonable substrate choice if it is used for oxidation of untreated natural saltwater (UNS). Under truly harsh seawater electrolysis conditions (*i.e.*, direct electrolysis of UNS at large *J*), NF would quickly dissolve. There is almost no literature claiming to have achieved the long-term (over 500 h) industrial-level *J* electrolysis in UNS using NF substrate. The substrate must be strongly resistant to corrosion from chlorine species (Cl⁻, Cl₂, HClO, ClO⁻, *etc.*) in order to directly split UNS. Table 5, which lists state-of-the-art and commercial electrocatalytic Cl⁻ oxidation systems, reveals that Ti is the material most frequently utilized to create CER anodes. Commercial Cl₂-evolving anodes are usually made of Ti substrates and catalytic coating (Ru + mixed metal oxides). Probably, the top options for resisting Cl-species corrosion in UNS remain Ti-based electrodes.

However, the spontaneous passivation of Ti to TiO_x, especially under anodic voltages, lead to bad OER activities. It may be attributable to both Ti passivation and the catalyst's deactivation if a Ti/catalyst electrode shows *J* degradation during oxidation electrolysis. Coating the surface of Ti with a noble metal layer (Pt, Au, Ru, *etc.*) is a way to extend O₂ evolution lifetime of Ti-based electrodes under harsh water electrolysis conditions [182], but at the expense of employing costly metals. We need to consider: (1) whether it is more cost-effective to coat the noble metal layer on the substrate than to use alkaline seawater; (2) is coating Ti with noble metals more effective than directly coating the catalyst surface with OER-active noble metals (Ir, Ru, Pt, *etc.*) as the catalytic layer? In addition, since Ti substrate can be protected with a noble metal layer prior to the growth of active catalysts to prevent passivation, and this noble metal layer may also

TABLE 5

Some representative electrochemical Cl⁻ oxidation systems.

Electrodes	Electrolyte	Supplemental description	Ref.
Ti-Ru-Ir based DSA (Siontech Inc., Korea) [39]	1.0 M NaCl	pH = 1, 25 °C	Nat. Commun. 412 (2020) 11
Ti-Ru based DSA (Ru _{0.3} Ti _{0.7} O ₂ , Bayer Materials, Germany) [184]	3.5 M NaCl	pH = 3, 80 °C	Phys. Chem. Chem. Phys. 14 (2012) 7392–7399
Ti-Ru based DSA (Ru _{0.3} Ti _{0.7} O ₂ , Bayer Materials, Germany) [185]	3.5 M NaCl	pH = 3, 50 °C	Chem. Mater. 22, (2010), 6215–6217
Ti-Ru-Ir based DSA (Bayer Materials, Germany) [186]	4.0 M NaCl	pH = 3, 25 °C	Phys. Chem. Chem. Phys. 16, (2014), 13741–13747
RuTiO _x /antimony-doped tin oxide [187]	4.0 M NaCl	pH = 2, 25 °C	Energy Environ. Sci. 12 (2019) 1241–1248
Porous Ir/TiO ₂ [188]	4.0 M NaCl	pH = 3, 40 °C	ACS Catal. 3 (2013) 1324–1333
RuO ₂ /Nb:TiO ₂ -A200 [189]	0.6 M NaCl	pH = 6	ACS Catal. 11, (2021) 12423–12432
Ir-Co mixed oxide/Ti foil [190]	2 M and 10 mM NaCl	N/A	J. Ind. Eng. Chem. 108 (2022) 514–521
Ti/Ir _{0.8} Nd _{0.2} O _x [191]	5 M NaCl	pH = 2	ChemElectroChem 8, (2021) 1204
RuO ₂ @TiO ₂ nanosheet array/Ti [192]	5 M NaCl	pH = 2	Small 13 (2017) 1,602,240
Ti-plate-supported catalysts mainly consisting of RuO ₂ –TiO ₂ [193]	5 M NaCl	pH = 2	Nature 617 (2023) 519–523

lower the contact resistance [183], (3) can the noble metal layer be replaced by non-noble metal-based alloys/sulfides/other materials? In fact, inert layer formation may be suppressed somewhat or with less catalytic activity loss by improving the catalyst preparation on the Ti surface.

Additionally, there are a lot of grades of Ti materials available (e.g., China's titanium and titanium alloy plate and sheet standard: GB/T3621-2007), each type with the own chemical composition, mechanical strength, tensile property, corrosion resistance, price, etc. This indicates that Ti and Ti alloys can be upgraded towards a better substrate, and such improvement should take the characteristics of DSS/ISS into consideration. We expect innovative electrode/substrate designs based on Ti of high-performance (small E_{onset} , >99% O₂ FE, and ultralong lifespan), low-cost and potential to scale up the manufacturing process.

NiFe LDH, the benchmark seawater oxidation catalysts?

Homemade/commercial RuO₂ and IrO₂ are not exactly the same for each work, and the activity comparisons are rarely normalized by electrochemical surface area or catalyst mass. Many work supports the claim that OER activities of nanoscale NiFe LDH were on par with or even better than those of well-known RuO₂ and IrO₂ in the alkaline media (e.g., $\eta_{500} = 274$ mV & Tafel slope = 32.8 mV dec⁻¹ for NF/NiFe LDH, $\eta_{500} = 441$ mV & Tafel slope = 74.7 mV dec⁻¹ for NF/IrO₂ [194]), but the stability of NiFe LDH seems to be a big issue. Despite its high OER activity, NiFe LDH cannot survive in an acidic solution. Even in PBS (pH from 7 to 9), slow diffusion of proton acceptors (e.g., OH⁻) between layers also makes the LDH structure unstable, especially under high J [195]. The local acidification issue is obvious in buffer solution, and disappears under alkaline environments. H⁺ is released after H₂O participate in OER, while the relatively large size of HPO₄²⁻ does not diffuse into the interlayer in time like smaller OH⁻. In fact, when J are sufficiently high (e.g., 500 mA cm⁻²), the LDH may encounter both chlorine corrosion and local acidification. Thus, how the LDH structure collapse during SO should be investigated to determine the primary cause. If the issue is local pH drop within interlayers, it may be effective to delaminate multi-layered LDH into thinner nanosheets or to increase the interlayer spacing. If the issue is chlorine corrosion, it is necessary to selectively repel Cl⁻ from catalytic surfaces. Our group demonstrated that benzoate (BZ) anions intercalation expanded the layer spacing of NiFe LDH and simultaneously introduced negative charges to hinder Cl⁻ oxidation [196]. The resulting BZ-NiFe LDH performed much better than NiFe LDH in alkalized seawater, and the conventional NiFe LDH array was severely etched, with large amount of KCl appears after electrolysis. Our group synthesized amorphous NiFe LDH nanosheet array on a robust NiMoS_x microcolumn array as well, which was able to run relatively stable at the J of 500 mA cm⁻² for 500 h in alkalized seawater [148]. With the co-action of NiFe LDH and NiMoS_x, activity and stability were both achieved. In addition to introducing anions (e.g., PO₄³⁻-intercalated NiFe-LDH [197]) or sulfides (e.g., partial sulfidation Ni₂Fe-LDH to Ni₂Fe-LDH/FeNi₂S₄ heterostructure [81]), we need more strategies to improve the stability of NiFe LDH. Cao and his co-workers developed 3d-5d hybrid NiIr LDH [73], which was superior to NiFe LDH coun-

terpart for O₂ electro-production in 1 M KOH + seawater. After long-term SO, impurities from seawater or NF produced nanoparticles on the NiIr LDH nanosheets. Though the V-t curve is stable, the catalyst surface has undergone a relatively obvious change after the 650-h of SO, indicating changed active phase of the catalyst.

The ideal electrodes for SESSs?

An acceptable electrode must first be chemically stable in seawater, after which it must maintain stability throughout long-term SR/SO at ampere-level J , and ultimately it must stay active and stable for natural SR/SO. For ASO, Fe-group-metals- and sulfides-based high-surface-area structures (e.g., hierarchical NiFe hydroxide/NiS_x/NF [30]) exhibit high stability. Even without alkali for enhancing selectivity (i.e., no OH⁻ or in-sufficient OH⁻), some metal sulfides demonstrated good stability. As an nice example, hollow sphere CoFeS_x afford 700-h and 20-h stable saltwater oxidation in (1) 0.1 M KOH + 0.6 M NaCl solution and (2) simulated seawater (0.6 M NaCl + 0.03 M SO₄²⁻ + 0.06 M Mg²⁺ + 0.01 M Ca²⁺), respectively [198]. This study well confirmed that *in situ* derived anticorrosion layer on CoFeS_x enabled a selectivity in favor of O₂ generation even when OH⁻ in electrolytes are not quantitatively superior to Cl⁻. Additionally, despite the fact that electrocatalysis takes place at the surface, multi-scale synergistic engineering (e.g., Cl⁻ repelling layer + synergistic co-action of Co and Fe + hollow structure-based bulk-level mass transfer improvement for CoFeS_x) to optimize performance is highly needed. Therefore, a genuine SO electrode may have the following design advantages/satisfy the following requirements: (1) improved bulk properties (conductivity, corrosion resistance, specific surface area, etc.), (2) optimal bulk-surface area volume ratio (no wasted bulk area), (3) Cl⁻-rejection ability, (4) higher intrinsic O₂-evolving activity (having sites that tend to synthesize O₂ and disfavor CER), and (5) nicely constructed local electrostatic field environments that guarantee a OH⁻-rich state and rapid OER kinetics in the Helmholtz layer [199]. Moreover, to further assist catalysts (e.g., sulfides) to make full use of H₂O in seawater for O₂ synthesis, (6) introducing extra sites that can facilitate H₂O adsorption/dissociation, like strong-proton-adsorption sites/Lewis acid sites [27,31], would be a viable option. The composite anode shall suppress Cl⁻ attack and make OH⁻ in large quantities near the local catalytic sites. (7) In addition, a superaerophobic/superhydrophilic anode [104,139], with uniform/consistent pores and channels [142] and optimal pore-throat aspect ratio [143], should be a precondition for easy bubble traffic at industrial-level J . (8) Last but not least, whether the electrodes are tested using MEA or other techniques, the cost of the electrodes must be considered. On the other hand, since the majority of previous SR works used alkaline seawater that contains less Ca²⁺/Mg²⁺, what is most required for SR is a genuine catalyst that can be electrolyzed in natural seawater at high J for months and even for years. While some metal phosphide-based electrodes [118,128] and alloyed Pt-Mo electrodes [200] appear to be able to more enduringly convert natural seawater into H₂ at relatively larger J than many metal sulfides [132] and metal nitrides-based electrodes [115], their performances still fall short of what are needed for practical use. Note that even a 3D nanoarray of NiCoN|Ni_xP|NiCoN with rich catalytic sites suffered from

notable and quick voltage loss at a small J of -10 mA cm^{-2} [116], indicating that conventional design strategies do not solve problems encountered in natural SR, and that the development of HER in this field is looking for pertinent strategies. Our section "Recent HER electrodes in natural seawater" makes it clear that there are no catalysts capable of achieving year-long natural SR electrolysis at high J .

OER versus CER

Electrochemical natural seawater oxidation (eNSO) catalysts are available (e.g., $\text{Cr}_2\text{O}_3\text{-CoO}_x$, supported by Ti fibre felt, which afforded a 100-h test at 500 mA cm^{-2} in PEM electrolyzer [27]), yet the corresponding tests on measuring H_2 FE and O_2 FE only last for 10 h (for $\text{Cr}_2\text{O}_3\text{-CoO}_x@\text{Ti}$), and there is no post-tests characterization of electrodes and PEM after 100-h reaction. Despite the best eNSO performance, 100-h electrolysis is not enough to show the practicability. Some other catalysts were evaluated in natural seawater with shorter time and smaller J , like TiO_2 array supported MoS_2 nanosheets with single atomic Ni and Ni phosphate clusters ($\text{Ni}_{\text{SA}}\text{-Ni}_{\text{Pi}}/\text{MoS}_2/\text{TiO}_2$) which showed a slight decay in only 15 h of electrolysis in natural seawater and the initial J of only $\sim 30 \text{ mA cm}^{-2}$ [201]. Thus, eNSO-to- O_2 is far more challenging than one might think, because depleting Cl^- in seawater is hard, so Cl^- always interferes with OER. That's why we can see that apart from catalyst design [27] and membrane optimization (e.g., electrochemical seawater-to- H_2 conversion using the PTPI Im^+ -based AEM [35]), the requisite costs of achieving long-time selective O_2 generation are concentrated alkaline seawater solutions (like 1 KOH + seawater) or the use of extra membranes (e.g., ion-selective hydrophilic semipermeable membrane-based seawater electrolysis reported by Xie et al. [28]; *in-situ* desalination-coupled stack device demonstrated by Kim et al. [29]).

Once OH^- dominates anion concentrations, high O_2 FE is totally predictable and in-sufficient to reflect the real selectivity of the catalyst. In other words, when Cl^- contents are equal to or much higher than OH^- contents, a catalyst still shows considerable O_2 evolution activity, and the corresponding catalytic sites are the ones that really tend to produce O_2 . More future research work is needed to fundamentally and properly define the competitive adsorption and subsequent activation of water/ OH^- and Cl^- on catalysts. A work showed that lithiation/delithiation treatments provided RuO_2 7 Å nanoscopic channels that enabled $^{*}\text{OOH}$ activation rather than $^{*}\text{Cl}$ activation in seawater [202]. It is known that compared to Cl^- , OH^- is a harder base, and phosphate ion group improved water (including alkaline seawater) splitting activity of $\text{NiCo}(\text{HPO}_4)_2@\text{Ni}_3\text{N}/\text{NF}$ [203], via preferential adsorption of OH^- . Similarly, partially crystalline NiFe-LDH excelled its crystalline counterpart for alkalized SO mainly because Cl^- would adsorb onto Ni^{2+} -rich crystalline planes more preferentially than OH^- , while OH^- would primarily adsorb onto the Ni^{3+} -rich boundaries [204]. In another work, $(\text{W}_2\text{O}_7)^{2-}$ intercalation improved Lewis acidity of NiFe LDH and thus higher affinity to OH^- rather than Cl^- , and DFT calculations also confirmed easier OH^- adsorption upon inserting $(\text{W}_2\text{O}_7)^{2-}$ [25]. A CeO_2 -decorated NiFe LDH catalyst with $(\text{W}_2\text{O}_7)^{2-}$ intercalation afforded 100-h SO at 1000 mA cm^{-2} in alkaline seawater. By introducing similar harder Lewis acid sites as mentioned above

to catalytic surfaces, strong Lewis base OH^- (even if Cl^- is likewise a hard Lewis base) would be preferentially adsorbed on such sites, providing not only a locally alkaline environment, but speed-up O_2 evolution. It is thus expected that work in this field to modify various Lewis acid layer/sites (e.g., Cr^{3+} [27], Ti^{4+} , and other M^{x+}) will increase and achieve more improvements.

Influence of other anions (SO_4^{2-} , Br^- , and HCO_3^- , etc.)

The chemical and physical makeup of seawater is exceedingly intricate. For electrolysis of natural seawater, the most challenging aspects for the cathode and anode during the operation are surface calcareous precipitation and chloride/active chlorine corrosion, respectively. Such issues stem from quantitatively dominant $\text{Mg}^{2+}/\text{Ca}^{2+}/\text{Cl}^-$. Other ions with high concentrations include $\text{Na}^+/\text{SO}_4^{2-}$, which can be viewed as Na_2SO_4 solution that facilitates seawater electrolysis to some extent. Ma et al. [70] even directly added Na_2SO_4 into (simulated) seawater to afford negative charged anodic surface and thus longer SO time. As the concentration of SO_4^{2-} increases (0 M, 0.125 M, 0.25 M, 0.5 M), the anode working lifespan gradually increases, indicating that the effect of SO_4^{2-} on performance is closely related to the concentration. In fact, except for Cl^- , $\text{Mg}^{2+}/\text{Ca}^{2+}$, Na^+ , and SO_4^{2-} , a wide variety of other ions with lower concentrations are present in seawater (e.g., K^+ , Br^- , Sr^{2+} , F^- , and HCO_3^-) [28], and the exact effects of these ions on the activity/stability of the catalyst/membrane during electrolysis remain unclear. There are still few comprehensive work examining the effect of these low-concentration ions like F^- on seawater electrolysis catalysts, which is to be expected in future studies.

Learn from ocean life for electrocatalytic system design

Although *in situ* desalination coupled electrolysis, reverse osmosis treatment followed by electrolysis, or filtering Ca/Mg salts followed by alkaline seawater electrolysis can afford relatively stable H_2 synthesis due to environments with relatively few impurities, almost no catalysts can withstand the harsh natural seawater splitting conditions (e.g., ultralong industrial-level J electrolysis operation, interference of impurities in untreated seawater, local high acidity).

In fact, the ocean with great levels of dissolved salt directly and indirectly nurtures a huge variety of life. The ability of sea creatures (plants, animals, and microbes) to adapt to the ocean where they reside for generations has reached the most affordable and dependable levels, so it would be attractive learn from the ocean life toward retrofitting existing electrocatalytic systems and innovating new ones. Take a deep dive into the structure's functioning (*i.e.*, physical and biological characteristics) of various marine organisms (e.g., osmoregulation in fish, the skin structure of a shark, chemical structure and shape of corals) may help us solves tricky problems that cannot be solved using conventional design strategies. Therefore, learning from these ocean natives (from Open Ocean, deep-sea, coastal, *etc.*) may be beneficial to designing efficient and stable seawater electrolysis systems with new general mechanisms.

CRediT authorship contribution statement

Jie Liang: Investigation, Writing - original draft, Writing - original draft, Writing - review & editing. **Zixiao Li:** Investigation.

Xun He: Investigation. **Yongsong Luo:** Investigation. **Dong-dong Zheng:** Investigation. **Yan Wang:** Investigation. **Ting-shuai Li:** Investigation. **Binwu Ying:** Investigation. **Shengjun Sun:** Investigation. **Zhengwei Cai:** Investigation. **Qian Liu:** Investigation. **Bo Tang:** Supervision, Funding acquisition. **Xuping Sun:** Supervision, Funding acquisition.

Data availability

Data will be made available on request.

Declaration of Competing Interest

The authors declare that they have no known competing financial interests or personal relationships that could have appeared to influence the work reported in this paper.

Acknowledgments

This work was supported by the Free Exploration Project of Frontier Technology for Laoshan Laboratory (No. 16-02) and the National Natural Science Foundation of China (Nos. 22072015 and 21927811).

References

- [1] Hydrogen: A renewable energy perspective (IRENA, 2019).
- [2] The Future of Hydrogen (IEA, 2019).
- [3] Global Hydrogen Review (IEA, 2021).
- [4] R.F. Service, *Science* 324 (5932) (2009) 1257.
- [5] N. Mac Dowell et al., *Joule* 5 (10) (2021) 2524.
- [6] M. Chatenet et al., *Chem. Soc. Rev.* 51 (11) (2022) 4583–4762.
- [7] R. Sofi et al., *Sci. Total Environ.* 859 (2023) 160288.
- [8] E. Jones et al., *Sci. Total Environ.* 657 (2019) 1343.
- [9] Annual Percentage Change in Renewable Energy Generation (2021). (Our World in Data). <https://ourworldindata.org/grapher/annual-change-renewables>
- [10] I. Staffell et al., *Energ. Environ. Sci.* 12 (2) (2019) 463–491.
- [11] W. Tong et al., *Nat. Energy* 5 (5) (2020) 367.
- [12] J. Liu et al., *Angew. Chem. Int. Ed.* 61 (45) (2022) e202210753.
- [13] F. Dingenen, S.W. Verbruggen, *Renew. Sustain. Energy Rev.* 142 (2021) 110866.
- [14] B. Xu et al., *Green Chem.* 25 (10) (2023) 3767–3790.
- [15] X. Xiao et al., *Small* 18 (11) (2022) 2105830.
- [16] F. Zhang et al., *Trends Chem.* 3 (6) (2021) 485.
- [17] S. Khatun et al., *J. Mater. Chem. A* 9 (1) (2021) 74–86.
- [18] Q. Zhou et al., *Mater. Today Phys.* 26 (2022) 100727.
- [19] S. Dresp et al., *ACS Energy Lett.* 4 (4) (2019) 933–942.
- [20] M. Maril et al., *Int. J. Hydrog. Energy* 47 (6) (2022) 3532.
- [21] S. Jiang et al., *Catalysts* 12 (3) (2022) 261.
- [22] A.J. Esswein et al., *Energy and Environmental Science* 4 (2) (2011) 499.
- [23] S.-H. Hsu et al., *Adv. Mater.* 30 (18) (2018) 1707261.
- [24] L. Yu et al., *Nat. Commun.* 10 (1) (2019) 5106.
- [25] M. Li et al., *Appl. Catal. B Environ.* 330 (2023) 122612.
- [26] N. Nie et al., *Appl. Catal. B Environ.* 322 (2023) 122100.
- [27] J. Guo et al., *Nat. Energy* 8 (3) (2023) 264–272.
- [28] H. Xie et al., *Nature* 612 (7941) (2022) 673–678.
- [29] B.-J. Kim et al., *Desalination* 551 (1) (2023) 116431.
- [30] Y. Kuang et al., *Proc. Natl. Acad. Sci.* 116 (14) (2019) 6624–6629.
- [31] N. Wang et al., *Adv. Mater.* 35 (2023) 2210057.
- [32] L. Wu et al., *Appl. Catal. B Environ.* 294 (2021) 120256.
- [33] A.R. Zeradjanin, *Nat. Catal.* 6 (2023) 458–459.
- [34] X. Zhang et al., *Inorg. Chem. Front.* 10 (2023) 3103–3111.
- [35] M.L. Frisch et al., *ACS Energy Lett.* 8 (5) (2023) 2387–2394.
- [36] M. Hu et al., *Appl. Catal. B Environ.* 317 (2022) 121774.
- [37] X. Kang et al., *Nat. Commun.* 14 (2023) 3607.
- [38] F. Dionigi et al., *ChemSusChem* 9 (9) (2016) 962–972.
- [39] T. Lim et al., *Nat. Commun.* 11 (1) (2020) 412.
- [40] D. Jin et al., *Adv. Funct. Mater.* 33 (2023) 2301559.
- [41] E. Enkhtuvshin et al., *Adv. Funct. Mater.* 33 (2023) 2214069.
- [42] S.S. Veroneau, D.G. Nocera, *Proc. Natl. Acad. Sci.* 118 (9) (2021).
- [43] W. Fujita et al., *J. Electrochem. Soc.* 170 (3) (2023) 036507.
- [44] J.G. Vos, M.T.M. Koper, *J. Electroanal. Chem.* 819 (2018) 260–268.
- [45] J.G. Vos et al., *J. Am. Chem. Soc.* 140 (32) (2018) 10270–10281.
- [46] Y. Yokoyama et al., *Chem. Lett.* 49 (2) (2020) 195–198.
- [47] W. Zhang et al., *Chem. Rev.* 123 (11) (2023) 7119–7192.
- [48] S. Dresp et al., *Energ. Environ. Sci.* 13 (6) (2020) 1725–1729.
- [49] J. Chang et al., *Adv. Mater.* 33 (2021) 2101425.
- [50] T. Zhao et al., *Small* (2023), <https://doi.org/10.1002/smll.202208076>.
- [51] R. Pärnamäe et al., *J. Membrane Sci.* 617 (2021) 118538.
- [52] S.Z. Oener et al., *Science* 369 (6507) (2020) 1099–1103.
- [53] P.K. Giesbrecht, M.S. Freund, *Chem. Mater.* 32 (19) (2020) 8060–8090.
- [54] F. Sun et al., *Angew. Chem. Inter. Ed.* 61 (31) (2022) e202203929.
- [55] L.-C. Janie et al., in: *Energy Conversion-Current Technologies and Future Trends*, IntechOpen, Rijeka, 2018, pp. 56–70.
- [56] Z.M. Bhat et al., *Joule* 4 (8) (2020) 1730–1742.
- [57] S.S. Veroneau et al., *ACS Appl. Energy Mater.* 5 (2) (2022) 1403–1408.
- [58] D.H. Marin et al., *Joule* 7 (4) (2023) 765–781.
- [59] C. Huang et al., *Energy and Environmental Science* 15 (11) (2022) 4647–4658.
- [60] E. Asghari et al., *Curr. Opin. Electrochem.* 31 (2022) 100879.
- [61] C. Wang et al., *Nanoscale* 13 (17) (2021) 7897–7912.
- [62] J. Li et al., *Int. J. Hydrog. Energy* 47 (69) (2022) 29685–29697.
- [63] H. Zhang et al., *J. Alloy. Compd.* 922 (2022) 166113.
- [64] S.-C. Ke et al., *Energy Fuels* 35 (16) (2021) 12948–12956.
- [65] S. Jiang et al., *Catalysts* 12 (2) (2022) 123.
- [66] X. Liu et al., *Adv. Energy Mater.* (2023), <https://doi.org/10.1002/aenm.202301438>.
- [67] J.-T. Ren et al., *Small* (2023), <https://doi.org/10.1002/smll.202300194>.
- [68] Y. Li et al., *Electrochim. Acta* 390 (2021) 138833.
- [69] J. Li et al., *Adv. Funct. Mater.* 31 (27) (2021) 2101820.
- [70] T. Ma et al., *Angew. Chem. Inter. Ed.* 60 (42) (2021) 22740–22744.
- [71] S.Y. Jung et al., *Appl. Surf. Sci.* 568 (2021) 150965.
- [72] T.u. Haq, Y. Haik, *Catal. Today* 400–401 (1) (2022) 14–25.
- [73] H. You et al., *J. Am. Chem. Soc.* 144 (21) (2022) 9254–9263.
- [74] A. Badreldin et al., *ACS Appl. Energy Mater.* 4 (7) (2021) 6942–6956.
- [75] A. Badreldin et al., *ACS Omega* 7 (6) (2022) 5521–5536.
- [76] J. Chen et al., *J. Mater. Chem. A* 11 (3) (2023) 1116–1122.
- [77] A. Wang et al., *Adv. Mater.* 34 (49) (2022) 2204247.
- [78] B. Cui et al., *Nano Res.* 14 (4) (2021) 1149–1155.
- [79] X. Luo et al., *Adv. Sci.* 9 (7) (2022) 2104846.
- [80] J. Sun et al., *Appl. Surf. Sci.* 567 (2021) 150757.
- [81] L. Tan et al., *Adv. Funct. Mater.* 32 (29) (2022) 2200951.
- [82] Y. Zhao et al., *Adv. Energy Mater.* 8 (29) (2018) 1801926.
- [83] W.H. Hung et al., *Mater. Today Energy* 19 (2021) 100575.
- [84] C.-X. Zhao et al., *Energ. Environ. Sci.* 15 (2022) 3257–3264.
- [85] T.X. Nguyen et al., *Adv. Funct. Mater.* 31 (48) (2021) 2106229.
- [86] T. Wang et al., *Adv. Mater.* 30 (27) (2018) 1800757.
- [87] K. Feng et al., *Appl. Catal. B Environ.* 325 (15) (2023) 122365.
- [88] S. Feng et al., *Catalysis Communications* 162 (2022) 106382.
- [89] T. Li et al., *Chem. Eng. J.* 460 (15) (2023) 141413.
- [90] Z. Chen et al., *Nano Res.* 13 (2020) 293–314.
- [91] C. Fu et al., *J. Colloid Interf. Sci.* 634 (15) (2023) 804–816.
- [92] K. Fujimura et al., *J. Appl. Electrochem.* 29 (6) (1999) 769–775.
- [93] H. Habazaki et al., *Scr. Mater.* 44 (8) (2001) 1659–1662.
- [94] N.A. Abdel Ghany et al., *Electrochim. Acta* 48 (1) (2002) 21–28.
- [95] Z. Wang et al., *Inorg. Chem.* 61 (38) (2022) 15256–15265.
- [96] T. Okada et al., *Langmuir* 36 (19) (2020) 5227–5235.
- [97] H. Abe et al., *Electrocatalysis* 10 (2) (2019) 195–202.
- [98] L. Bigiani et al., *Appl. Catal. B Environ.* 284 (2021) 119684.
- [99] T.P. Keane et al., *J. Am. Chem. Soc.* 145 (9) (2023) 4989–4993.
- [100] G. Capilli et al., *ACS Nano* 16 (8) (2022) 12488–12499.
- [101] A.A. Bhardwaj et al., *ACS Catal.* 11 (3) (2021) 1316–1330.
- [102] L. Zhuang et al., *Adv. Funct. Mater.* 32 (25) (2022) 2201127.
- [103] R.-Y. Fan et al., *Inorg. Chem. Front.* 9 (16) (2022) 4216–4224.
- [104] F. Sun et al., *Nat. Commun.* 12 (1) (2021) 4182.
- [105] H.-Y. Wang et al., *ACS Nano* 17 (11) (2023) 10965–10975.
- [106] Z. Li et al., *Adv. Funct. Mater.* (2023), <https://doi.org/10.1002/adfm.202304079>.
- [107] Z. Yu et al., *Adv. Funct. Mater.* 32 (38) (2022) 2206138.
- [108] L. Zhang et al., *Adv. Mater.* 34 (16) (2022) 2109321.
- [109] Z. Xiao et al., *Adv. Funct. Mater.* 33 (7) (2023) 2212183.
- [110] Y. Yang et al., *Green Chem.* 25 (10) (2023) 4104–4112.
- [111] Q. Mao et al., *Adv. Funct. Mater.* 32 (31) (2022) 2201081.
- [112] J. Zheng, *Appl. Surf. Sci.* 413 (2017) 72–82.

- [113] J. Zheng, *Appl. Surf. Sci.* 413 (2017) 360–365.
- [114] H. Li et al., *Journal of Materials Chemistry A* 4 (17) (2016) 6513–6520.
- [115] H. Jin et al., *ACS Nano* 12 (12) (2018) 12761–12769.
- [116] L. Yu et al., *ACS Energy Lett.* 5 (8) (2020) 2681–2689.
- [117] X. Wu et al., *Adv. Energy Mater.* 9 (34) (2019) 1901333.
- [118] Y.-Y. Ma et al., *Energ. Environ. Sci.* 10 (3) (2017) 788–798.
- [119] Y. Huang et al., *Appl. Catal. B Environ.* 251 (2019) 181–194.
- [120] L. Zhao et al., *Appl. Catal. B Environ.* 338 (5) (2023) 122996.
- [121] L. Zeng et al., *J. Mater. Chem. A* 7 (2019) 25628–25640.
- [122] S. Ye et al., *J. Mater. Chem. A* 8 (2020) 11246–11254.
- [123] X. Bu et al., *Chem. Eng. J.* 438 (2022) 135379.
- [124] J. Miao et al., *Adv. Funct. Mater.* 29 (8) (2019) 1805893.
- [125] C. Yang et al., *Appl. Catal. B Environ.* 304 (2022) 120993.
- [126] M. Maleki et al., *J. Electroanal. Chem.* 916 (2022) 116379.
- [127] R. Ding et al., *Green Chem.* 23 (12) (2021) 4551–4559.
- [128] S. Liu et al., *J. Mater. Chem. A* 8 (48) (2020) 25768–25779.
- [129] X. Lu et al., *Energ. Environ. Sci.* 11 (7) (2018) 1898–1910.
- [130] Q. Zhang et al., *ACS Appl. Mater. Inter.* 13 (45) (2021) 53798–53809.
- [131] P. Gnanasekar et al., *ACS Sustainable Chemistry & Engineering* 9 (25) (2021) 8572–8580.
- [132] Y. Li et al., *Appl. Catal. B Environ.* 318 (2022) 121832.
- [133] Y. Lin et al., *J. Energy Chem.* 55 (2021) 92–101.
- [134] W. Xu, *Adv. Funct. Mater.* (2023), <https://doi.org/10.1002/adfm.202302263>.
- [135] H. Chen et al., *Appl. Catal. B Environ.* 293 (15) (2021) 120215.
- [136] F. Yang et al., *Adv. Funct. Mater.* 31 (21) (2021) 2010367.
- [137] C. Zhang et al., *Sci. Adv.* 9 (2023) eadd6978.
- [138] H. Liu et al., *Nat. Commun.* 13 (2022) 6382.
- [139] J. Shen et al., *Energy Environ. Mater.* (2023), <https://doi.org/10.1002/eem2.12462>.
- [140] A. Ambrosi, M. Pumera, *Adv. Funct. Mater.* 28 (27) (2018) 1700655.
- [141] X. Su et al., *Adv. Sci.* 6 (6) (2019) 1801670.
- [142] T. Kou et al., *Adv. Energy Mater.* 10 (46) (2020) 2002955.
- [143] F. Yang et al., *Adv. Energy Mater.* 10 (25) (2020) 2001174.
- [144] J. Zhu et al., *Energy Environ. Mater.* 6 (2) (2023) e12318.
- [145] L. Zhang et al., *Small* 17 (28) (2021) 2100832.
- [146] Y. Song et al., *Adv. Funct. Mater.* (2023), <https://doi.org/10.1002/adfm.202214081>.
- [147] P. Zhai et al., *Nat. Commun.* 14 (1) (2023) 1873.
- [148] L. Zhang et al., *Inorg. Chem. Front.* 10 (9) (2023) 2766–2775.
- [149] S. Feng et al., *J. Mater. Chem. A* (2023), <https://doi.org/10.1039/D3TA01585H>.
- [150] C. Ros et al., *ChemSusChem* 14 (14) (2021) 2872–2881.
- [151] X. Wang et al., *ACS Applied Mater. Interf.* 14 (37) (2022) 41924–41933.
- [152] Q. Wang et al., *Inter. J. Hydrot. Energy* 47 (25) (2022) 12629–12641.
- [153] F. Ma et al., *Appl. Catal. B Environ.* 307 (2022) 121198.
- [154] L. Li et al., *Adv. Energy Mater.* 10 (30) (2020) 2001600.
- [155] L. Yang et al., *Applied Surface Science* 607 (2023) 154885.
- [156] L. Wang et al., *Nat. Commun.* 13 (1) (2022) 5785.
- [157] S.A. Grigoriev et al., *Inter. J. Hydrot. Energy* 36 (3) (2011) 2721–2728.
- [158] M. Schalenbach et al., *Inter. J. Hydrot. Energy* 38 (35) (2013) 14921–14933.
- [159] D.V. Esposito, *Joule* 1 (4) (2017) 651–658.
- [160] X. Yan et al., *Nat. Commun.* 12 (1) (2021) 4143.
- [161] E.T. Ojong et al., *Inter. J. Hydrot. Energy* 42 (41) (2017) 25831–25847.
- [162] J. Torrero et al., *Adv. Energy Mater.* (2023), <https://doi.org/10.1002/aenm.202204169>.
- [163] Y. Zhao et al., *Adv. Energy Mater.* 13 (10) (2023) 2203595.
- [164] M. Sartory et al., *Inter. J. Hydrot. Energy* 42 (52) (2017) 30493–30508.
- [165] M. Espinosa-López et al., *Renew. Energy* 119 (2018) 160–173.
- [166] M. Sánchez et al., *Inter. J. Hydrot. Energy* 45 (7) (2020) 3916–3929.
- [167] M. Sánchez et al., *Inter. J. Hydrot. Energy* 43 (45) (2018) 20332–20345.
- [168] M.T. de Groot et al., *Inter. J. Hydrot. Energy* 47 (82) (2022) 34773–34783.
- [169] Z. Lei et al., *Small* (2023), <https://doi.org/10.1002/smll.202301247>.
- [170] L. Yu et al., *Proc. Natl. Acad. Sci.* 119 (18) (2022).
- [171] A. Kumar et al., *ACS Energy Lett.* 6 (2) (2021) 354–363.
- [172] Y. Liu et al., *Nat. Commun.* 14 (1) (2023) 2475.
- [173] S. Anantharaj, V. Aravindan, *Adv. Energy Mater.* 10 (1) (2020) 1902666.
- [174] P. Li et al., *Small* 15 (13) (2019) 1805103.
- [175] Z. Zhou et al., *Energ. Environ. Sci.* 13 (10) (2020) 3185–3206.
- [176] J.-X. Feng et al., *J. Am. Chem. Soc.* 140 (15) (2018) 5118–5126.
- [177] W. Zhu et al., *ChemCatChem* 9 (10) (2017) 1721–1743.
- [178] Y. Wang et al., *Chem Catal.* 3 (7) (2023) 100643.
- [179] L. Yu et al., *Energ. Environ. Sci.* 13 (10) (2020) 3439–3446.
- [180] D. Liu et al., *Adv. Energy Mater.* 10 (45) (2020) 2002464.
- [181] B. Wu et al., *Adv. Mater.* 34 (43) (2022) 2108619.
- [182] A. Li et al., *Nat. Catal.* 5 (2) (2022) 109.
- [183] C. Feng et al., *Nat. Commun.* 12 (1) (2021) 5980.
- [184] R. Chen et al., *PCCP* 14 (20) (2012) 7392–7399.
- [185] R. Chen et al., *Chem. Mater.* 22 (23) (2010) 6215–6217.
- [186] A.R. Zeradjanin et al., *PCCP* 16 (27) (2014) 13741–13747.
- [187] I.A. Moreno-Hernandez et al., *Energ. Environ. Sci.* 12 (4) (2019) 1241–1248.
- [188] N. Menzel et al., *ACS Catal.* 3 (6) (2013) 1324–1333.
- [189] H.W. Lim et al., *ACS Catal.* 11 (20) (2021) 12423–12432.
- [190] S. Han et al., *J. Ind. Eng. Chem.* 108 (2022) 514–521.
- [191] J. Hu et al., *ChemElectroChem* 8 (6) (2021) 1204–1210.
- [192] M. Jiang et al., *Small* 13 (4) (2017) 1602240.
- [193] J. Yang et al., *Nature* 617 (7961) (2023) 519–523.
- [194] M. Ning et al., *Mater. Today Phys.* 19 (2021) 100419.
- [195] R. Chen et al., *Adv. Mater.* 31 (41) (2019) 1903909.
- [196] L. Zhang et al., *Nano Res. Energy* 1 (2022) e9120028.
- [197] B. Zhang et al., *Small* 18 (45) (2022) 2203852.
- [198] J. Li et al., *Adv. Sci.* 9 (25) (2022) 2202387.
- [199] R. Li et al., *Appl. Catal. B Environ.* 318 (2022) 121834.
- [200] J. Zheng et al., *RSC Adv.* 8 (17) (2018) 9423–9429.
- [201] M.S. Kim et al., *Energy Environ. Mater.* 5 (4) (2022) 1340–1349.
- [202] S. Shin et al., *Small* 19 (11) (2023) 2206918.
- [203] H. Sun et al., *ACS Appl. Mater. Inter.* 14 (19) (2022) 22061–22070.
- [204] Q. Tu et al., *ACS Appl. Energy Mater.* 4 (5) (2021) 4630–4637.
- [205] Y.S. Park et al., *J. Mater. Chem. A* 9 (15) (2021) 9586–9592.
- [206] M. Ning et al., *Energ. Environ. Sci.* 15 (9) (2022) 3945–3957.